DISSERTATION

MANAGEMENT OF CONTAMINANTS IN LOW PERMEABILITY MEDIA

Submitted by

Kevin R. Saller

Department of Civil and Environmental Engineering

In partial fulfillment of the requirements

For the Degree of Doctor of Philosophy

Colorado State University

Fort Collins, Colorado

Summer 2014

Doctoral Committee:

Advisor: Tom Sale

Domenico Bau
Charles Shackelford
Michael Ronayne

<div align="center">ABSTRACT</div>

<div align="center">MANAGEMENT OF CONTAMINANTS IN LOW PERMEABILITY MEDIA</div>

Groundwaters contaminated with chlorinated solvents represent one of the largest challenges to the groundwater remediation profession. Due to their large storage potential, addressing contaminant releases from the low permeability (herein k) zones of source zones and plumes is of interest. Building off of a perceived knowledge gap regarding the effectiveness and mechanisms behind common treatments of low k zones, the overarching objective for this research is to develop insights into the physical processes controlling treatment of contaminants stored in low k zones.

A laboratory experiment using six (6) identical laboratory tanks with alternating layers of transmissive and low k soils was employed to produce a comparative analysis of common treatment technologies. The experiments involved flushing with a saturated TCE solution for 52 days, followed by a 28 day water-only flush, and then a 27 day treatment window. Post treatment flushing with only water was then conducted for an additional 82 days to determine the post-treatment outcome of each approach. Treatments were: 1) no-action as a control, 2) enhanced water flushing, 3) potassium permanganate flushing, 4) flushing with KB-1 microbial inoculum and lactate, 5) a KB-1 inoculum, lactate and xanthan gum injection, and 6) flushing with sulfate-reducing bacterial (SRB), lactate and magnesium sulfate.

Order-of-magnitude (herein OoM) (i.e., 3 OoM = 99.9%) reductions in effluent TCE concentrations at the end of the study, relative to the end of the TCE flushing (day 52) were: no-action control (2.59), enhance flushing (2.58), permanganate (3.05), KB1-lactate (3.15), KB1-lactate-xanthan gum (3.19), and SRB-lactate-sulfate (3.75). At the end of the

study (day 189), effluent TCE concentrations from the tanks range from 2.79 (control) to 1.63 (SRB-lactate-sulfate) OoM above the MCL for TCE.

Results from the enhanced flushing treatment suggest limited long-term advantages to using this treatment technology for the chosen heterogeneous soil architecture. Observations from the permanganate treatment include limited penetration of the oxidant solution into the low k zones, resulting in post-treatment TCE rebound. This result was most likely caused by limitations imposed by an oxidant demand of the low k soils, such as from reduced mineral species or oxidation of organic matter. All three of the biologically mediated treatments (treatments 4-6) saw more than 3 OoM reductions in effluent TCE after injection of lactate, followed by rebound. This result is most likely due to metabolic exhaustion of the lactate in the tanks resulting in carbon starvation of the microbes. The results of this study reveal that even under ideal laboratory conditions (e.g., sweep efficiency of treatments, high contact of treatments to contaminated soils), these common treatment technologies applied to systems with contaminants stored in low k zones were limited to 1.16 OoM (93%) improvements in TCE water quality relative to the no-action control at the conclusion of the 189 day study. Analysis of total effluent chlorinated volatile organic compounds (CVOC) (i.e., cis-DCE) from the tanks at the end of the study further limits these improvements.

Results from the tank studies provided an opportunity to develop and test conceptual models addressing the treatment of contaminants in low k zones. These models provided evidence to confirm or deny the validity of insights gained on treatment mechanisms from the laboratory treatments. The reactive-transport code *MIN3P* provided a convenient opportunity to advance numerical models using laboratory-scale data.

Laboratory conceptual models for the six laboratory studies were developed and implemented. Laboratory-scale modeling results from the control tank indicate that *MIN3P* is

capable of simulating the transport and natural attenuative processes involved in the spatial evolution of TCE throughout the 189 day experiment. Modeling the five active treatments demonstrate that *MIN3P* accommodates for the complexities necessary to model processes such as intra-aqueous reaction (e.g., permanganate ISCO), mineral-phase dissolution, biological growth, and biological decay. Findings from this laboratory-scale modeling study indicate that our understanding of the interaction of an oxidative treatment, such as permanganate, is mostly complete and can be satisfactorily modeled at this scale. Results from the study also indicate that the use of *MIN3P* to model microbial growth, decay and intra-aqueous dechlorination is viable given the incorporation of Monod kinetics and inhibition terms.

The laboratory-scale conceptual models were applied to two field-scale scenarios using the laboratory derived biogeochemical input parameters. This up-scaling of the models was done to gain insights concerning treatment outcomes at larger domains. Field-scale modeling studies demonstrated the relative performances of each of the treatments under two different aquifer scenarios. Although geometrically and chemically simplified, results from the field-scenarios indicate that the treatments considered would be relatively ineffective at sites with large low k bodies (such as an aquitard), but may be more effective at treating sites where contaminants are limited to thin interbeds of low k media.

The validity of coupling transverse hydrodynamic dispersion to seepage velocity at the laboratory-scale was investigated in two distinct experiments. The first was an experiment to clarify the validity of using a diffusion-only transverse hydrodynamic dispersion term in a contaminant plane-source model (Bird et al., 1960). Results from this experiment suggest that diffusion alone was unable to account for the observed mass flux emanating from a dissolving gypsum ($CaSO_4$) pool above a flowing transmissive layer. This finding suggests

that processes beyond diffusion (e.g., flow-path tortuosity) were at work in transversely spreading the aqueous sulfate. A second experiment developed a method of quantifying the transverse spreading of a fluorescein tracer in a uniform flow field as a function of distance and time. Quantifying the transverse spreading of the fluorescein tracer was accomplished using image-analysis and function minimization techniques provided by *MATLAB*. Results from this second experiment suggest that: 1) the transverse spreading of the fluorescein tracer was not linear with distance from the source, 2) molecular diffusion alone is not enough to account for the transverse spreading at the chosen seepage velocities, and 3) at a specific time from source, transverse hydrodynamic dispersion within the steady-state plumes seemed to increase as the seepage velocity was increased. Physical explanations regarding this phenomenon are discussed, and include the presence of non-laminar flow at the microscopic pore-scale due to soil electrostatic forces or flow-path tortuosity. Non-laminar flow at this scale may result in pore-space micro-eddies that can result in enhanced transverse spreading of contaminants perpendicular from the mean flow-path.

Insights from this work indicate a need for further investigation of novel solutions for managing contaminants in low k zones. This topic is the focus of a state-of-the-science report that was submitted to the Strategic Environmental Research and Development Program (SERDP) in March 2014. Furthermore, there is an apparent lack of consensus on the processes controlling transverse spreading of contaminants in plumes. Further study of the processes controlling transport in plumes is warranted. In the absence of a clear understanding of biogeochemical processes in low k zones, site managers will likely continue to struggle in implementing effective remedies for subsurface releases of chlorinated solvents.

TABLE OF CONTENTS

Thesis Introduction

The following provides an introduction to this thesis, including: 1) a problem statement, 2) background on subsurface releases of chlorinated solvents, 3) a review of common treatments for chlorinated solvent plumes, 4) a review of laboratory studies addressing treatment of contaminants stored in low k media, 5) the research goals for modeling the treatment studies with the reactive-transport code *MIN3P*, 6) background regarding transverse hydrodynamic dispersion investigated in Chapter 4, 7) objectives of the research, and 8) the overall organization for this Thesis. This information provides a foundation for the subsequent Chapters.

1.1. Problem Statement

Advancements in site characterization tools have demonstrated that the extent and distribution of contaminants in heterogeneous media are more complex than previously thought. Correspondingly, historical subsurface conceptual models for contaminants based on uniform porous media have often been flawed. Limited field-scale successes with the remediation of subsurface contaminants over the last three decades (NRC, 1994; NRC, 2005; NRC, 2013) provides additional evidence supporting flawed site conceptual models. This suggests that our understanding of contaminant transport within heterogeneous media to be incomplete, and more importantly, that modern hydrogeologists need to rethink the strategies involved in efforts to remediate contaminants in the subsurface. Herein, a vision for modern contaminant hydrology is advanced that embraces the concepts of transport in heterogeneous media.

1.2. Groundwater Contamination by Chlorinated Solvents

The extensive use of chlorinated solvents as degreasing products during industrial and military activities gave rise to a significant groundwater contamination problem in the U.S. and abroad that has spanned decades (Pankow and Cherry, 1996). Groundwaters contaminated with chlorinated solvents represent one of the largest challenges to the groundwater remediation profession (Stroo et al., 2012). To date, site owners and governments have spent billions of dollars in often unsuccessful remediation efforts (NRC, 2013). Recent field and modeling studies have demonstrated that common remediation efforts for impacted subsurface media can be ineffective, and the time-frame of care can be on the order of centuries.

Through best management practices of the 1950's, 60's, 70's and 80's, chlorinated solvents were dumped onto dry ground as a form of waste management based on evaporation. Chlorinated solvents were typically released at the surface as dense non-aqueous phase liquids (DNAPLs), which can migrate down through porous media until a low permeability (k) layer is encountered. Low k layers act as capillary barriers that create DNAPL pools (Johnson and Pankow, 1992; Feenstra et al., 1996; Dekker and Abriola, 2000; Saenton et al., 2002). DNAPL constituents can then dissolve into the surrounding groundwater flow, forming contaminant plumes within aquifers. Furthermore, dissolved phase DNAPL constituents can diffuse into low k layers, sorb to and within solids, and partition into soil gas. Due to the potential carcinogenic effects of chlorinated solvents such as perchloroethene (PCE) and trichloroethene (TCE) (U.S. EPA), aqueous and vapor plumes can result in a potential health risk to the public that uses the groundwater or are impacted by vapor intrusion into indoor-air.

1.3. Common Treatment Technologies for Contaminant Plumes

One of the earliest technologies for chlorinated solvent plumes in groundwater was pump and treat. Limitations of pump and treat have lead to a suite of *in situ* treatments centered on delivery of chemical and/or biological amendments. Modern treatments for plumes include: 1) *In-Situ* Chemical Oxidation (ISCO) treatments such as potassium permanganate or persulfate, 2) biologically Enhanced Reductive Dechlorination (ERD) which relies on dechlorinating microbes (natural or augmented) with a supplied carbon substrate (such as lactate or vegetable oil), 3) the use of chemical/biological injections to precipitate out reactive mineral phases (e.g., biogeochemical reductive dechlorination), or 4) chemical reductants. These treatments are usually delivered to the subsurface via delivery wells or point-injections. Unfortunately, poor contact between the contaminant and reactants can occur due to the complex flow-paths in natural heterogeneous media. Specifically, the biggest problem is often poor contact of treatments with contaminants in low k zones. After extended periods of exposure, low k zones can act as persistent secondary sources for groundwater contamination. This is commonly seen in the case of source removal/isolation activities (Sudicky et al., 1985; Liu and Ball, 2002; Chapman and Parker, 2005; Sale et al., 2008). Transport in low k zones is often diffusion dominated and is governed by biogeochemical conditions that are often consequentially different than the conditions present in transmissive zones. These observations suggest that the consideration of low k zones can be critical to anticipating the benefits of site remedies.

1.4. Laboratory Studies Addressing Treatment of Contaminants in Low Permeability Zones

Chapter 2 of this work uses side-by-side heterogeneous laboratory tanks to investigate: 1) the efficacies of six (6) common field treatments for contaminants in low k zones, and 2) the chemical and biological processes occurring during these treatments. This knowledge can aid in better decision making concerning the management of contaminant releases from low k zones at field sites. A timeline of the laboratory treatment studies is shown in Figure 1.1. The six treatments were:

(1) Constant flushing with clean water (control)

(2) Enhanced flushing with clean water

(3) Potassium permanganate ISCO flushing

(4) KB-1 (microbial inoculum) bioaugmentation with sodium lactate

(5) KB-1 bioaugmentation with sodium lactate and xanthan gum

(6) Sulfate reducing bacteria (SRB) bioaugmentation with magnesium sulfate and lactate

Post-treatment flushing was employed to evaluate contaminant rebound after treatment. Detailed background information on each of these six treatments is presented in Section 2.3. Effluent samples were collected from each tank throughout the experiment to determine the efficacy of the treatments in reducing releases of chlorinated volatile organic compounds (CVOC) from low k zones.

1.5. Modeling Using *MIN3P*: Laboratory and Field Studies

Chapter 3 presents a two-part modeling effort using the reactive-transport code *MIN3P* (Mayer et al., 2002). First, results from the laboratory studies in Chapter 2 are used to
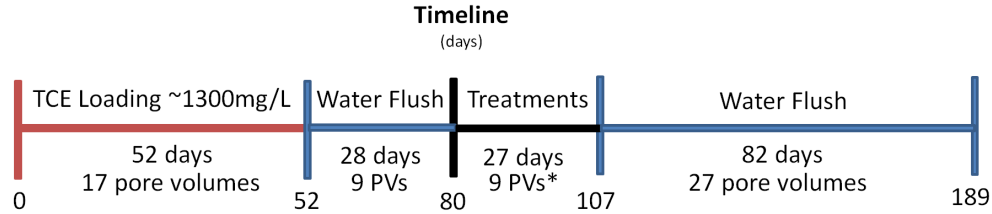
FIGURE 1.1. Experimental timeline of TCE loading, treatment and flushing periods from the treatment studies explored in Chapter 2 (*enhanced flushing and xanthan gum treatments received 42 and 1.33 P.V.s, respectively). Post-treatment flushing is shown as the 82-day water flush after the 27-day treatments.

develop numerical models for each of the six laboratory treatments. These laboratory-scale models explore theoretical treatment mechanisms observed during the laboratory treatment studies. Once satisfied with the development of the laboratory-scale models, a second modeling effort explores the concept that *MIN3P* can be used to upscale the laboratory results to explore the relative efficacy of the treatments within two field-scale scenarios. Results from upscaling models have the potential to provide a tool for site-managers to better apply treatment schemes without the costs associated with field-trials.

Published literature concerning the development and testing of the code against field data can be found in Mayer et al. (2001a), (2001b), (2002) and Henderson et al. (2009). Published literature concerning upscaling laboratory treatment results to the field-scale using *MIN3P* was not found. This provided the motivation for this portion of the research.

1.6. LABORATORY STUDIES ON HYDRODYNAMIC TRANSVERSE DISPERSION

Historically, data showing transverse spreading of miscible solutes in aqueous flow fields has been widely attributed to the phenomenon of transverse hydrodynamic dispersion. Since the 1950's, this phenomenon has been described and formulated in a number of ways. The

most prevalent has been the approach by Bear (1972). Combining current theory and mathematics of the time, Bear (1972) defined this phenomenon as the combined effects of molecular diffusion and a velocity-dependent mechanical dispersion term. This formulation is shown in Equation 1.

$$D = \alpha \cdot v + D^*,$$ (1)

where α is the dispersivity coefficient (L), v is the seepage velocity (L $\cdot$ T^{-1}) and D^* is effective molecular diffusion (L^2 $\cdot$ T^{-1}). In modeling efforts to describe plume evolution, dispersion has historically been applied both longitudinally and transversely to the direction of groundwater flow. A qualitative representation of how this formulation of transverse hydrodynamic dispersion acts on a plume is shown in Figure 1.2. Notice the larger and larger volume of aquifer inhabited by the plume with distance and time. Since its publication, this concept of dispersion from the textbook of Bear (1972) has become ingrained within a large number of modeling and teaching efforts.
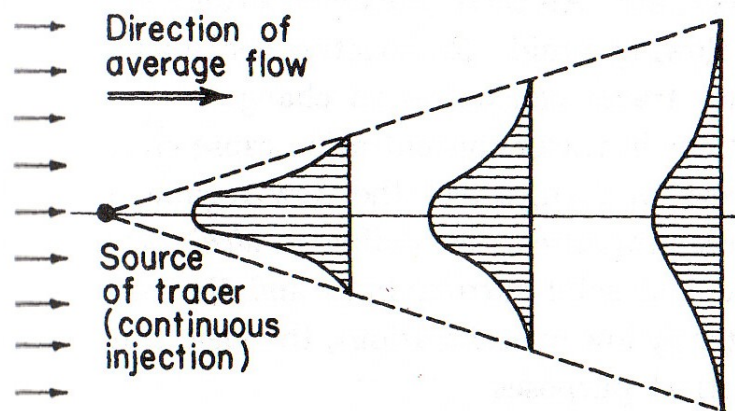
FIGURE 1.2. From Bear (1972), the widening solute front in a porous media due to the effects of transverse dispersion, modified from Danel (1952). Each of the 3 shown vertical-transect concentration profiles represents a normal-distribution curve for the transverse dispersion of the particles.

By studying field data from monitoring wells, many studies have attempted to quantify the value of α within Equation 1. Some studies concluded that α can be defined as a scalar which depends on the longitudinal length of the domain of interest. Since defining α in this way greatly simplifies the system of the soil heterogeneities, solid/liquid phase interactions, pore-space flow variations and many of the other known and unknown phenomena occurring in the subsurface flow, this depiction of such a complex phenomenon can be criticized as being short sighted.

Advancement of high-resolution subsurface site-characterization techniques over the last two decades has produced interesting results, an example of which is the 'narrow' contaminant plume situation shown in Figure 1.3 (Rivett et al., 2001). These types of results suggest a disconnect between the definition of the transverse hydrodynamic dispersion seen in Equation 1 and observed field-scale plume evolution. In conjunction with the recent recognition that 1) contaminant storage and release from low k zones can explain missing contaminant mass at the distal ends of plumes which was previously attributed to transverse hydrodynamic dispersion, and 2) the use of monitoring and injection wells to produce water quality data can artificially spread a contaminant within the formation, the observation of narrow contaminant plumes over long distances provides the motivation for investigating this phenomenon.

The results and analysis from two laboratory experiments to investigate the coupling of transverse hydrodynamic dispersion and seepage velocity are provided in Chapter 4. The first experiment tests a contaminant plane-source model (based on Bird et al., 1960) using a diffusion-only transverse dispersion term. The second experiment develops a computational imaging technique in *MATLAB* to analyze the transverse spreading of laboratory-scale fluorescein plumes. Using the results from these experiments, the objectives for this portion
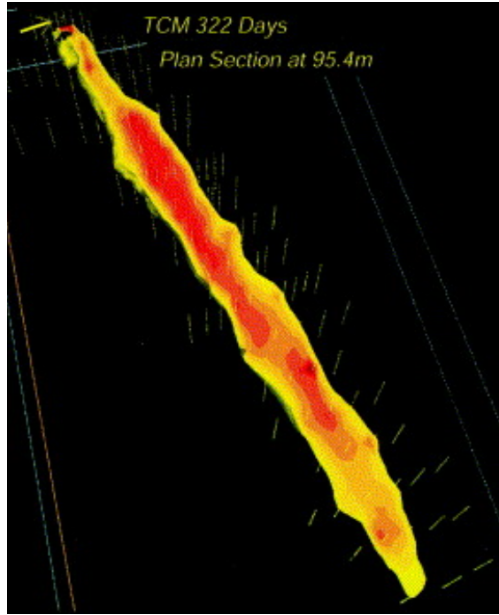
FIGURE 1.3. High-resolution profile of a TCM plume in a sandy aquifer demonstrating minimal transverse dispersion (from Rivett et al., 2001).

of the research are to: 1) determine the validity of a diffusion-only dispersion term inside the contaminant plane-source model (Bird et al., 1960), and 2) to qualitatively demonstrate how a dissolved contaminant will transversely spread when moving through a porous media under different seepage velocities at the laboratory scale.

1.7. RESEARCH HYPOTHESES AND OBJECTIVES

The hypotheses which are tested in Chapters 2, 3 and 4 are:

- That laboratory-scale tank studies can be used to evaluate the relative efficacy of common treatments for chlorinated solvents in low k zones.

- That it is possible to develop laboratory-scale models using the reactive-transport code *MIN3P* to accurately capture the complex biogeochemical processes occurring in each of the treatments presented in Chapter 2.

- That laboratory-scale treatment models can be used to explore and compare the relative efficacy of the laboratory treatments from Chapter 2 at the field-scale.

- That the contaminant plane-source model presented by Bird et al. (1960) can be used with a purely diffusive dispersion term to explain laboratory data of a gypsum pool dissolving into a transmissive layer.

- That the phenomenon of transverse hydrodynamic dispersion in a porous media can be explained at the laboratory-scale by the processes of diffusion.

- That the current prevailing definition of transverse hydrodynamic dispersion is in need of further study and consideration.

Overall, the broad objectives for this work center on: 1) improving our understanding of the processes controlling the outcomes of treatments applied to contaminants stored in the low k zones of aquifers, and 2) to clarify the effect of seepage velocity on transverse mixing of contaminants in plumes. Additional objectives include:

- Quantifying the fate and transport of a dissolved phase TCE pulse in a laboratory controlled heterogeneous system.

- Quantifying the treatment mechanisms and outcomes of six (6) treatment options in the presence of low k zones.

- Supporting sound decision making regarding treatment of subsurface releases of anthropogenic contaminants.

- Using laboratory derived and published biochemical parameters, determine if the reactive-transport code *MIN3P* can be used to accurately model the treatments.

- Addressing concerns from emerging controversy regarding the phenomenon of transverse hydrodynamic dispersion.

1.8. Thesis Content and Publication Status

Chapter 2 presents a laboratory tank treatment study employing six, layered soil system tanks saturated with aqueous TCE. Reactive-transport modeling in support of these laboratory treatments is presented in the first part of Chapter 3. Results from the laboratory models are expanded in the second part of Chapter 3, which upscales the lab models to field-scale to determine the outcome of treatments given two field scenarios. Chapter 4 presents the results from two laboratory experiments that provide two unique types of analyses of transverse hydrodynamic dispersion in porous media. The first experiment is a laboratory analysis of a gypsum pool dissolving into a transmissive zone to test a model presented by Bird et al. (1960). The second experiment presents a new method to analyze transverse mixing using a fluorescein-dye point-source in a uniform flow field and subsequent analysis of plume images using *MATLAB*.

Chapter 1 presents an introduction relevant to the laboratory and modeling studies conducted herein, and is not intended for journal publication. An abbreviated version of Chapter 2 (lab studies) has been submitted to the Journal of Contaminant Hydrology. The results from modeling the six laboratory treatment studies and two field-scenarios presented in Chapter 3 are being finalized for submission to the Journal of Contaminant Hydrology. The results from the two laboratory experiments in Chapter 4 which analyze laboratory-scale transverse hydrodynamic dispersion in a porous media is also intended for publication in the Journal of Contaminant Hydrology. Chapter 5 presents a summary of the results and implications from Chapters 2, 3 and 4, as well as recommendations for future work and is not intended for journal publication.

CHAPTER 2

Treatment of Contaminants in Low Permeability Zones - Laboratory Studies

2.1. Chapter Synopsis

An emerging concern in subsurface contaminant hydrology is what can be done to address contaminants stored in low permeability (k) layers in source zones and plumes. In the first part of this two-part study, six identical laboratory tanks with alternating 5-cm thick layers of transmissive and low k soils were employed to produce a comparative analysis of treatment technologies for contaminant in low k zones. The experiments involved flushing with a saturated TCE solution (52 days), flushing with water (28 days), treatment (27 days), and post treatment flushing with water (82 days). Treatments were: 1) no-action control, 2) enhanced water flushing, 3) potassium permanganate flush, 4) KB-1 microbial inoculum with lactate, 5) KB-1 with lactate and xanthan gum injection, and 6) sulfate-reducing bacteria (SRB) inoculum with lactate and magnesium sulfate. Order-of-magnitude (OoM) (i.e., 3 OoM = 99.9%) reductions in effluent TCE concentrations at the end of the study, relative to the end of the TCE flushing were: no-action control (2.59), enhance flushing (2.58), permanganate (3.05), KB1-lactate (3.15), KB1-lactate-xanthan gum (3.19), and SRB-lactate-sulfate (3.75). Effluent TCE concentrations from all tanks range from 2.79 (control) to 1.63 OoM (SRB-lactate-sulfate) above the TCE MCL at the end of the study.

Primary findings from this study include: 1) consequential contaminant storage and release time-frames associated with low k zones, 2) enhanced flushing failed to sufficiently drive the TCE out of the low k zones to produce a long-term reduction in effluent concentrations, 3) penetration of permanganate into the low k zones was limited by the oxidant demand of

the low k soils and potential clogging of pore space by manganese dioxide, and 4) all three of the biologically mediated treatments saw multiple OoM reduction of TCE followed by rebound, most likely from exhaustion of the electron donor. Overall, constrained performance in the tanks studies is consistent with observed treatment and rebound of chlorinated solvent concentrations at many field sites.

Furthermore, results indicate that even under ideal laboratory conditions, common treatment technologies applied to systems with contaminants in low k zones were limited to a 1.16 OoM (93%) improvement in TCE water quality (relative to no-action). This finding suggests that in addition to providing a long-term source for contaminants, low k zones rendered the considered remediation methods ineffective at large OoM reductions in long-term effluent CVOCs. Findings indicate that care is needed in setting the strategies and expectations involved in these treatments at field sites with low k zones.

2.2. Introduction

Chlorinated solvents are a member of a broad class of anthropogenic contaminants that can persist in subsurface settings for extended periods of time. Groundwaters contaminated with these solvents represent one of the largest challenges to the groundwater remediation profession (Stroo et al., 2012). Chlorinated solvents were extensively used historically as degreasing products for various types of machinery, such as aircraft engines, along with their uses in dry-cleaning (Pankow and Cherry, 1996). Best management practices of the 1950's, 60's, 70's and 80's has caused widespread contamination of groundwaters throughout the United States, and indeed the world. Due to its extensive use, a particular contaminant of concern is trichloroethene (TCE). TCE and other chlorinated solvents were typically released to the subsurface as a dense non-aqueous phase liquid (DNAPL). Once released, DNAPLs

migrate down through the porous media until they reach a low k layer that acts a capillary barrier (Johnson and Pankow, 1992; Feenstra et al., 1996; Dekker and Abriola, 2000; Saenton et al., 2002). DNAPLs perched above capillary barriers partition into the groundwater and are subsequently transported via advection and diffusion into both the transmissive and low k zones of the aquifer. Commonly, chlorinated solvents persist in groundwater even after large monetary expenditures and numerous treatment options have been exercised (Stroo et al., 2012). In part, the limitations of our efforts to address chlorinated solvent releases can be attributed to gaps in our understanding of treatment behavior in heterogeneous subsurface media.

Following Gillham et al. (1984), Sudicky et al. (1985), Mackay and Cherry (1989), Parker et al. (1994), Chapman and Parker (2005), Sale et al. (2008) and Parker et al. (2008), a key element in the understanding of subsurface migration of contaminants and the treatments used to remediate these contaminants was missing - namely, the storage and release of contaminants from low k zones in aquifers. Depending on the exposure time of the contaminant (along with other factors), low k zones can store large quantities of contaminant that have migrated into the layers via diffusion and slow advection. Research and field data mentioned previously have shown that once the transmissive zones have been cleared of a contaminant, the low k zones in heterogeneous aquifers can behave as persistent secondary sources for significant periods of time (Sudicky et al., 1985; Liu and Ball, 2002; Chapman and Parker, 2005; Sale et al., 2008). Work done by Liu and Ball (2002), Chapman and Parker (2005) and Sale et al. (2008) has shown that the slow diffusive process that governs dissolved phase contaminant loading into and out of these low k soils can cause down-gradient wells to produce contaminated water above the Maximum Contaminant Level (MCL) for decades or even centuries after source zone removal.

While often successful, chemical oxidative treatments such as potassium permanganate can sometimes fail because of these diffusion dominated soils, as it relies on direct contact with the contaminant. Once the treatment has finished and begins flushing out of the transmissive zones, any untreated TCE stored in the low k soils is again driven into the transmissive zones via diffusive and slow advection processes, causing a "rebound" in down-gradient concentrations. A particularly relevant example of this type of failure is Spill Site 7 located at F.E. Warren Air Force Base in Cheyenne, Wyoming. To date, potassium permanganate flushing, source excavation, soil vapor extraction, pump and treat, biologically enhanced reductive dechlorination and a zero-valent iron permeable reactive barrier have been employed. Despite these efforts, TCE remains above the U.S. E.P.A. MCL of 5 μg/L in a down-gradient stream.

Building off of a perceived knowledge gap regarding the effectiveness and mechanisms of treatment in low k zones, the objective for this portion of research is to develop insights into the physical processes controlling the treatment of contaminants in low k zones via laboratory tank studies. By employing highly controlled conditions and a contaminant mass balance, side-by-side treatment comparisons for heterogeneous soils in the laboratory offers a unique way to investigate the effectiveness of treating contaminants stored in low k zones. This Chapter presents the results of research in which six (6) heterogeneous sand tanks filled with field soils were concurrently flooded with a saturated aqueous solution of TCE, after which six commonly used treatments were employed:

(1) Constant flushing with clean water (Control)

(2) Enhanced flushing with clean water

(3) Potassium permanganate flushing

(4) KB-1 (microbial inoculum) bioaugmentation with sodium lactate

(5) KB-1 bioaugmentation with sodium lactate and xanthan gum

(6) Sulfate reducing bacteria (SRB) bioaugmentation with magnesium sulfate and lactate

The first four treatments were chosen because of their common use at contaminated field sites. Treatments 5 and 6 were used because they appear to be promising novel remediation technologies for chlorinated solvents. To provide a foundation for interpreting the results from the tank studies, this paper will first provide some of the theory behind each of these treatments. Second, the experimental and analytical methods are discussed. Lastly, this paper presents the results and conclusions from the experiments. These laboratory studies provide a basis for the modeling studies presented in Chapter 3.

2.3. Treatment Theory and Mechanisms

The following subsections provide background information for each of the treatments as a basis for subsequent interpretation of the results.

2.3.1. No Action-Control. Due to the effects of sorption and diffusion of TCE into and out of the low k zones, an asymmetrical effluent breakthrough curve will form when given a pulse source. After the TCE source is removed, this effluent curve will present a 'tailing' behavior. This behavior occurs as a result of TCE desorption and diffusion out of the low k zones (Sudicky et al., 1985). Depending on natural attenuative processes and the architecture of the transmissive and low k zones, this can maintain a down-gradient TCE concentration profile orders of magnitude above the MCL for extended periods of time (Chapman and Parker, 2005; Sale et al., 2008). It is worth noting that a pulse source with no-action is analogous to source removal and/or containment.

2.3.2. ENHANCED AQUEOUS FLUSHING. Enhanced flushing of water to deplete contaminants can be achieved by pumping and/or the injection of water through a target volume of porous media (Sale, 1996). This method can be further modified with a corresponding system of extraction wells and possible above-ground treatment facilities. Treated water can either be re-injected or discharged at surface (Mackay and Cherry, 1989). Injection/extraction wells are placed at strategic locations relative to the contaminant plume to maximize the flow of the water throughout the target zone. This treatment technology works by displacing contaminants in transmissive zones and increasing local concentration gradients driving desorption and diffusion of contaminants out of low k zones. Potential limitations of this treatment technology include the low solubility of some contaminants, sorption to media and storage in low k zones where advective processes are significantly reduced (Mackay, 1996). These limitations suggest that this treatment would most likely be effective at sites where either containment is a goal, the hydrogeology is relatively transmissive, and/or when the contaminant has a relatively high solubility in water.

From the perspective of treating contaminants stored in low k zones, this treatment will increase the removal of contaminants by maintaining a higher concentration gradient between the transmissive and low k zones than during normal groundwater velocities. This process increases contaminant diffusion from the low k soils as described by Fick's First Law:

$$(2) \qquad\qquad J_D = n \cdot D^* \cdot \frac{dC}{dx}$$

where J_D is the diffusive flux ($M \cdot L^{-2} \cdot T^{-1}$), C is the concentration of the contaminant ($M \cdot L^{-3}$), n is the soil porosity (/), x is position (L) and D^* is the effective diffusion coefficient ($L^2 \cdot T^{-1}$). Equation 2 suggests that an increase in the concentration gradient, dC/dx, produces a higher diffusive contaminant flux from the low k zones (secondary sources) to

the continuously flushed transmissive zones (C $\approx$ 0). This treatment can also be used as a hydraulic containment or control system, where the migration of a contaminant plume is of concern (Mackay and Cherry, 1989).

2.3.3. POTASSIUM PERMANGANATE FLUSHING. Subsurface delivery of potassium permanganate, an *In Situ* Chemical Oxidation (ISCO) technology, has been shown to be effective at treating chlorinated ethenes at both the laboratory and field scales (Schnarr et al., 1998; MacKinnon and Thomson, 2002; Thomson et al., 2007; Hønning et al., 2007; Siegrist et al., 2011). Combined with its high solubility in water ($\approx$ 63.8 g/L at 20° C), these characteristics make it an attractive and popular option for groundwater remediation of chlorinated solvents such as TCE. Laboratory experiments have shown that the reaction of TCE and $KMnO_4$ proceeds as shown in Equation 3 (Schnarr et al., 1998). No hazardous products are created from this reaction.

(3) $$C_2Cl_3H + 2MnO_4^- \rightarrow 2CO_2 + 2MnO_2(s) + 3Cl^- + H^+$$
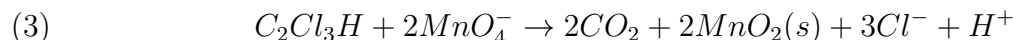
A potential drawback of this treatment is an increase in water turbidity along with the precipitation of MnO_2 minerals. Solid phase MnO_2 has been shown to cause clogging problems in the transmissive zones (MacKinnon and Thomson, 2002; Thomson et al., 2007), in addition to clogging in the screens, filters and surrounding soil of the wells used for the treatment injections. These issues, however, are more typical of a permanganate treatment when TCE exists as a DNAPL. Precipitation of MnO_2 can make it difficult for the ISCO treatment to reach the contaminated zones, and may be one of the primary factors responsible for contaminant rebound in heterogeneous soils. Another potential drawback of permanganate ISCO is the depletion of permanganate via reactions with the naturally occurring

aquifer materials, such as the organic matter present in the soils (Yan and Schwartz, 1999; Marvin et al., 2002; Mumford et al., 2005; Urynowicz et al., 2008; Hønning et al., 2007; Siegrist et al., 2011). This interaction imposes a natural oxidant demand (NOD) within the subsurface which can reduce the amount of oxidant that is able to react with the target compound. A possible benefit of this interaction between the organic matter and the permanganate is the destruction of the organic phase. This could potentially aid in releasing a portion of sorbed contaminant, which exposes a greater mass to the treatment solution. Lastly, perhaps the single greatest limitation of this ISCO treatment is that its effectiveness in combating post-treatment rebound is dependent on its persistence over extended periods in which contaminant diffusion from low k zones can occur.

2.3.4. KB-1 CULTURE AND LACTATE. In this experiment, a microbial inoculum was employed to drive enhanced reductive dechlorination (ERD). This technology involves the subsurface injection of dechlorinating microbes along with fermentable organic substrates to increase the degradation of undesirable compounds to unharmful end products (Damgaard et al., 2012; Field and Sierra-Alvarez, 2004). Early investigations into the use of microbes to degrade chlorinated ethenes include those by Bouwer and McCarty (1983), Parsons et al. (1984), Vogel and McCarty (1985) and Freedman and Gossett (1989). These studies found through various methods that Perchloroethene (PCE) can be reductively dehalogenated in anaerobic systems to produce TCE, cis-dichloroethene (cis-DCE), trans-DCE, vinyl chloride (VC), dichloromethane and carbon dioxide (CO_2). Furthermore, Freedman and Gossett (1989) found that methanogens may play an important role in the dechlorination of PCE and TCE. In an extensive literature review conducted by Field and Sierra-Alvarez (2004), they note many field and laboratory studies that followed this line of investigation. These include the works of Pavlostathis and Zhuang (1993), Lee et al. (1998), Vancheeswaran

et al. (1999) and a microcosm study by Fennell et al. (2001), which found various levels of dechlorination of PCE and TCE from field soils impacted with these solvents. Ellis et al. (2000) conducted an early field validation at a site where TCE dechlorination had stalled at cis-DCE. Conducted over a 509-day period at Dover Air Force Base, the authors were able to demonstrate full conversion of TCE and cis-DCE to ethene using an injected microbial culture brought in from a site contaminated with chlorinated compounds in Pinellas, Florida. More recently, Scheutz et al. (2010) conducted a more successful field trial of this technology in a clayey till. The authors injected a soybean oil and *Dehalococcoides* solution into a sand-filled hydraulic fracture establishing a bioactive zone, which after 148 days, dechlorinated all cis-DCE in the fracture into ethene. Scheutz et al. (2010) further found that due to the diffusion of the fermentation products into the clay, a bioactive zone extended approximately 5 to 6 cm into the clay matrix developed, which has potential implications for other sites with contaminated low k zones.

Although many genera of halorespiring microorganisms can partially dechlorinate chlorinated ethenes to cis-DCE, only bacteria from the genus *Dehalococcoides* which contain the functional genes encoded for synthesizing VC reductase (VCr) are able to completely dechlorinate to ethene (Maymo-Gatell et al., 1999; Magnuson et al., 2000; Field and Sierra-Alvarez, 2004; Muller et al., 2004; Lookman et al., 2007; Scheutz et al., 2008; Lee et al., 2013). Work by Hendrickson et al. (2002) helped clarify why some field sites see a stalling of PCE and TCE dechlorination at cis-DCE by demonstrating that when *Dehalococcoides* 16S rRNA genes are absent, full dechlorination to ethene does not occur. Conversely, ethene is the major end product of PCE degradation at field sites with this gene expression. The process of microbial attenuation of these chlorinated ethenes requires an organic electron-donating substrate (e.g., petroleum hydrocarbons, lactate) (Field and Sierra-Alvarez, 2004). Microbially ERD

of a contaminant, such as TCE, is possible in this case because a microorganism can benefit energetically from using TCE as an electron acceptor during the oxidation of an electron rich organic compound. Although aerobic cooxidation of PCE and TCE has been observed, the KB-1 inoculum (*Dehalococcoides* sp., *Geobacter* sp. and *Methanomethylovorans* sp.) used in this experiment prefers methanogenic or sulfate-reducing conditions. Microbial degradation of these chlorinated compounds proceeds through reductive hydrogenolysis, shown in Figure 2.1. As hydrogen replaces the chlorine substituents, each reduction yields less and less favorable energy for the microbes.
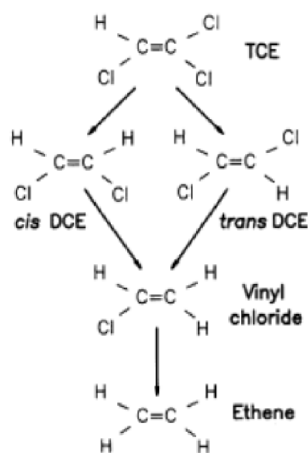
FIGURE 2.1. Anaerobic biotransformation pathway of PCE through ethene (Mohn and Tiedje, 1992).

Similar to a permanganate ISCO treatment, the success of this microbially ERD is dependent on the contaminant coming into contact with the bioactive zones. Although many high k sites have proven successful using microbially ERD (e.g., Ellis et al., 2000; Lookman et al., 2007; Scheutz et al., 2008), the challenge for these sites remains. The biological treatment must overcome distributing these organisms such that the KB-1 inoculum would be able to degrade any remaining contaminants stored in low k zones and any potentially harmful by-products over the extended release times from low k zones. In a heterogeneous system,

the microbial inoculum must either: 1) stay active in the high k zones over the entire duration of contaminant diffusion from the low k zones, or 2) the bioactive zone must migrate or grow into the low k zones and degrade the contaminant(s) stored there. This biological migration into the low k zones, however, is not supported by most field data and modeling efforts that suggest that most dechlorination occurs in the more transmissive zones and at the interfaces between the low and high k layers. Lima and Sleep (2007) demonstrated the limitations of microbial growth within heterogeneous columns fed with methanol and carbon tetrachloride. They observed no significant microbial growth beyond the interface with the transmissive zones over a 400 day period, partly attributed to the small pore space of low k zones. This finding implies that this type of aerobic dechlorination occurs mostly in higher k zones. Modeling done by Chambon et al. (2010), Manoli et al. (2012) and field work done by Damgaard et al. (2012) support this idea; although some biological migration occurs, the lack of bioactivity of these specific microbes in the lower k layers could mean a significant period of time may be required for meaningful dechlorination to occur at heterogeneous sites.

2.3.5. KB-1 CULTURE WITH LACTATE AND XANTHAN GUM. Using a KB-1 culture and lactate injection augmented with a 1 gm/L solution of xanthan gum provides interesting possibilities for treating contaminants in low k zones. Xanthan gum was used in this experiment for two reasons: 1) theoretically, to increase the sweep efficiency of the biological treatment solution throughout the tank when compared to a normal injection, and 2) to create a 'plug' of the natural groundwater flow around the injection area to inhibit having the injected KB-1 and carbon sources flushed away off-site. In the field, this option potentially helps sustain more favorable conditions for the dehalogenating bacteria to establish within and populate the contaminated zone(s) for treatment.

Xanthan gum is a polysaccharide, and has applications in food processing such as a stabilizer, or in the oil and gas industry to thicken drilling mud. For groundwater purposes, it has other properties that could be useful in remediating contaminated low k zones. When mixed with water, it creates a shear-thinning fluid. This means that the viscosity of a xanthan gum solution decreases as shearing forces increase. The transmissive sand zones within the test tanks (and aquifers) are low-shear, which means the viscosity of the treatment solution in these zones is higher than in the low k layers. Potentially, the use of xanthan gum could increase or 'force' a treatment media further into the low k zones than would otherwise happen under normal diffusive processes. Furthermore, solutions of xanthan gum are usually stable under wide ranges of pH, and does not impede the dechlorinating capability of KB-1 inoculum (McCray et al., 2010). Since xanthan gum is an ineffective electron donor for complete dechlorination to occur, another electron donor (e.g. lactate, methanol) is needed (McCray et al., 2010).

2.3.6. SULFATE REDUCING BACTERIA WITH LACTATE AND SULFATE. Sulfate-reducing bacteria (e.g., *Desulfovibrio desulfuricans*) in anoxic conditions use aqueous sulfate as a terminal electron acceptor and generate sulfide species. After dissolving naturally occuring iron minerals (e.g., goethite, FeOOH), these dissolved sulfide species form iron-sulfide mineral species (Goldhaber and Kaplan, 1974; Jeong and Hayes, 2007). An example mineral formed in this process is the black-colored tetragonal FeS_{1-x} reactive mineral mackinawite (Wolthers et al., 2003). Mackinawite has been shown to degrade chlorinated solvents under select conditions of formation (Butler and Hayes, 1999; Butler and Hayes, 2000; Butler and Hayes, 2001; Jeong and Hayes, 2003; Jeong and Hayes, 2007; Hyun and Hayes, 2009). Other metal sulfides form in these systems, such as NiS, CuS and ZnS, but iron sulfides accumulate in

comparatively significantly greater quantities at sites where these other metals are in trace amounts (He et al., 2008).

The reaction of TCE and mackinawite primarily produces the dichloroelimination product acetylene with intermediate chloro-acetylene with little to no production of cis-DCE and VC (Butler and Hayes, 1999; Butler and Hayes, 2000; Butler and Hayes, 2001; Jeong and Hayes, 2007; Jeong et al., 2007; Brown et al., 2007). Since these deposited iron sulfides are highly insoluble in water, this reaction most likely occurs at the mineral surface (Butler and Hayes, 2000). Work by Rickard (1995) showed that the way the mackinawite mineral forms may be pH dependent. This pH dependence is relevant because Wolthers et al. (2003) demonstrated that more reactive FeS minerals form at higher pH values (>7), which helps explain previous studies using mackinawite that showed no reactivity with chlorinated solvents. This pH dependency on mineral reactivity was confirmed by Hyun and Hayes (2009) who showed that, in addition to pH dependency, an Fe:S molar ratio close to 1, the addition of citrate, the age of the mineral, and the interaction of native metals (e.g., Cr, Cu, Co, Ni) with the mackinawite all affect the TCE dechlorinating capabilities of mackinawite. Lastly, sulfate-reducing cultures have been shown to degrade chlorinated ethenes and ethanes as part of a cometabolic process (Bagley and Gossett, 1990; Grostern and Edwards, 2006). This could help drive dechlorination under sulfate reducing conditions.

2.4. Methods

This section describes the experimental methods used in the setup, execution and analysis of the laboratory experiments.

2.4.1. Tank Setup. A set of six identical dual-permeability, 2-dimensional tanks were constructed (Figure 2.2). The tanks are 1-meter tall, by 0.5-m wide, and 2.54-cm deep. The

soils lay within a 2.54 cm deep gasketed aluminum sidewall that spans along the perimeter of the front and backplates. The front and back walls of the tank are composed of glass and stainless steel, respectively. Stainless steel 1/8" T joints (seen at the bottom of Figure 2.2) were installed at the bottom (inlet) and top (outlet) of the sidewall. The T joints were connected on one side to piezometers (1/8" glass tubing) to detect pore-space plugging, and connected on the other side for delivery and recovery of the fluids.
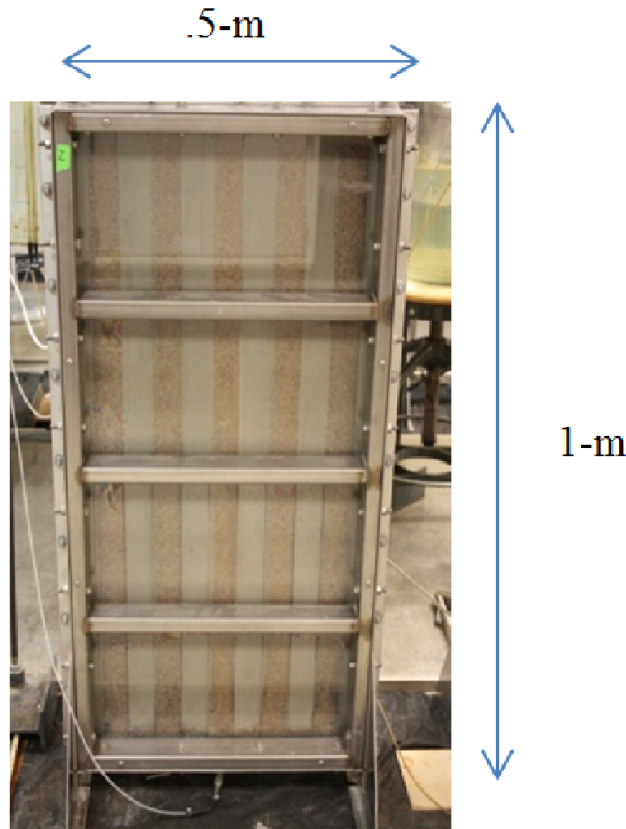
FIGURE 2.2. Tank geometry from the laboratory treatment studies. Image shows the alternating transmissive/low k soil striping, where the gray soils are the low k soils. Depth of tank = 2.54 cm. Flow is from bottom to top.

The soils were obtained from TCE impacted field soils from Spill Site 7 at F.E. Warren Air Force Base, Cheyenne, Wyoming. Soils were sieved in the lab to produce a 10-35 sand for the transmissive layers, and a minus 100 sieve for the low k layers. The sands (transmissive soil) were washed with tap water to remove fines. The low k soils were examined using XRD

and determined to be composed primarily of calcium and magnesium carbonate minerals, shown in Figure 2.3.

Coupled TwoTheta/Theta

2Theta WL=1.54056
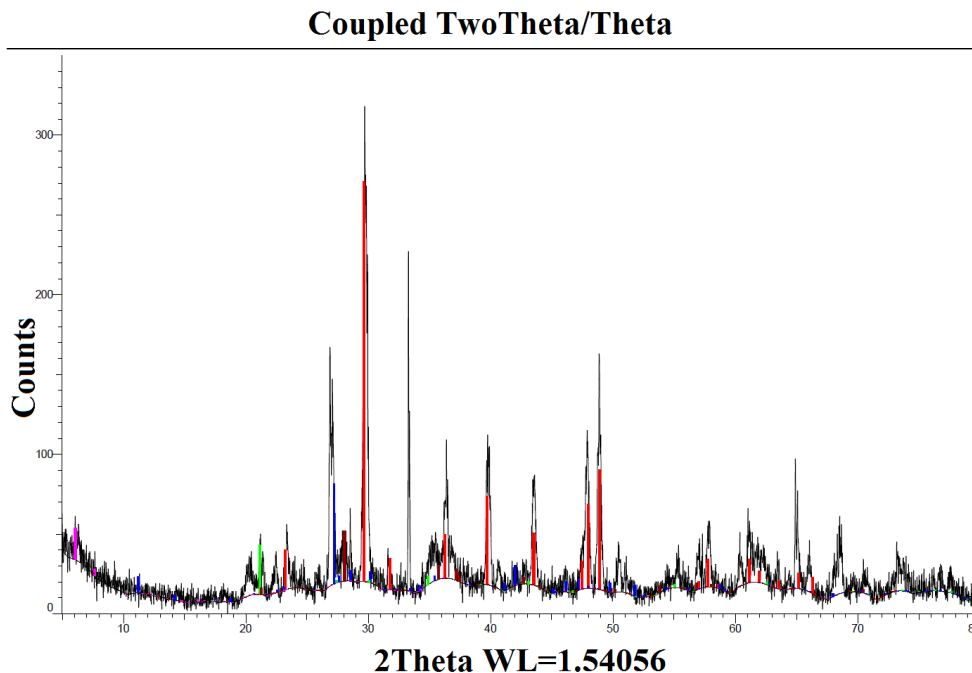
FIGURE 2.3. XRD results from low k soils. Red lines indicate (Ca, Mg) CO_3 peaks.

The transmissive soil had an unquantifiable organic carbon content (f_{oc}), while the low k soils were 0.3% f_{oc}. Laboratory TCE sorption tests with the low k soils demonstrated a distribution coefficient, K_d, of 0.69. This result is shown in Figure 2.4, and demonstrates a linear sorption isotherm ranging 3 orders of magnitude from 0.5 mg/L to 500 mg/L. Hydraulic conductivities of the transmissive and low k soils were determined using constant head column permeameters. Properties of the transmissive and low k soils are summarized in Table 2.1.

TCE Sorption Test on Silts

$$y = 0.693x - 0.9856$$
$$R^2 = 0.9997$$
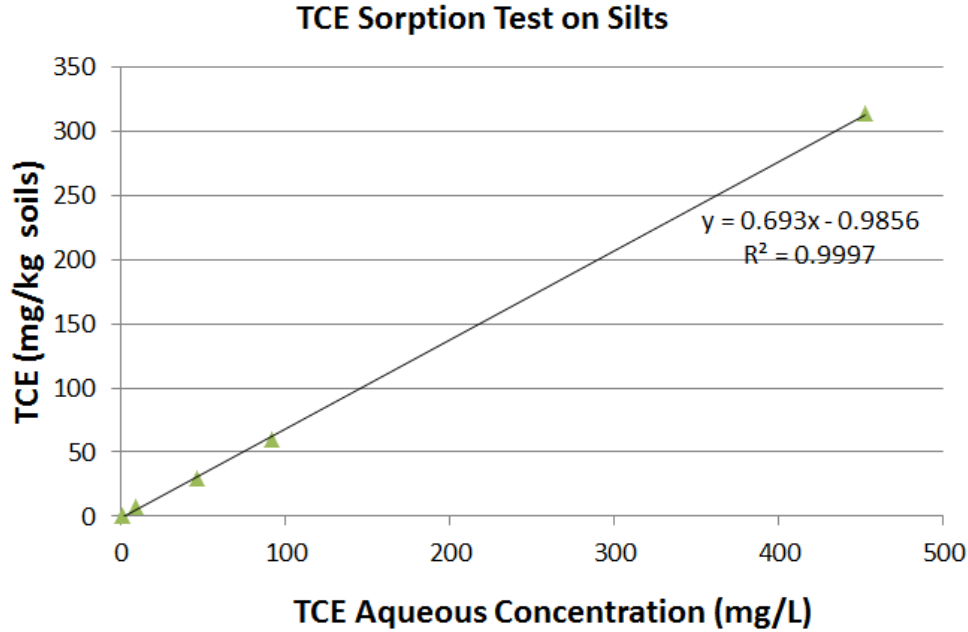
FIGURE 2.4. Results from batch sorption tests on low k soils using TCE. The match of the fit line suggests a linear sorption isotherm, where the slope is equal to the distribution coefficient K_d.

TABLE 2.1. Laboratory derived soil parameters of the transmissive and low k soils used in the treatment studies.

Soil	Hydra. Cond.	Porosity	f_{oc}(% w/w)	$K_{d,TCE}$ (mL/gm)
Transmissive	2.3E-1 cm/s	0.39	ND	ND
Low k	2.0E-4 cm/s	0.49	0.3	0.7

To maximize the surface contact for contaminant storage and release from the low k layers, the soils within the tank were arranged in 9 alternating, 5-cm thick layers with an additional 2, 2.5-cm thick low k layers at each end. The 2, 2.5-cm thick low k layers on the sides of the tank were placed as such for diffusive symmetry of the TCE into the low k zones, since these 2 low k layers are only in contact with 1 transmissive layer each. These layers spanned from the bottom to the top of the tank (Figure 2.2). To ensure even flow upwards through the transmissive layers and to prevent movement of the soil layers, 1-cm tall, reinforced stainless steel screens were placed at the top and bottom of the tank. This

soil striping pattern was employed to create a large surface contact for contaminant storage and release from the low k layers. Soils were placed in the tank by removing one of the 4 sidewalls and pouring the soils into the tank. The contents of the tank were vibrated and leveled at intervals during soil placement. Once filled, the tanks were rotated to the vertical orientation shown in Figure 2.2 to 1) prevent settlement from forming preferential flow paths and 2) eliminate gravity driven transport between the high and low k zones. The difference in hydraulic conductivity between the soils ensures advective flow in the tanks would dominate through the transmissive zones, and the low k layers would be be influenced by diffusive processes. Each tank was given its own separate 1/8" glass tubing system and positive displacement piston pump (Fluid Metering Inc., Syosset, NY, model #RHSY) to deliver all fluids throughout the experiment.

2.4.2. AQUEOUS FLUSHING. After the soil layers were emplaced and the tank sealed, 10 pore volumes (herein P.V.s) of CO_2 (Airgas, 99%) was flushed into the tank in intervals to displace the oxygen and nitrogen contained in the pore-space of the soils. CO_2 dissolves faster in water than oxygen and nitrogen, facilitating the depletion of entrapped gases. Next, de-gassed tap water (Fort Collins, Colorado) was flushed through the tanks from bottom to top. The influent de-gassed water contained 80 mg/L calcium-carbonate with 4 mg/L chloride and 11 mg/L sulfate. Each pump was set to produce a 0.33 m/day seepage velocity in the transmissive layers for the entire duration of the experiment. Exceptions include the enhanced flushing and KB-1 with xanthan gum treatments. This is discussed in Section 2.4.3. Flow-rates for each pump were measured twice a month throughout the experiment to verify steady flow.

Following a 21-day water flood, a de-gassed aqueous solution of TCE (J.T. Baker, 99.8%) near solubility ($\approx$ 1300 mg/L, 0.99E-2 mol/L) and 2978 mg/L (0.25E-1 mol/L) bromide (J.T.

27

Baker, 99.9%) was flushed through the tanks concurrently. TCE flushing was at the same transmissive zone seepage velocity of 0.33 m/day, and lasted for 52 days. Effluent samples were collected using 10-mL flow-through vials, and sealed with zero head-space using Teflon lined septa caps, labeled and stored at 4°C until quantitative analysis. Flushing a constant TCE saturated aqueous solution into the tanks was achieved using a 1-m tall, 5.2-cm wide hollow glass column that was filled halfway with glass beads (6 mm diameter) and 40 grams of Sudan IV dyed TCE (Figure 2.5).

FIGURE 2.5. 1-m long TCE exchanger with dyed TCE in 6 mm glass beads, used to saturate influent water with TCE for delivery to tanks. Flow direction from bottom to top.

Non-aqueous phase TCE was added to the exchanger daily as it was depleted. Sudan IV was added to the TCE so that the distribution and amount of TCE in the exchanger

was visually apparent. The de-gassed water (from a carboy containing 2000 mg/L bromide) flowed from a bottom port to a top glass port, where it was distributed to the tanks using their individual pump and glass piping system. The glass beads in this TCE exchanger column were added to maximize the surface area of the TCE contacting the water as the water passed upwards through the column. The system was gas tight to minimize TCE losses from volatilization. Measured TCE influent concentrations throughout the experiment had an average value of 1298 +/- 36 mg/L

Following the 52-day contaminant loading phase, the TCE and bromide source was removed from the influent, and de-gassed water was once again flushed through the tanks for a period of 28 days. Following this 28-day flushing period, the 27-day long treatments began. Following treatment, another 82-day flushing with clean de-gassed tap-water was imposed. A timeline for the experiment is shown in Figure 2.6.

Timeline
(days)

TCE Loading ~1300mg/L	Water Flush	Treatments	Water Flush
52 days 17 pore volumes	28 days 9 PVs	27 days 9 PVs*	82 days 27 pore volumes

0   52   80   107   189
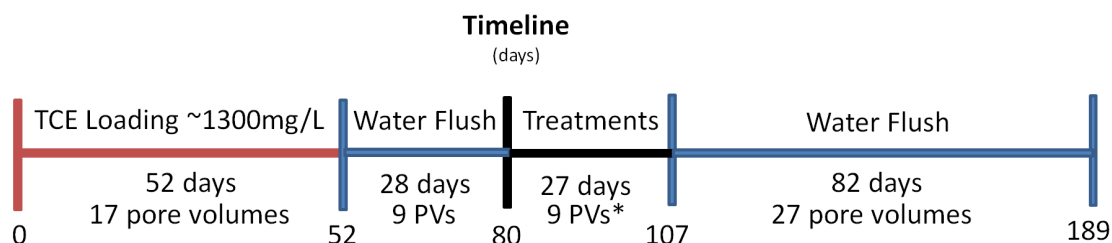
FIGURE 2.6. Experimental timeline of TCE loading, flushing and treatment periods (*enhanced flushing and xanthan gum treatments received 42 and 1.33 P.V.s, respectively) for the laboratory treatment studies.

2.4.3. TREATMENTS. The 27-day treatments were initiated on day 80. A summary of the treatments is listed in Table 2.2. The flow through the control tank remained unchanged at 0.33 m/day (transmissive) during the course of the treatment period, and no treatment chemicals were flushed through. The same de-gassed tap water used in the initial water flood was used throughout the rest of the experiment for this tank. The enhanced flushing

treatment was subjected to an increased flow-rate of approximately 5-times, at 1.56 m/day of the same de-gassed water as the control. The third tank received a solution of 2657 mg/L potassium permanganate (J.T. Baker, A.C.S. Reagent), dissolved in de-gassed water, and delivered at an unchanged flow-rate of 0.33 m/day. Since pore-space plugging from manganese dioxide (MnO_2) precipitates is usually of concern anytime permanganate is used as a treatment in soils, 2000 mg/L of sodium hexametaphosphate was added to the potassium permanganate solution as a dispersing agent to attempt to limit the formation of MnO_2 deposits.

The fourth tank received an anaerobic injection of KB-1 culture (approximate population of 5.0E10 dechlorinating cells/L) grown at SiREM labs (Guelph, Ontario) injected using a syringe pump (Chemvx Inc., model #Fusion 100) into the tank concurrently with a 2000 mg/L de-gassed aqueous solution of sodium lactate (Alfa Aesar, Stock #41529) at a 0.33 m/day flow-rate. A mineral and vitamin mixture supplied by SiREM Labs to aid the KB-1 inoculum was added to the injection aqueous solution as well. KB-1 consists of halorespiring bacteria, such as strains in the *Dehalococcoides*, *Geobacter* and *Methanomethylovorans* genus. The fifth tank received an anaerobic injection of KB-1 culture (approximate population of 5.0E10 dechlorinating cells/L) grown at SiREM labs (Guelph, Ontario) injected using a syringe pump (Chemvx Inc., model #Fusion 100) into the tank concurrently with a de-gassed aqueous solution of 1000 mg/L dissolved xanthan gum (Essential Depot, E415 USP FCC Food Grade) and 2000 mg/L sodium lactate (Alfa Aesar, Stock #41529) at a 0.33 m/day flow-rate. The aqueous lactate and xanthan gum solution was only injected for a 4 day period, corresponding to 1.33 transmissive P.V.s of flow. The tank was then sealed for the remaining 23 days of the treatment period. This scenario better represents field sites where the groundwater would flow around a zone injected with xanthan gum instead

of being forced through, as it would with this experimental setup. As with the previous KB-1 treatment, a minerals and vitamin mixture supplied by SiREM Labs was added to the influent aqueous solution.

The sixth tank received an anaerobic injection of Sulfate Reducing Bacteria (SRB) (*Desulfovibrio desulfuricans* American Type Culture Collection 13541) injected using a syringe pump (Chemvx Inc., model #Fusion 100) into the tank concurrently with a de-gassed aqueous solution of 2880 mg/L dissolved anhydrous magnesium sulfate (Fisher Scientific, M65-501 99.9%) and 5370 mg/L sodium lactate (Alfa Aesar, Stock #41529) at a 0.33 m/day flow-rate. The aqueous magnesium sulfate and lactate solution was injected for the duration of the 27-day treatment. The SRB was grown using a modified Baars medium for sulfate reducers (ATCC #1249), where ferrous chloride was used in lieu of ferrous ammonium sulfate. These treatments lasted a total of 27 days, upon which de-gassed tap water was again pumped through the tanks.

To quantify the long-term behavior of the effluent TCE concentrations, flushing of the tanks with clean water continued for a period of 82 days after the end of the treatments. The total sampling period lasted a total of 189 days after the start of the TCE flushing. Effluent samples from the 10-mL flow-through vials were taken daily during times of significant changes in effluent concentrations, such as at the start and end of the treatment period, but were taken less often during periods where effluent concentrations were more stable. ORP measurements were taken periodically throughout the experiment using a Ag-AgCl probe to determine the redox state of each tank.

2.4.4. ANALYTICAL METHODS. Concentrations of TCE and degradation products were determined by pipetting 2 mL out of the 10 mL effluent aqueous sample vial and using a 1:1 liquid:liquid extraction of Methyl-Tert-Butyl-Ether (MTBE) (OmniSolv, MX0826-6,

TABLE 2.2. Details of the treatments used in the laboratory treatment studies.

Tank Number	Treatment
1 - No-Action as a Control	Flush with de-gassed tap water at base transmissive zone seepage rate of 0.33 m/day
2 - Enhanced Flushing	Enhanced flushing with water at 5 times the base transmissive zone seepage rate to 1.56 m/day
3 - Potassium Permanganate	Flushing 2000 mg/L permanganate at the base seepage rate of 0.33 m/day, in conjunction with 2000 mg/L sodium hexametaphosphate to reduce tank plugging from the formation of MnO_2 minerals
4 - KB-1 and Lactate	Flushing a 2000 mg/L sodium lactate aqueous solution at the base seepage rate of 0.33 m/day with an initial inoculation of KB-1 culture
5 - KB-1, Lactate and Xanthan Gum	Delivery of 1.33 transmissive P.V.s of 2000 mg/L solution of sodium lactate and 1000 mg/L xanthan gum at the base seepage rate of 0.33 m/day with an initial inoculation of KB-1 followed by zeroing the flow through the tank for 23 days
6 - SRB, Lactate, Magnesium Sulfate	Flushing a 5370 mg/L sodium lactate and 2880 mg/L magnesium sulfate at the base seepage rate of 0.33 m/day with an inoculation of sulfate reducing bacteria

99.99%). Extraction samples were put on a vortex machine for 20 minutes (SMI Model #2600 Multi-Tube Vortexer). The MTBE portion of these extractions was analyzed for TCE and DCE using an ECD detector on an HP 5890 GC with a DB-624 column (J&W Scientific). An Agilent GCMS 5973 detector with a RTX-624SIL MS column was later used on the MTBE extracts to determine cis-DCE concentrations below ≈ 350 μg/L and to determine if VC was produced. TCE concentrations were determined by using 16-point calibration curves that ranged from known values of the chlorinated solvents in MTBE of 100 mg/L to 3 μg/L, while cis-DCE and VC concentrations used a 11 point calibration curve with values ranging from 50 mg/L to 48 μg/L.

The remaining 8 mL of the 10 mL effluent samples were analyzed for bromide and sulfate concentrations using a Metrohm Advanced Compact Ion Chromatograph 861 with an A Supp5 250 column, which used a 5 point calibration curve with bromide values ranging from 100 mg/L to 1 mg/L. The data from both of these analytical methods were stored and analyzed using *Microsoft Excel.*

Analysis of effluent sample ratios of ^{13}C to ^{12}C for the TCE and cis-DCE were done using Gas Chromatography-Combustion-Isotope Ratio MS (GC-C-IRMS) with a DB-624 column. At the conclusion of the experiment, biological analysis of soil sediments was conducted at SiREM labs with their method of Gene-Trac testing using Nano-drop Spectrophotometry tests to determine the population of the *Dehalococcoides* contained within the extracted soil cores.

2.5. Experimental Results and Discussion

This section presents the analytical results from each of the six tank studies including effluent TCE, cis-DCE and VC concentration data.

2.5.1. Control. The first tank considered is the control. Figure 2.7 shows the effluent concentrations of TCE and cis-DCE for the control over the 189 days. This plot reveals an asymmetrical effluent breakthrough curve. During the 52-day loading phase, effluent TCE concentrations approach the influent and then decrease sharply as the transmissive zones clear of the contaminant once the source was removed. The prolonged tailing observed is due to TCE diffusion out of the low k zones. This down-gradient behavior is common after contaminant removal or source isolation at heterogeneous sites with low k layers. Effluent bromide data was unremarkable, so the data is not shown on these plots. Cis-DCE was first detected at 43 μg/L (4.5E-7 mol/L) and rose to values over 4 mg/L near the end of the

experiment. Rising levels of cis-DCE is indicative of some form of natural attenuation in these field impacted soils. No VC was detected in the control tank throughout the experiment.

When the remaining 5 tanks began treatment at day 80, the control had an effluent TCE concentration of 78 mg/L (5.9E-4 mol/L), 1.18 orders of magnitude (OoM) lower than day 52 concentrations. At the end of treating the other tanks (day 107), effluent TCE concentrations had fallen to 37 mg/L (2.8E-4 mol/L), or 1.5 OoM below day 52 levels. At the end of the experiment (189 days), the effluent concentration of TCE had decreased 2.59 OoM from that of the TCE flood to 3.1 mg/L (2.3E-5 mol/L). This value is almost 3 OoM above the MCL (5 μg/L) and detection limits of available analytical methods. The effluent TCE signal shown in Figure 2.7 demonstrates the long periods of time required to deplete low k zones contaminated with TCE to acceptable levels. A mass balance analysis for this tank is shown in Figure 2.8, which demonstrates the total CVOC flux into and out of the control tank. This figure helps to partially validate the level of control that laboratory conditions provide when using these tanks to analyze the storage, release and treatment of chlorinated solvents under these conditions.

2.5.2. ENHANCED FLUSHING. Tank 2 was treated via enhanced flushing of de-gassed tap water only, simulating a transmissive zone depletion treatment strategy. Figure 2.9 shows the effluent concentrations of TCE (red) and cis-DCE (black) for this treatment. For reference, effluent TCE concentrations from the control tank are shown in blue on each plot.

The treatment window is shown by the cyan stripping beginning at day 80 and ending at day 107. During treatment, effluent TCE mass removal was 1635 mg, or 1.36 times that of the control over the same period. After treatment, effluent TCE concentrations remained slightly below the control tank for the remainder of the experiment. Effluent cis-DCE concentrations also increased as the experiment progressed, indicating some form of
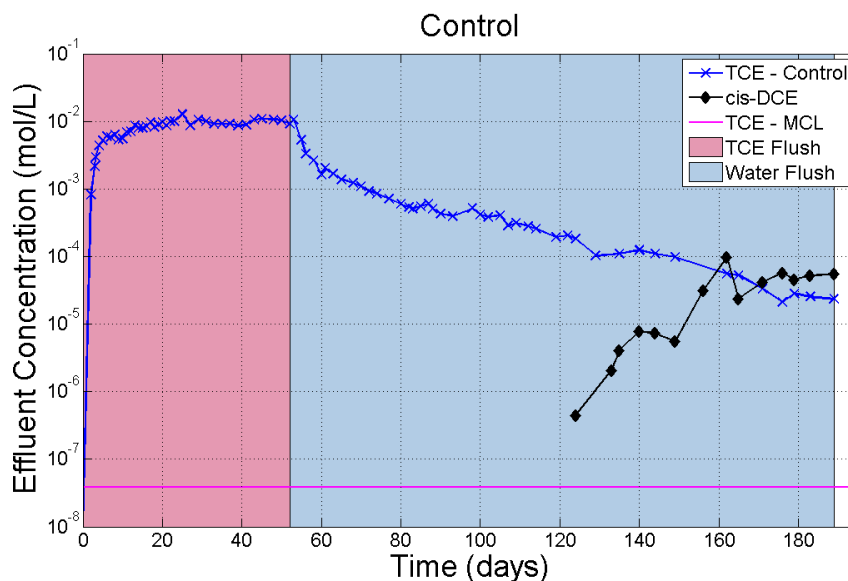
FIGURE 2.7. Control tank effluent TCE (blue) and cis-DCE (black) concentrations over the course of the 189-day experiment. The red shading denotes the TCE flushing period, while the light blue shading denotes flushing with clean water only. The elongated tailing of TCE concentrations after the TCE pulse source was removed is due to desorption, diffusion and slow-advection from the soils. At 189-days, effluent TCE levels are still almost 3 OoM above MCL. Increasing effluent cis-DCE indicates natural attenuative processes occurring.

natural attenuation in the tank. As with the control, VC was not detected throughout the 189 days. At the start of treatment (day 80), effluent TCE concentrations had fallen to 76 mg/L (5.8E-4 mol/L), or 1.17 OoM below day 52 levels. At the end of treatment (day 107), effluent TCE concentrations had fallen to 5.7 mg/L (4.9-5 mol/L), or 2.29 OoM below day 52 levels. At the end of the experiment, the effluent TCE concentration was 3.0 mg/L (2.3E-5 mol/L) or 2.58 OoM below day 52 concentrations. Overall, reductions in effluent TCE concentrations seen at the conclusion of the experiment are effectively equal to the control (3.0 vs. 3.1 mg/L, respectively). It is anticipated that enhanced flushing would be more effective if the water was driven perpendicular to the low k bedding instead of parallel. Further study is needed to determine the TCE depletion benefits with further flow increases and different soil architectures.
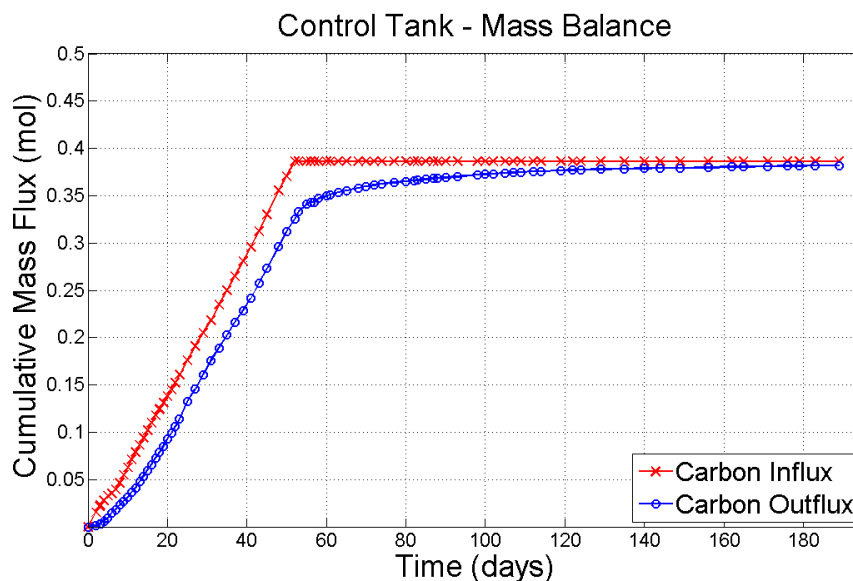
FIGURE 2.8. CVOC mass balance for the control tank demonstrating nearly complete recovery of injected carbon.

2.5.3. POTASSIUM PERMANGANATE. Figure 2.10 presents the concentrations of TCE (red) and cis-DCE (black) for the permanganate ISCO treatment overlain by the control tank TCE concentrations. The treatment window is again shown by the cyan window. Effluent TCE and cis-DCE levels dropped to non-detect shortly after treatment began and throughout, but the TCE rebounded to roughly an OoM less than the control tank after the permanganate treatment was stopped, and then had a lower slope than the control for the remainder of the experiment. At the start of treatment, effluent TCE concentrations had fallen to 107 mg/L (8.1E-4 mol/L), or 1.1 OoM below day 52 concentrations. At the end of treatment, effluent TCE concentrations had fallen below detection limits, but by day 122 had risen back to 5.4 mg/L (3.1E-5 mol/L), or 2.38 OoM below day 52 levels. No VC was detected throughout the 189 days. At the end of the experiment the effluent TCE concentration was 1.2 mg/L (9.0E-6 mol/L), 3.05 OoM below day 52 levels. Just as with the first two tanks, Figure 2.10 also shows increasing levels of cis-DCE after treatment and illuminates the possible presence of biological activity that remained within the untreated

36
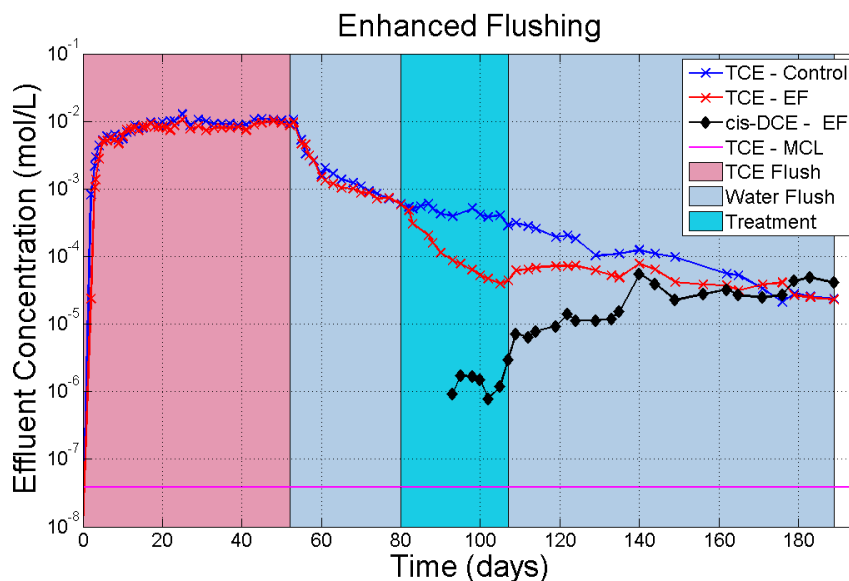
FIGURE 2.9. Enhanced flushing tank effluent TCE (red) and DCE (black) concentrations, with control TCE (blue). The red shading denotes the TCE flushing period, the light blue shading denotes flushing with clean water only, and the cyan shading denotes the treatment flushing window. This shading is typical of all remaining CVOC effluent breakthrough curve plots. A reduction in effluent TCE concentrations during treatment is observed, but continued reductions in effluent TCE relative to the control for the remainder of the experiment were not observed. Effluent cis-DCE is indicative of natural attenuative processes.

portions of the low k zones after the permanganate flood had finished. As with the enhanced water flood, improvements in effluent TCE concentrations for this ISCO treatment at the end of the experiment are modest when compared to the control, and represents a 62% reduction in effluent TCE (1.18 vs. 3.1 mg/L, respectively).

To help explain this rebound behavior of the TCE, Figure 2.11 presents a picture of a typical low k layer within the tank at the beginning and end of treatment. This figure illustrates incomplete penetration of the treatment (purple and brownish colors) into the low k zones. The contributing factors may include: not using a highly enough concentrated permanganate treatment solution, the low k soil oxidant demand consuming the permanganate,
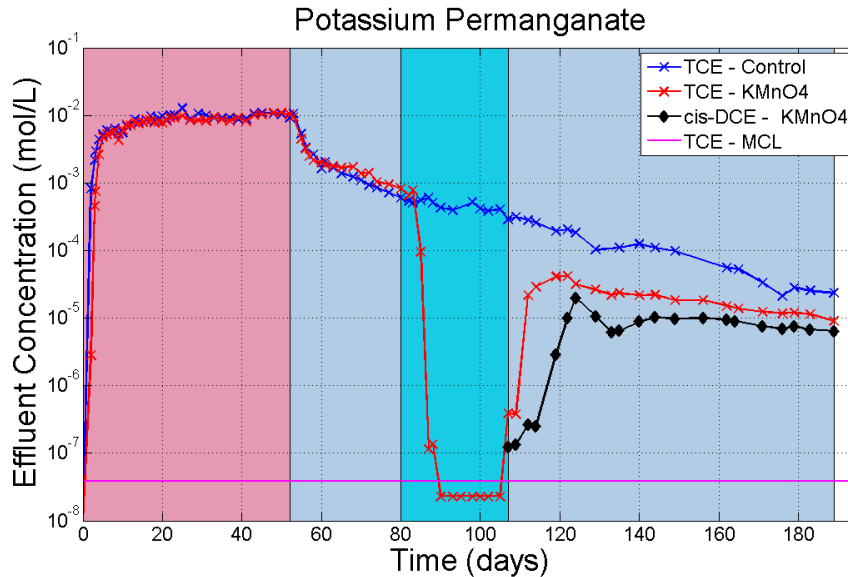
FIGURE 2.10. Permanganate tank effluent TCE (red) and cis-DCE (black) concentrations, with control TCE (blue). The drop in effluent TCE during the permanganate flushing is apparent, but the rebound afterwards indicates incomplete treatment of the soils. Effluent cis-DCE is indicative of natural attenuative processes.

or the insoluble MnO_2 mineral deposition causing plugging of the low k zones thereby decreasing the diffusion of the permanganate into these zones. Figure 2.12 shows the extent of the mineral deposits two weeks after treatment had finished. When using a permanganate injection, these deposits can significantly decrease the hydraulic conductivity of the soil and cause soil plugging (Schroth et al., 2001; Thomson et al., 2008), which has consequences for treatment delivery. The results from dissolving sodium hexametaphosphate into the permanganate solution to deter MnO_2 formation are unclear, as no comparison is available of MnO_2 mineral deposition in an identical tank setup without this dispersing agent. Overall, results provide a qualitative and quantitative demonstration of how soil oxidant demand and the precipitation of MnO_2 minerals can limit the benefits of permanganate ISCO treatments.

2.5.4. KB-1 CULTURE AND LACTATE. Figure 2.13 shows effluent concentrations of TCE, cis-DCE and VC for the KB-1 inoculum and lactate treatment. Figure 2.13 shows

38
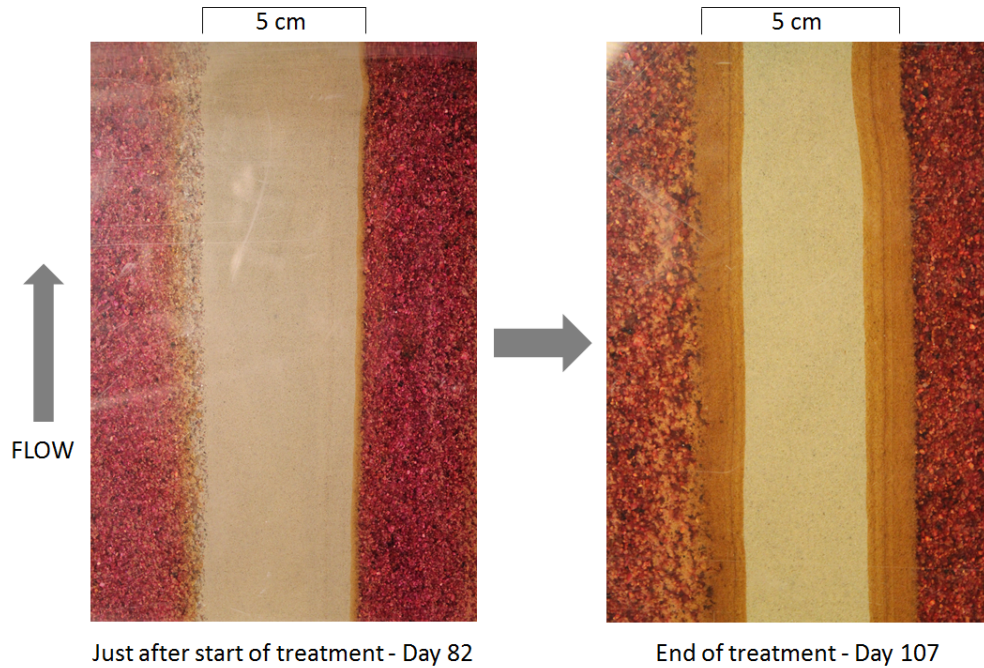
FIGURE 2.11. Permanganate migration into low k zones over the course of the 27-day treatment flushing period. Note the lack of complete migration of the treatment solution into the low k soils, which resulted in a post-treatment TCE rebound (see Figure 2.10).

FIGURE 2.12. Post-treatment MnO_2 deposits in the transmissive and low k soils in the permanganate treatment tank.

effluent TCE levels quickly dropping several OoM below the control during and after treatment. Starting at day 100, effluent TCE concentrations stayed below 100 μg/L for roughly a 56-day period. The rise in effluent TCE at the start of the lactate flood could be explained by a change in sorption equilibrium conditions within the tank. Effluent cis-DCE levels rose during and after the lactate treatment injection as well. Analysis showed relatively steady effluent levels of VC production during and after treatment. At the start of treatment, effluent TCE levels had fallen 1.13 OoM below day 52 levels to 104 mg/L (7.9E-4 mol/L). At the end of the lactate flush, effluent TCE levels had fallen to 30 μg/L (2.3E-7 mol/L), or 4.66 OoM below day 52 levels. The effluent levels of TCE eventually rebounded to within an OoM of the control near day 170. This rebound could be due to a lack of available lactate within the tank for meaningful dechlorination to continue. At the end of the experiment, the effluent TCE concentration was 1.0 mg/L (7.6E-6 mol/L), 3.15 OoM below day 52 levels. This concentration represents a 68% reduction in effluent TCE relative to the control (1.0 vs. 3.1 mg/L, respectively). However, total effluent CVOC levels from TCE, cis-DCE and VC casts doubt on the effectiveness of this treatment scenario.

The rebound of TCE near the end of the experiment suggests that the KB-1 did not populate into the low k zones and degrade the stored TCE. To test this idea, gene-trac testing was run at SiREM Labs on soil samples collected at the end of the experiment to determine if the *Dehalococcoides* are populating the transmissive zones, low k zones or the interface between the two. Table 2.3 shows the results of these tests on 3 soil samples for *Dehalococcoides*. These results agree with previous lab and field findings that, within this time-frame, the microbes prefer to populate high-low k interfaces as opposed to within the low k layers.
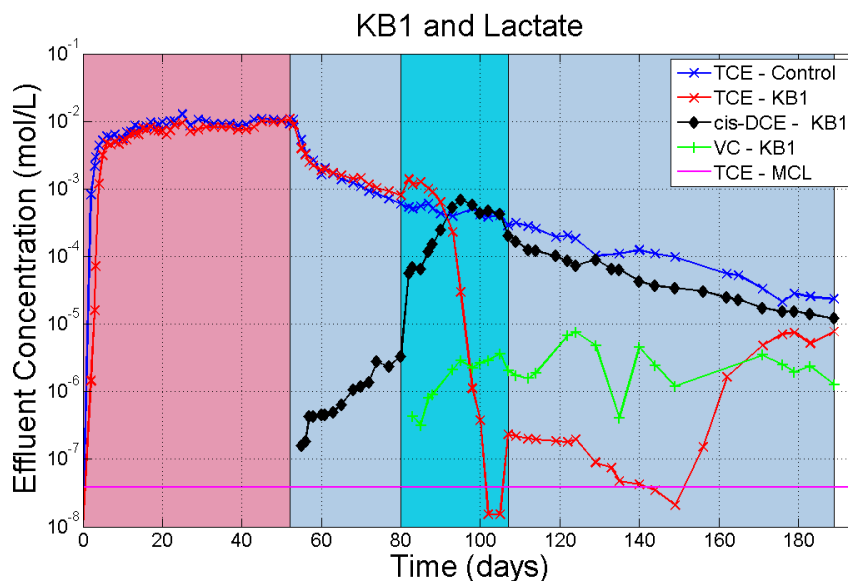
FIGURE 2.13. KB-1 and lactate tank effluent TCE (red), cis-DCE (black) and VC (green) with control TCE (blue). The drop in effluent TCE and rise in dechlorination by-products (e.g., cis-DCE) during treatment is apparent (cyan shading), indicating treatment. Late-stage rebound of TCE indicates metabolic constraints were imposed on the microbes, which resulted in a stalling of the treatment.

The shape of effluent concentration data in Figure 2.13 and the findings shown in Table 2.3 suggest that this treatment with the KB-1 inoculum mostly occurred at the interfaces between transmissive and low k zones and stalls once available electron donor has been exhausted, which has been observed and hypothesized previous (Scheutz et al., 2010; Chambon et al., 2010, Manoli et al., 2012). The issues resulting from treating contaminants in low k zones with a KB-1 inoculum can most likely be resolved by further injections of lactate until the KB-1 has mined enough contaminant from the low k zones to meet down-gradient concentration standards.

2.5.5. KB-1 CULTURE, LACTATE AND XANTHAN GUM. Figure 2.14 presents effluent concentrations of TCE, cis-DCE and VC for the KB-1, lactate and xanthan gum treatment. Following treatment, Figure 2.14 illustrates effluent TCE levels (red) had fallen 3.2 OoM below the control after the pump had been restarted. Effluent TCE stayed in this range

(≈5-100 ppb) for approximately the same period of time as the previous KB-1 treatment. As with the previous treatment, effluent cis-DCE levels in the tank increased approximately 3 OoM after the addition of KB-1 and tailed off as flushing continued. Although data points are limited, VC concentrations peaked after restarting the pumps and slowly decreased in concentration with time. At the start of treatment, effluent TCE levels had fallen to 112
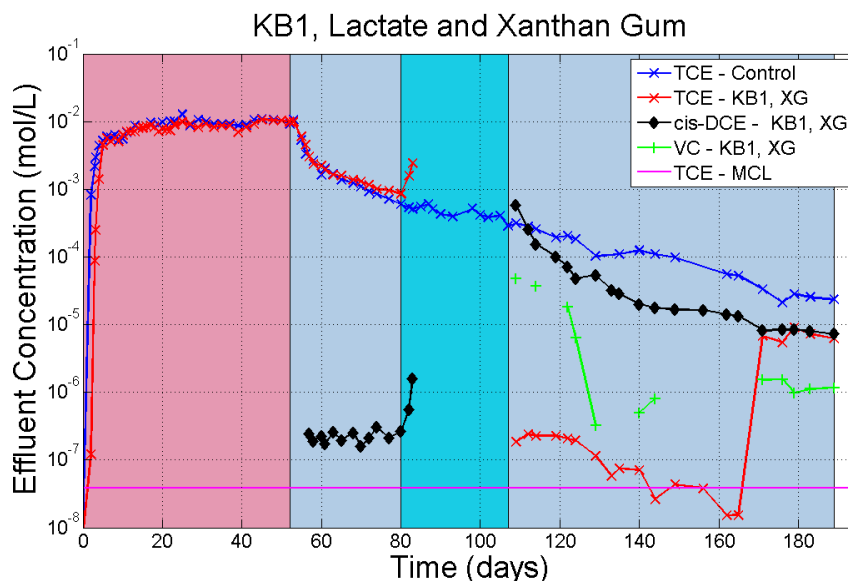
FIGURE 2.14. KB-1, lactate and xanthan gum tank effluent TCE (red), cis-DCE (black) and VC (green) with control TCE (blue). The lack of effluent data during the treatment window was due to shutting off the pump when 1.33 transmissive P.V.s of the treatment solution had passed through the tank. As with the previous KB-1 treatment, late-stage rebound of TCE indicates metabolic constraints were imposed on the microbes, resulting in a stalling of the treatment.

mg/L (8.5E-4 mol/L), or 1.06 OoM below day 52 levels. At day 109, effluent TCE levels fell to 24 μg/L (1.8E-7 mol/L), or 4.72 OoM below day 52 levels. As with the previous KB-1 treatment, effluent levels of TCE stayed below 100 μg/L (7.6E-7 mol/L) for a period of about 2 months, eventually reaching 4 μg/L at day 156, but then rebounded to within an OoM of the control around day 170, most likely for the same reasons as the previous KB-1 treatment. At the end of the experiment, the effluent TCE concentration was 0.82

TABLE 2.3. *Dehalococcoides* populations (enumerations/gram soil) within the KB-1 treatment tanks at day 189. '*' denotes an analytical estimate between the detection limit of method and quantification limit. The transmissive and low k soil samples were taken at the mid-points of the soil layers using a 1-cm wide brass tube, while the interface sample was taken from the interface zone between the two soils. The interface zones are shown in this case to have higher populations of *Dehalococcoides*.

Soil	Tank 4	Tank 5
Low k	4E3 *	2E3 *
Interface	3E4	1E4
Transmissive	3E2 *	2E3 *

mg/L (6.2E-6 mol/L), or 3.19 OoM below day 52 levels. This concentration represents a 73% reduction in effluent TCE relative to the control (0.82 vs. 3.1 mg/L, respectively). As with the previous KB-1 treatment, total effluent CVOC levels may cast doubt on the effectiveness of this treatment scenario.

Soil samples were taken from this tank as well to determine *Dehalococcoides* populations. Table 2.3 shows the populations of 3 soil samples tested for *Dehalococcoides*. As with the previous KB-1 treatment, Table 2.3 and the shape of effluent TCE in Figure 2.14 indicate that the population of *Dehalococcoides* is mostly located at the transmissive-low k interfaces. This finding can indicate that either the xanthan gum was not successful in forcing the treatment media into the low k zones, or that the KB-1 inoculum simply prefers to populate at soil interfaces.

2.5.6. SULFATE REDUCING BACTERIA, MAGNESIUM SULFATE AND LACTATE. The deposition of black minerals was observed during the last treatment of SRB, lactate and sulfate, as shown in Figure 2.15. By the end of the experiment, nearly all of the sediments in the tank were black. A plot of effluent sulfate over the course the experiment is shown in Figure 2.16 and demonstrates the growth and reduction of sulfate by the SRB over the 27-day treatment window (black lines).

FIGURE 2.15. SRB, lactate and sulfate treatment at day 10 of the 27-day treatment (influent treatment solution was clear). Image shows deposition of black mineral phase in the transmissive and low k soils.
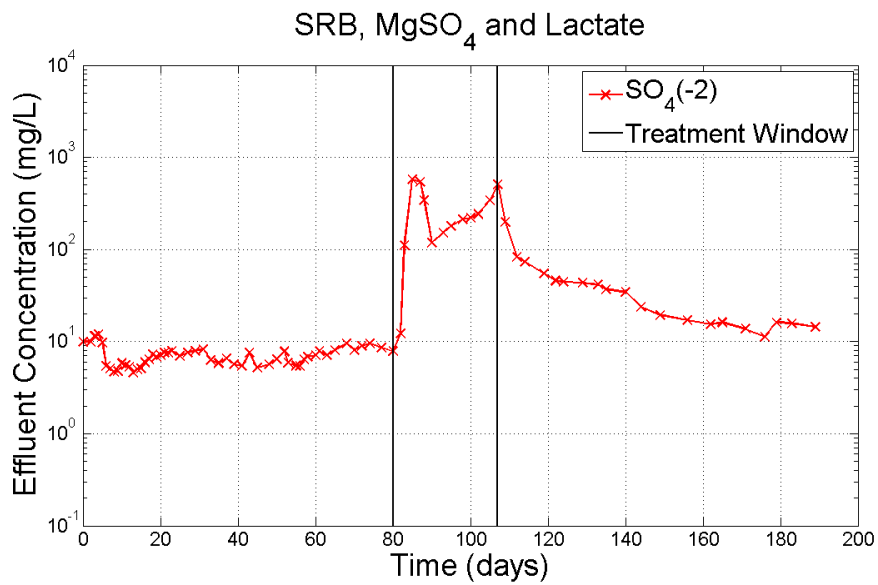
FIGURE 2.16. Effluent sulfate concentrations through time in the SRB, lactate and sulfate treatment tank.

Figure 2.17 shows effluent concentrations of TCE and cis-DCE for the SRB inoculum, lactate and magnesium sulfate treatment. At the start of treatment, effluent TCE levels fell to 141 mg/L (1.0E-3 mol/L), or 0.94 OoM below day 52 levels. At the end of the sulfate and lactate flood, effluent TCE levels fell to 25 mg/L (1.9E-4 mol/L), or 1.69 OoM below day 52 levels. Similar to the two KB-1 treatments, an increase in effluent TCE was observed
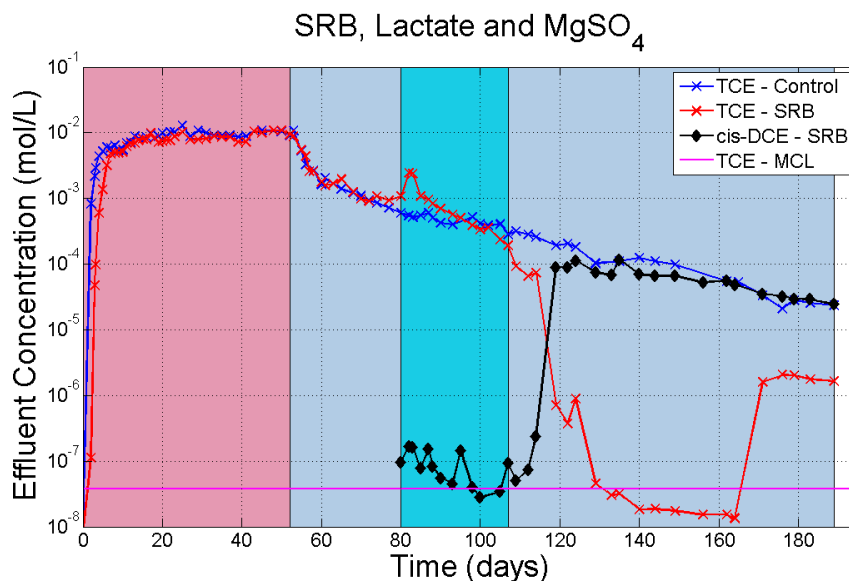
FIGURE 2.17. SRB, lactate and sulfate treatment tank effluent TCE (red) and cis-DCE (black) with control TCE (blue). During treatment no meaningful reduction in effluent TCE was observed, while post-treatment reductions in TCE and increases in cis-DCE indicate a primarily microbial treatment mechanism. This finding is reinforced by the late-stage rebound of TCE, which indicates similar metabolic constraints were imposed on the microbes to the KB-1 treatments, resulting in a stalling of the dechlorination.

immediately after the lactate flush began. As shown, the levels of TCE did not substantially decline during the course of the treatment itself, but dropped to below MCL around day 130. These effluent concentrations remained in this range (below 5 μg/L) until around day 170. As with the KB-1 treatments, effluent TCE levels eventually rebounded, with a final effluent TCE concentration of 0.21 mg/L (1.6E-6 mol/L) at day 189, which was 3.75 OoM below day 52 levels. This final concentration was 1.15 OoM below the control, making this method the most effective at reducing effluent TCE concentrations of the treatments used, but not for total CVOC flux. No effluent VC was detected over the course of the experiment.

Figure 2.17 shows that during the sulfate flushing, no meaningful dechlorination occurred. Possible explanations are that the sulfate was acting as the preferred electron acceptor in the tank, or the SRB out-competing the naturally occurring halorespiring bacteria (Hyun and

45

Hayes, 2009), or sulfide toxicity affecting the microbes. The combination of no meaningful dechlorination and the production of large concentrations of cis-DCE once the treatment was finished indicate a biological dechlorination mechanism. Since mineralogical treatments have been shown to degrade TCE through β-elimination to acetylene with little or no cis-DCE (Butler and Hayes, 1999; Butler and Hayes, 2001), this data suggests that the biological portion of the tank as the treatment mechanism was substantial, as effluent molar cis-DCE concentrations were in the same range as the effluent TCE from the control. Another line of evidence for the lack of mineralogical degradation is the pH of formation for these minerals. Effluent pH values measured between 6.9 and 7.2 during the treatment window, which has been shown to produce non-reactive iron-sulfide minerals (Hyun and Hayes, 2009). Consistent with the KB-1 biological treatments, a rebound in effluent TCE concentrations occurred around day 170 day of the experiment. This finding indicates that either the treatment was mostly biotic and lactate starvation is to blame for the rebound, and/or an unfavorable change in redox state occurred in tanks 4-6 around this time.

Soil samples were taken from this treatment to determine the locations (if any) of *Dehalococcoides*. Results showed no quantifiable *Dehalococcoides* population in any of the core samples. This could indicate either another bacteria is responsible for dechlorinating the TCE to cis-DCE or another treatment mechanism is present. These microbial results from this SRB treatment mirror those from the control tank, which also found no quantifiable population of *Dehalococcoides* present during the coring activities at the end of the experiment. To further investigate this line of evidence, ^{13}C isotope analysis was conducted on effluent TCE and cis-DCE samples from this treatment in order to determine if the appearance of cis-DCE was due to biological dechlorination, but results were inconclusive.

Table 2.4 summarizes some these results by listing the treatment strategy behind each tank, and the OoM reduction in effluent TCE concentrations relative to the end of the aqueous TCE flood (day 52 levels).

TABLE 2.4. Summary of quantitative results of treatments, strategy types and TCE OoM reductions at day 189 versus day 52 (end of aqueous TCE flushing).

Treatment	Treatment strategy	TCE day 189 (mg/L)	Day 52 to 189 OoM Reduction
1. Control	Source removal via barrier, excavation	3.07	2.59
2. Enhanced flushing	Transmissive zone depletion	3.01	2.58
3. Potassium permanganate	Low k depletion or containment	1.18	3.05
4. KB1 and lactate	Low k depletion	1.0	3.15
5. KB1, lactate and xanthan gum	Low k depletion or containment	0.82	3.19
6. SRB, lactate and sulfate	Low k depletion or containment	0.21	3.75

2.5.7. INTRA-TANK ORP COMPARISON. Using a Ag-AgCl probe, the recorded redox conditions from the tank effluents are shown in Figure 2.18. This Figure shows that the three biological treatments were under highly reducing conditions during the bulk of the treatment period, but became less reducing near the end of the experiment. This observation in the change in redox state for the three biological treatments helps explain the observed changes in treatment that these tanks experienced as their effluent TCE concentrations increased at this time in the experiment.

2.6. SUMMARY AND CONCLUSIONS

The laboratory experiments presented herein demonstrate governing processes and limitations of common field treatments. A 52-day aqueous TCE flood produced an asymmetrical effluent breakthrough curve that approached the solubility value of TCE in water, followed
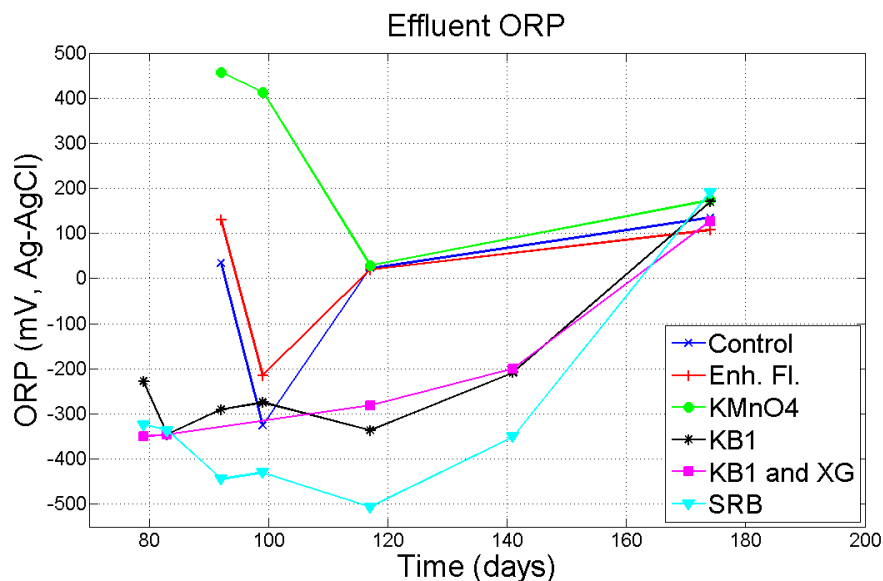
FIGURE 2.18. Effluent ORP measurements (Ag-AgCl electrode) of the six tanks. The rise in effluent ORP in the biological treatments near the end of the experiment agrees with previously shown CVOC breakthrough data that presents a stalling of treatment.

by a slowly falling TCE signal due to releases from the low k zones. Once the source was removed, 'tailing' behavior commonly seen in laboratory experiments and heterogeneous field sites was observed. 137 days after the source was removed, effluent TCE from the control tank was still 3.1 mg/L (2.3E-05 mol/L), which is still almost 3 orders of magnitude above drinking water standards. This tailing occurs in spite of the relatively short duration of the TCE loading phase when compared to the prolonged DNAPL releases at field sites.

Effluent TCE concentrations for the enhanced flushing treatment fell relative to the control during the treatment window, but stabilized to nearly the same levels as the control tank afterwards for the remainder of the experiment. This type of treatment has been extensively used in the field as a form of pump and treat systems, and there are numerous ways to modify this treatment from the way that this particular laboratory flush was done. These modifications include a much larger increase in the flow-rate, changing the architecture of the low k zones, or by using chemical enhancements to increase the rate at which TCE is

mined from the low k zones. Under these specific flushing conditions and soil architecture, results from an enhanced flushing of water indicate no discernible long-term advantage in reducing effluent CVOCs.

The potassium permanganate treatment produced an effluent with non-detect TCE and cis-DCE levels during treatment. Oxidant demand and the precipitation of MnO_2 appears to have caused limited penetration of the permanganate treatment into the low k zones, resulting in an observed TCE rebound to within an OoM of the control. Because of this lack of permanganate penetration, effluent TCE and cis-DCE levels rebounded and remained within an OoM of the control after treatment. These observations suggest that sites with large oxidant demands and/or large numbers of low k lenses might not be good candidates for this ISCO treatment, which is consistent with conclusions drawn from previous lab and field studies.

The two KB-1 biological treatments demonstrate that large reductions in effluent TCE levels can be achieved. However, within systems of short retention times, corresponding increases in effluent cis-DCE and VC concentrations can be expected. Results from the two KB-1 treatments demonstrate an effluent TCE rebound near the end of the experiment corresponding to an increase in ORP, and that *Dehalococcoides* prefer to inhabit the interfaces between high and low k soil zones. Coring samples showed that the distribution of the KB-1 within the tank had a quantifiable *Dehalococcoides* population at the transmissive/low k interface, compared to the center of the soil layers where populations were below the quantification limits of the method. Given a longer experimental time-frame and sufficient electron donor, these populations might have eventually migrated far enough into the low k zones to enhance the treatment, and further study on this matter is needed. These observations

49

indicate two treatment processes: 1) that continued treatment relies heavily on the avail-ability of an electron donor, and 2) the microbes preferentially dechlorinate contaminants as they diffuse out of the low k layers. These results suggest that this treatment could continue indefinitely as long as the microbes are continually provided with an electron donor. Results indicate little to no advantage to using a 1000 mg/L solution of xanthan gum to increase the sweep efficiency of a KB-1 inoculum. The advantage of using xanthan gum to cause a 'plug' or zone of minimal water circulation for treatment is still an option and should be explored further.

The last treatment of SRB, lactate and magnesium sulfate produced some interesting results. Effluent TCE levels remained approximately unchanged compared to the control during the treatment. However, upon removal of the influent sulfate, TCE levels dropped quickly to method detection limits around day 156. This suggests that the sulfate was acting as the preferred electron acceptor, thereby inhibiting TCE dechlorination. As with the two previous microbial and lactate treatments, effluent TCE concentrations rebounded around day 170. This result suggests that the majority of the treatment was occurring biologically and not mineralogically (or some combination thereof), as the timing of the rebound behavior coincides with the rebounds of the KB-1 treatments. The presence of cis-DCE is furthermore indicative of a biological treatment pathway, as mineralogical treatments tend to degrade TCE through chloro-acetylene to acetylene. PCR analysis on soil samples from this tank after the experiments finished showed no quantifiable *Dehalococcoides* sp. in either of the soil layers or at the soil interface. This result indicates that if the treatment was mostly biological, the dechlorination would have been done by a microbe other than *Dehalococcoides*, such as *Dehalobacter*, which is known to dechlorinate TCE to cis-DCE. These findings to indicate a

biological treatment mechanism is supported by the work of Hyun and Hayes (2009), which showed that mackinawite formed below pH=8 is effectively non-reactive with TCE.

Overall, the results of this study are illuminating with respect to achieving MCLs in drinking water. Results demonstrate that common treatments can have limited benefits with respect to depleting contaminants in low k zones to the levels needed for achieving MCLs in transmissive zones. This finding suggests a need for rethinking the strategies involved in managing contaminants in low k zones. Results furthermore point to a need to manage expectations of treatment outcomes at heterogeneous sites, as the time-frame of care could be significant, on the order of decades or even centuries. Since the implications of this study at field-scales are not clear, the next Chapter of this research will involve the use of the reactive-transport code *MIN3P* to model these systems at both the laboratory and field scale.

CHAPTER 3

UPSCALING LABORATORY TANK STUDIES USING MIN3P: TREATMENT STUDIES AND FIELD SCENARIOS

3.1. CHAPTER SYNOPSIS

Results from the tank studies from Chapter 2 provided an opportunity to develop and test conceptual models addressing the treatment of contaminants in low k zones. These models provided evidence to confirm or deny the validity of insights gained on treatment mechanisms from the laboratory treatments. The reactive-transport code *MIN3P* provided a convenient opportunity to advance numerical models using laboratory-scale data.

Laboratory conceptual models for the six laboratory studies were developed and implemented. Laboratory-scale modeling results from the control tank indicate that *MIN3P* is capable of simulating the transport and natural attenuative processes involved in the spatial evolution of TCE throughout the 189 day experiment. Modeling the five active treatments demonstrate that *MIN3P* accommodates for the complexities necessary to model processes such as intra-aqueous reaction (e.g., permanganate ISCO), mineral-phase dissolution, biological growth, and biological decay. Findings from this laboratory-scale modeling study indicate that our understanding of the interaction of an oxidative treatment, such as permanganate, is mostly complete and can be satisfactorily modeled at this scale. Results from the study also indicate that the use of *MIN3P* to model microbial growth, decay and intra-aqueous dechlorination is viable given the incorporation of Monod kinetics and inhibition terms.

The laboratory-scale conceptual models were applied to two field-scale scenarios using the laboratory derived biogeochemical input parameters. This up-scaling of the models was

done to gain insights concerning treatment outcomes at larger domains. Field-scale modeling studies demonstrated the relative performances of each of the treatments under two different aquifer scenarios. Results suggest that up-scaling laboratory models is warranted to better understand the implications of larger domains, larger time frames, more realistic geologic architectures, and the implications of non-uniform contact of treatment media with zones of contamination. Up-scaled results indicate persistent exceedance of down-gradient Maximum Contaminant Levels (MCLs) in groundwater for hundreds of years after application of remedial measures. Although geometrically and chemically simplified, results from the field-scenarios indicate that the treatments considered would be relatively ineffective at sites with large low k bodies (such as an aquitard), but may be more effective at treating sites where contaminants are limited to thin interbeds of low k media. A limitation of this work is that short-term lab studies may be missing long-term attenuation processes that could reduce the overall period in which MCLs are exceeded, which may be significant at field-scales and large time-frames.

3.2. Introduction and Background

Understanding and anticipating the behavior of contaminants stored in low k zones are possibly the most important concepts for managing remediation efforts of chlorinated solvents at field sites (Sale et al., 2014). The six laboratory treatments presented in Chapter 2 provide fundamental insights regarding processes controlling different treatments of contaminants in low k zones. These treatments were a: 1) no-action control, 2) enhanced water flushing, 3) potassium permanganate flush, 4) KB-1 microbial inoculum with lactate, 5) KB-1 with lactate and xanthan gum injection, and 6) sulfate-reducing bacteria (SRB) inoculum with lactate and magnesium sulfate.

Developing and evaluating conceptual laboratory-scale models using the reactive-transport code *MIN3P* (Mayer et al., 2002) provides a tool to further analyze and investigate the findings from Chapter 2. Within this investigation, the models can also highlight discrepancies between the conceptual framework of the model and observed data, which may help illuminate unforeseen biogeochemical processes. This modeling effort is divided into two parts. First, using the 2-D soil architecture and laboratory derived parameters, in conjunction with the chemical/biological treatments described in Chapter 2, *MIN3P* is used to develop conceptual models for each of the six laboratory treatments. These laboratory-scale conceptual models then provide a basis for the second part of this modeling effort, which involves up-scaling the laboratory models to field-scales.

The second portion of this modeling effort explores the idea of using the *MIN3P* models to determine the efficacy of the six treatments given two field scenarios. The field scenarios can be summarized as: 1) five TCE DNAPL pools dissolving into a high and low k zone field-scale architecture for 30 years, followed by 2) treatments applied to the aquifer system. The field-scale architecture is composed of discontinuous low k bedding layered in a continuous transmissive zone. The two field-scale soil architectures are distinguished by the presence and absence of an aquitard.

Previously published modeling studies done using *MIN3P* include Mayer et al. (2001a), Mayer et al. (2001b), Mayer et al. (2002) and Henderson et al. (2009). In relation to this modeling effort, no current publications explore the use of *MIN3P* to scale laboratory treatment data to field scenarios. The lack of equivalent modeling studies illuminates a niche that deserves further consideration. Overall, the objective of this work is to investigate the hypothesis that up-scaling laboratory reactive-transport treatment models to the field-scale

can help determine relative treatment outcomes. Benefits of this insight include potential cost-savings through the design of more efficient treatment and delivery systems.

First, this Chapter presents a brief introduction to *MIN3P*. Second, conceptual models for the six treatments are advanced. Third, results from the laboratory and the two field-scale modeling efforts are presented. Lastly, the conclusions drawn from these modeling efforts are discussed.

3.3. Background and Literature on *MIN3P*

This section will provide a brief overview of the *MIN3P* code, as well as previously published modeling and field data that uses the code.

3.3.1. MIN3P Background. *MIN3P* is a reactive-transport model developed by Dr. Uli Mayer as part of his Ph.D. research at the University of Waterloo (1999). Mayer et al. (2002) describes each part of the theory and mathematical formulation of this code in detail. The code was created to investigate reactive transport in both saturated and unsaturated porous media under partial equilibrium systems. *MIN3P* supports advective-dispersive aqueous transport and diffusive gas transport in one, two or three spatial dimensions.

Using the global implicit solution approach (Steefel and Lasaga, 1994), *MIN3P* calculates the interactions of reaction and transport processes by enforcing a mass balance between solid, surface, dissolved and gas phase species. The program considers both homogeneous and heterogeneous aqueous-phase reactions such as complexation, oxidation-reduction, ion exchange, surface complexation, mineral dissolution-precipitation and gas exchange. The model accounts for variable saturation and multiple components for transport, deposition and reaction. In addition to geochemical reactions, the code is also capable of simulating microbial growth and decay. *MIN3P* utilizes Monod and inhibition terms to account for

changes in the geochemical state of the tank, such as the availability of nutrients or from chemical toxicity. Key points in the implementation of *MIN3P* are that the code uses: 1) Newton's method to iteratively solve the nonlinear reactive transport equations, 2) the block-centered finite difference method for spatial discretization (Patankar, 1980), 3) fully implicit time weighting for temporal discretization of the governing equations, 4) reactions, rates and model inputs contained in external input files, 5) dissolution-precipitation reactions are considered kinetically controlled, while all other reactions are considered to be at equilibrium, and 6) WATSOLV to solve the systems of matrices, which is a sparse iterative solver package (VanderKwaak et al., 1997).

MIN3P inputs, including reaction and rate parameters, reaction networks and the user input's for soil parameters, geometry, dispersivities, chemical species etc. are read from a user defined text file. When provided with all of the hydrogeologic, transport and chemical parameters of the tank system, the code outputs data that describes the solute concentrations, redox conditions, mineralogical, pH, pe, chemical fluxes, and many other parameters at any spatial point and time. Furthermore, *MIN3P* gives the user the ability to define the reaction pathways. This allows *MIN3P* to be applied to each of the six treatments considered in the previous chapter, and is especially relevant in the case of the SRB, lactate and sulfate treatment, where multiple minerals and microbes were present and the reaction pathways are not perfectly clear.

3.3.2. PUBLISHED LITERATURE. Besides providing the mathematical details imbedded within *MIN3P*, Mayer et al. (2002) discusses two hypothetical scenarios to test the code under complex field conditions. The first is a Light Non-aqueous Phase Liquid (LNAPL) spill that results in the system shown in Figure 3.1. This figure shows LNAPL hydrocarbon

at 1% volume fraction in the unsaturated zone extending over a length of 10 m, and a zone of 10% hydrocarbon volume fraction spread over 20 m at the water table.
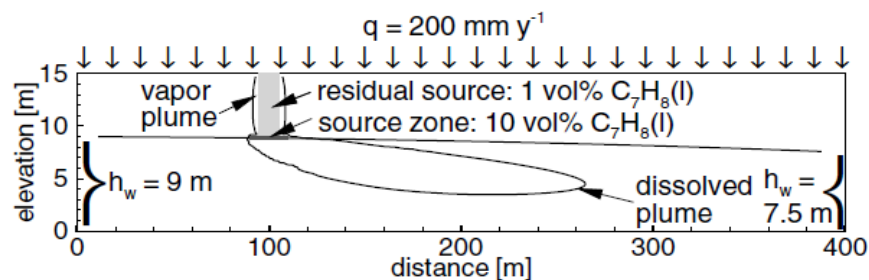
FIGURE 3.1. Hydrocarbon spill situation for scenario 1 from Mayer et al. (2002).

The focus of this scenario was to illustrate the ability of the code to model the degradation of contaminants by aerobic and anaerobic processes via reductive dissolution of iron oxides and methanogenesis. Using a 300 year simulation, their results mimicked the behavior of these types of plumes at field sites, and resulted in some interesting observations during attenuation. Namely, that for the simulation to match observed field sites with limited downgradient methane concentrations, secondary redox reactions within the model had to be considered (oxidation of methane by dissolved oxygen, ferric hydroxides and dissolved ferric iron), and that aerobic degradation is limited to the source area and upgradient fringe zones due to the consumption of oxygen by the re-oxidation of reduced reaction products.

The second scenario in Mayer et al. (2002) was a simulation of sulfide mineral oxidation and reactive transport in a 1-D profile against collected field data at a tailings impoundment. The results demonstrated that the code could replicate field-observed concentration data for most of the quantified components (Mg, Ca, Na, K, Ni, Cu, Si, Al, SO_4, Fe(III)), as well as the system pH with depth.

Other modeling studies done with *MIN3P* include the work of Mayer et al. (2001a), which simulated natural attenuation of a plume of phenolic compounds (phenols, cresols and

xylenols) in West Midlands, UK, by using microbial biodegradation with different electron acceptors. Mayer et al. (2001b) studied the effects of a zero-valent iron barrier on a Cr(VI) plume with chlorinated solvents, and found some interesting interactions happening in the barrier itself. For instance, they found that secondary mineral formation can decrease the barrier porosity over long periods of time, which corresponds to currently observed barrier data.

Most recently, Henderson et al. (2009) demonstrated the impressive capabilities of this code during a field treatment of permanganate injection of a sandy aquifer contaminated with TCE. The code was able to closely reproduce the observed concentrations of the permanganate, dissolved TCE and the Cl- from a cross section of 11 multilevel wells (121 total points), 5 m on each side of the permanganate injection. This data is shown in Figures 3.2a and 3.2b. The code was also able to reproduce other chemical parameters from two observation wells (such as pH, K^+, Mg^{2+}, Ca^{2+}), as well as a rebound in TCE in one of these wells.
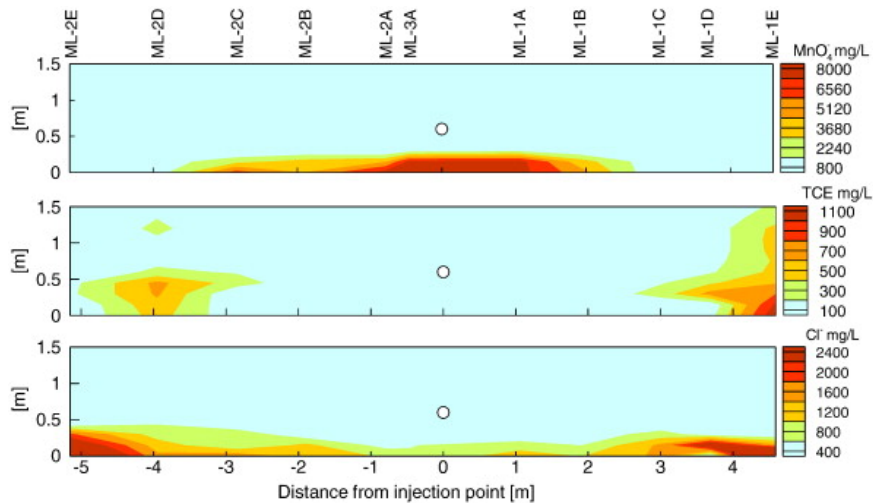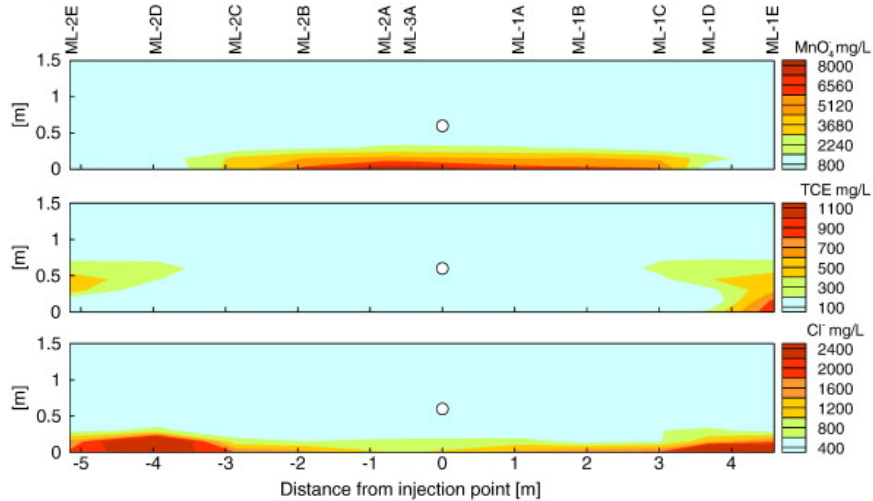
FIGURE 3.2. a) Observed and b) simulated MnO_4^{-2}, TCE and Cl- at day 55 after permanganate injection, from Henderson et al. (2009).

There are other publications that used MIN3P to model field sites and scenarios with similarly successful outcomes, but it would be repetitive to discuss them here. In relation to the this portion of the research, no publications were discovered that deal with using MIN3P to scale laboratory data to field scenarios. This illuminates a niche that deserves further consideration.

The two field scenarios in this paper are based on the transmissive/low k zone architecture in Parker et al. (2008). Parker et al. (2008) is a study in the storage and release of TCE from low k zones embedded in a continuous transmissive zone. Parker et al. (2008) was one of the first publishings to show through a field and modeling study that the storage and releases from low k zones can cause down-gradient concentrations to remain above MCLs for centuries. An important finding of this paper is that unless a high level of care is taken during coring activities, thin layers of low k bedding can hide contaminants which may mislead investigators during site-characterization activities about the scope of the problem they are facing.

3.4. Laboratory-Scale Model Setup

The following describes the methods used to setup the models that address processes controlling transport and treatment of contaminants in the six laboratory tank studies from the Chapter 2.

3.4.1. Laboratory-Scale Model Setup. The simulation domain for the laboratory models were setup to match the architecture of the transmissive and low k zones provided by the laboratory studies (Part 1). Figure 3.3 presents the dimensions of the laboratory with the selected geologic architectures. The timeline for the aqueous flushing and treatments are identical to the schemes used in Chapter 2. The domain for each tank had a total of 18540 nodes (X - 180, Y - 1, Z - 103). The silts and sands were given a horizontal nodal distance of 0.0024-m and 0.0047-m, respectively. Within the transmissive layers, a 2-mm thick zone at the soil interfaces had 0.0005-m horizontal discretization. Vertical nodal distances in the soil were set to 1-cm. Testing showed that increases in vertical discretization did not noticeably affect results. The maximum residual error tolerance was set to 1.0e-10 through

100 allowable solver iterations, with a maximum allowable time-step of 0.5 days. Table 3.1 provides important physical model input parameters. Each of these input parameters was experimentally derived, with the exception of the free-phase diffusion coefficient and the DCE distribution coefficient. The free-phase diffusion coefficient was averaged from published studies (Merck, 2013; Henderson et al., 2009; Hunt et al., 1988), and the DCE distribution coefficient is estimated from Kassenga et al. (2003).
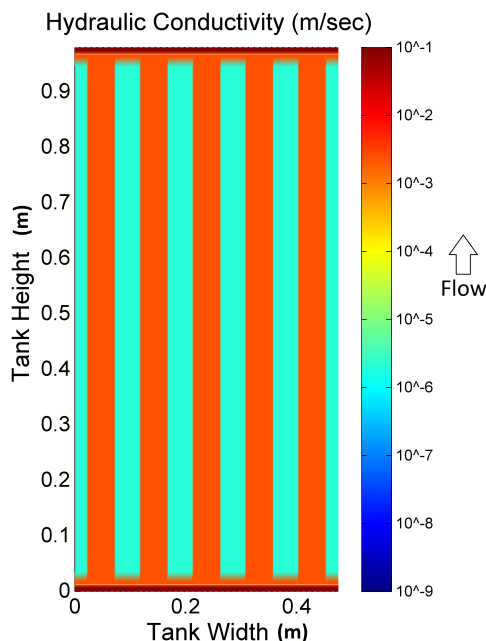
FIGURE 3.3. Model domain and hydraulic conductivities of the laboratory-scale model. Orange and cyan colors indicate transmissive and low k zones, respectively.

The top and bottom cross-sections were designated as flux boundaries, which remained constant in the control, permanganate, KB-1 & lactate, and the SRB, lactate and sulfate treatments. The enhanced flushing and KB-1 with lactate and xanthan gum treatments required a transient influent (lower) boundary condition during the treatment window. Since the experimental tanks had a 1-cm tall inflow and outflow plenum, this feature was incorporated into the model (i.e., porosity = 1, no retardation in this zone). Sorption of VC

61

TABLE 3.1. Model input soil and chemical parameters taken from the laboratory studies.

Component	Value	Units
Doman width	0.475	m
Doman height	0.98	m
Doman depth	0.0254	m
Sand hydraulic conductivity	2.3E-3	m/sec
Silt hydraulic conductivity	2.0E-6	m/sec
Sand porosity	0.39	V/V_{bulk}
Silt porosity	0.49	V/V_{bulk}
Sand longitudinal, transverse dispersivity	0.001^a, 0.0	m
Silt longitudinal, transverse dispersivity	0.0, 0.0	m
Sand distribution coeff., K_d	0.0	mL/gm
Silt TCE distribution coeff., K_d	0.7	mL/gm
Silt DCE distribution coeff., K_d	0.75^b	mL/gm
Averaged free-phase diffusion coeff.[c]	$5.0E-10^d$	m^2/sec
TCE flushing solution (day 0-52)	9.89E-03	mol/L

[a]Fitting parameter, estimated.

[b]Estimated

[c]Applied to all dissolved species.

[d]Calibrated from 8.0E-10 m^2/sec for TCE provided by Merck (2013), 6.4E-10 m^2/sec from Henderson et al. (2009), 2.7E-10 m^2/sec from Hunt et al. (1988)

was not accounted for due to previous studies showing relatively negligible VC distribution coefficients (Kassenga et al., 2003). Depending on the chemical complexity of each system, the time to run the model for each of these individual treatments ranged from one-half to six hours on an *Intel(R)* Core i5 2.8 GHz CPU with 4 GB of RAM. Table 3.2 provides the initial concentrations of the aqueous and biological species. Lastly, Table 3.3 provides the aqueous treatment concentrations used in modeling the treatments.

3.4.2. REACTION NETWORKS. Equation 4 demonstrates how intra-aqueous kinetic reactions are carried out in the model (modified from Lichtner (1996b); Lasaga (1998)). This equation contains the Monod and inhibition terms that allow the modeling of chemically

TABLE 3.2. Model domain initial biogeochemical conditions. Cl^- and CO_3^{-2} components were measured parameters from the influent water. The initial biomass component population was estimated. The Bio-block component is used as a part of these conceptual models to partially inhibit microbial growth in the low k soils.

Component	Initial Concentration	Units
TCE	1E-10	mol/L
cis-DCE	1E-7	mol/L
VC	1E-10	mol/L
lactate	1E-10	mol/L
MnO_4^-	1E-10	mol/L
$MnO_{2(aq)}$	1E-10	mol/L
K^+	1E-10	mol/L
Cl^-	8.46E-5	mol/L
CO_3^{-2}	3.8E-04	mol/L
pH	7.0	pH
Biomass	1E3	cells/L
Bio-block[a]	1E-10 (sand), 1E-2 (silt)	mol/L
f_{oc}	1E-10 (sand), 4.03E-3 (silt)	V/V_{bulk}
$MnO_{2(am)}$	1E-10	V/V_{bulk}

[a]Parameter to limit biomass growth.

TABLE 3.3. Flushing treatment concentrations in the permanganate, KB-1 and SRB models (treatments 3-6) during days 80-107. Values taken from the laboratory treatment studies.

Treatment Number	Component	Treatment Concentration (mol/L)
3	MnO_4^-	1.68E-2
4, 5	lactate	1.78E-2
6	lactate	4.79E-2
6	SO_4^{-2}	2.39E-2

complex treatment scenarios:

$$(4) \qquad R_k^a = -k_k^a \left[\prod_{j=1}^{N_c} \left(T_j^a\right)^{\sigma_{kj}^{at}} \prod_{j=1}^{N_c} \frac{T_j^a}{K_{kj}^{a,Mo} + T_j^a} \prod_{j=1}^{N_c} \frac{K_{kj}^{a,In}}{K_{kj}^{a,In} + T_j^a} \right] \left[1 - \frac{IAP_k^a}{K_k^a} \right]$$

where R_k^a is the reaction rate (mol/(L bulk·sec)), k_k^a is the rate constant of the reaction (mol/(L H_2O·sec)), T_j^a are the total aqueous component concentrations (mol/(L H_2O)), σ_{kj}^{at} is the reaction order, $K_{kj}^{a,Mo}$ is the half saturation constant and $K_{kj}^{a,in}$ is the constant of

inhibition for component A_j^c, IAP_k^a is the ion-activity product, and K_k^a is the equilibrium

constant. These reaction networks use 11 aqueous components (TCE, DCE, VC, MnO_4,

$MnO_{2(aq)}$, K^+, lactate, Cl^{-1}, H^+, CO_3^{-2}, pH) 2 immobile mineral phases (MnO_2, f_{oc}) and

2 immobile biomass phases (biomass (BM), Bio-block (BB)). The reaction networks, rate

expressions and rate constants used in modeling the treatments are presented in Tables 3.4

and 3.5.

TABLE 3.4. Reactions used in modeling the six treatments. The reaction number is used to identify the reaction networks used in Table 3.5. The treatment numbers correspond to the models that use those particular reactions. Similarities in these reactions are distinguished in Table 3.5.

Reaction Number	Treatment Number	Reaction
1	1, 2, 3	$C_2HCl_{3(aq)} + H_2 \rightarrow C_2H_2Cl_{2(aq)} + HCl$
2	1, 2, 3	$Biomass_{growth}$
3	1, 2, 3	$Biomass_{decay}$
4	3	$C_2HCl_{3(aq)} + 2KMnO_4 + 2H_2O \rightarrow 2MnO_{2(aq)} + 3Cl^- + 2CO_3^{-2} + 5H^+ + 2K^+$
5	3	$3C_2H_2Cl_{2(aq)} + 8KMnO_4 + 2H_2O \rightarrow 8MnO_{2(aq)} + 6Cl^- + 6CO_3^{-2} + 10H^+ + 8K^+$
6	3	$3CH_2O + 4KMnO_4 \rightarrow 4MnO_{2(aq)} + 3CO_3^{-2} + 2H^+ + 2H_2O + 4K^+$
7	4, 5	$C_2HCl_{3(aq)} + H_2 \rightarrow C_2H_2Cl_{2(aq)} + HCl$
8	4, 5	$C_2H_2Cl_{2(aq)} + H_2 \rightarrow C_2H_3Cl_{(aq)} + HCl$
9	6	$C_2HCl_{3(aq)} + H_2 \rightarrow C_2H_2Cl_{2(aq)} + HCl$
10	4, 5, 6	$Biomass_{growth}$
11	4, 5, 6	$Biomass_{decay}$

In the laboratory-scale models, reactions used in modeling the control, enhanced flushing

and permanganate treatments include biomass growth and decay, with dechlorination of

TCE as a second-order function of the biomass population and TCE concentration. This

is shown in Tables 3.4 and 3.5 as reactions (1), (2) and (3). The dechlorinating biomass

growth rate was calibrated to achieve a 1.0E7 cells/L population at day 189, which is a typical

dechlorinating biomass population. Literature growth and dechlorination rates were not used

TABLE 3.5. Model kinetic reaction networks and rate constants for the six laboratory models. The reaction number corresponds to the reaction(s) shown in Table 3.4. 'BB' and 'Lac.' refer to the Bio-block and lactate components, respectively.

Reaction Number	Rate Expression	Rate Constant
1	$R_{red-TCE} = -k_{red-TCE}[\text{BM}]$	1.0E-17
2	$R_{growth} = -k_{growth}[\text{BM}][\text{TCE}]$	1.4E-3
3	$R_{decay} = -k_{decay}[\text{BM}]$	1.0E-5
4	$R_{TCE-MnO_4} = -k_{TCE-MnO_4}[\text{TCE}][\text{MnO}_4]\left[\frac{[\text{TCE}]}{\text{K}_{\text{Mo}}^{\text{ox}-\text{TCE}}+[\text{TCE}]}\right]$	0.7 [a]
5	$R_{DCE-MnO_4} = -k_{DCE-MnO_4}[\text{DCE}][\text{MnO}_4]\left[\frac{[\text{DCE}]}{\text{K}_{\text{Mo}}^{\text{ox}-\text{DCE}}+[\text{DCE}]}\right]$	1.5 [b]
6	$R_{ox-CH_2O} = -k_{ox-CH_2O}[\text{MnO}_4^-]\left(\frac{\psi_{\text{CH}_2\text{O}}}{\psi_{\text{CH}_2\text{O}}^{\text{o}}}\right)^{2/3}$ [c]	1.6d-5[d]
7	$R_{Bio-TCE} = -k_{Bio-TCE}[\text{BM}]\left[\frac{[\text{TCE}]}{\text{K}_{\text{Mo}}^{\text{red}-\text{TCE}}+[\text{TCE}]}\right]$	4.0E-14
8	$R_{Bio-DCE} = -k_{Bio-DCE}[\text{BM}]\left[\frac{[\text{DCE}]}{\text{K}_{\text{Mo}}^{\text{red}-\text{DCE}}+[\text{DCE}]}\right]$	5.0E-15
9	$R_{Bio-TCE} = -k_{Bio-TCE}[\text{BM}]\left[\frac{[\text{TCE}]}{\text{K}_{\text{Mo}}^{\text{red}-\text{TCE}}+[\text{TCE}]}\right]\left[\frac{\text{K}_{\text{In}}^{\text{sulfate}}}{\text{K}_{\text{In}}^{\text{sulfate}}+[\text{sulfate}]}\right]$	2.0E-14
10	$R_{growth} = -k_{growth}[\text{BM}][\text{TCE}][\text{Lac.}]\left[\frac{[\text{Lac.}]}{\text{K}_{\text{Mo}}^{\text{Lac.}}+[\text{Lac.}]}\right]\left[\frac{\text{K}_{\text{In}}^{\text{BB}}}{\text{K}_{\text{In}}^{\text{BB}}+[\text{BB}]}\right]$	varies
11	$R_{decay} = -k_{decay}[\text{BM}]\left[\frac{\text{K}_{\text{In}}^{\text{Lac.}}}{\text{K}_{\text{In}}^{\text{Lac.}}+[\text{Lac.}]}\right]$	1.0E0

[a]Averaged from Yan and Schwartz (1999) and Huang et al. (2001).
[b]From Huang et al. (2001).
[c]Mineral update according to Lichtner (1996a).
[d]Similar to Henderson et al. (2009).

in these scenarios due to the unique biogeochemical nature and history of the soils. Reactions (4) and (5) show how the permanganate treatment uses a second order kinetic reaction to model the oxidation of TCE and DCE by permanganate (Yan and Schwartz, 1999). Reaction (6) demonstrates the reaction of permanganate and the soil oxidant demand is assumed to be first-order with respect to aqueous MnO_4^-. A rate constant of 1.6E-5 mol/(m^3 bulk·sec) was found to accurately define the permanganate penetration into the low k zones. Aqueous manganese dioxide from reactions (4), (5) and (6) is assumed to instantaneously precipitate out of solution into a mineral phase.

The degradation of TCE and DCE in the KB-1 treatment models are given as first-order with respect to the biomass population, with a Monod term for the TCE/DCE concentrations. This is shown in Tables 3.4 and 3.5 as reactions (7) and (8). Lacking detailed effluent concentration data for VC and ethene, these two daughter products of dechlorination are grouped as a single compound in the lab and field-scale models for mass balance purposes only. Reaction (9) from Tables 3.4 and 3.5 demonstrate how the treatment of TCE in SRB, lactate and sulfate treatment was accomplished. This reaction uses a Monod term for TCE and an inhibition term for sulfate. This rate expression in the conceptual model is used to delay the use of TCE as an electron acceptor while a preferred electron acceptor (sulfate) is present in sufficient quantities.

Reaction (10) accounts for the growth of the biomass within treatments 4, 5 and 6. This reaction is third-order with respect to biomass, TCE and lactate concentrations. The reaction uses a Bio-block inhibition term to simulate data that suggests that biomass growth is suppressed in the low k zones relative to the transmissive of these heterogeneous systems. In the two KB-1 and lactate treatments, the biomass growth rate was set to 6.5E-01 cells/(L H$_2$O·sec). These two rates were calibrated to produce the observed *Dehalococcoides* population of $\approx$4.0E7 cells/L by day 140. The SRB, lactate and sulfate treatment from Chapter 2 was assumed to be biologically mediated. In the SRB treatment model, the microbial growth rate was set to 6.5E-01 cells/(L H$_2$O·sec).

The model assumes that the microbes dechlorinate the TCE only under specific conditions (i.e., availability of TCE and lactate) and inactivate when these conditions are no longer present. Deactivation of the biomass using reaction (11) begins when lactate concentrations fall below 5.0E-6 mol/L. Reaction (11) is first-order with respect to the biomass population, and has a lactate inhibition term which will suppress biomass inactivation while sufficient

lactate is present. Table 3.6 presents the Monod and inhibition values used in the model from Table 3.5.

Table 3.6. Monod and inhibition terms (reference Equation 4) from Table 3.5.

Parameter	Value (mol/L)
K_{Mo}^{ox-TCE}	1.0E-06
$K_{Mo}^{red-TCE}$	5.9E-6 [a]
$K_{Mo}^{red-DCE}$	6.6E-4 [b]
$K_{Mo}^{Lac.}$	5.0E-8
$K_{In}^{sulfate}$	5.0E-4[c]
K_{In}^{BB}	1.9E-6
$K_{In}^{Lac.}$	3E-5 [d]

[a]Averaged from Haston and McCarty (1999) and Cupples et al. (2004b).
[b]Averaged from Haston and McCarty (1999) and Chambon et al. (2010).
[c]Suppresses TCE as electron acceptor while sulfate is abundant.
[d]Fitting parameter to delay biomass inactivation.

3.5. Laboratory Model - Results and Discussion

The following compares the modeled versus observed effluent water quality for each of the treatments employed in Chapter 2.

3.5.1. No-Action Control. Figure 3.4 provides a plot of the TCE concentrations in the control tank at 2 and 100 days. TCE is seen flushing through the transmissive zones and diffusing into the low k zones during the first 52-days, after which TCE slowly diffuses out. Modeling the control tank uses reactions 1-3 in Tables 3.4 and 3.5, and assumes a growing biomass population is responsible for the transformation of TCE into DCE. The result of this modeling effort is shown in Figure 3.5, which compares the observed and modeled TCE and DCE effluent water quality with time. For all effluent water quality plots the laboratory TCE and DCE data are shown in red and black, respectively, while the model TCE and DCE data are shown in blue and green. Figure 3.5 demonstrates how the model closely matches effluent TCE values during and immediately after source removal, but shows a

slight divergence with laboratory data around day 80. Late-time laboratory effluent TCE appear similar to those predicted in the model. Effluent DCE concentrations appear to agree with the assumption of using a second-order growth rate with respect to biomass and TCE. Late-time total molar CVOC flux from the model is nearly identical to what was observed in the laboratory. These findings suggest that the control model provides a viable conceptualization of critical transport and treatment processes taking place.

(A)   (B)
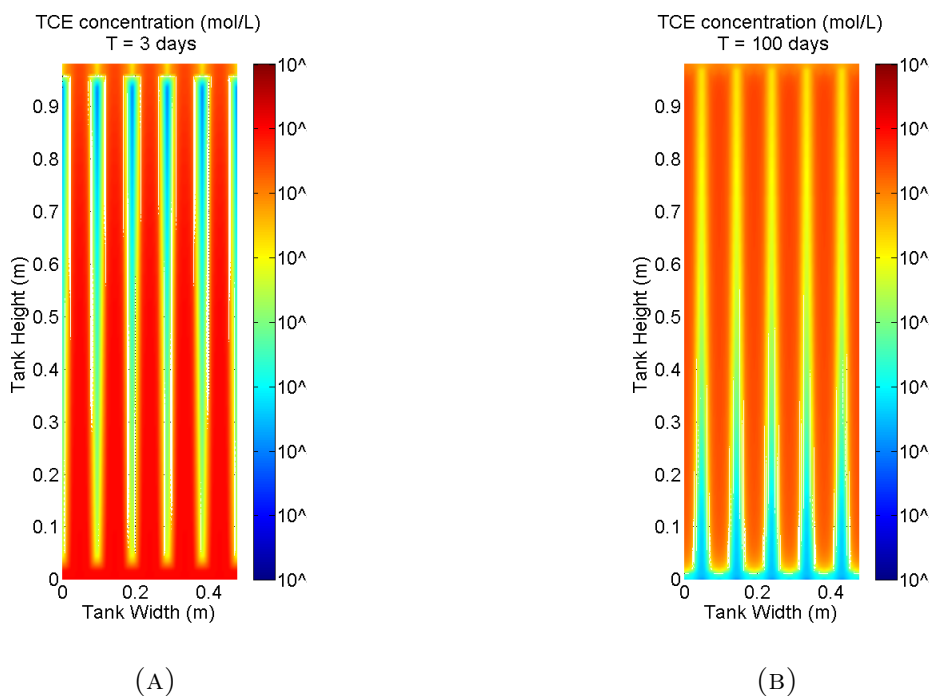
FIGURE 3.4. 2-D front view of laboratory-scale model TCE concentrations (A) during (day 3) and (B) after (day 100) pulse source. Note the transport of TCE into and then out of the low k zones

3.5.2. ENHANCED FLUSHING. Effluent TCE concentrations from the enhanced flushing treatment model are shown in Figure 3.6. This treatment model uses reactions 1-3 in Tables 3.4 and 3.5, and assumes a growing biomass population is responsible for the transformation of TCE into DCE. Before treatment, the model accurately predicted the evolution of the effluent TCE curve. During treatment, the model predicts a smaller drop in effluent TCE than was observed. The model overestimates the effluent TCE rebound after treatment,
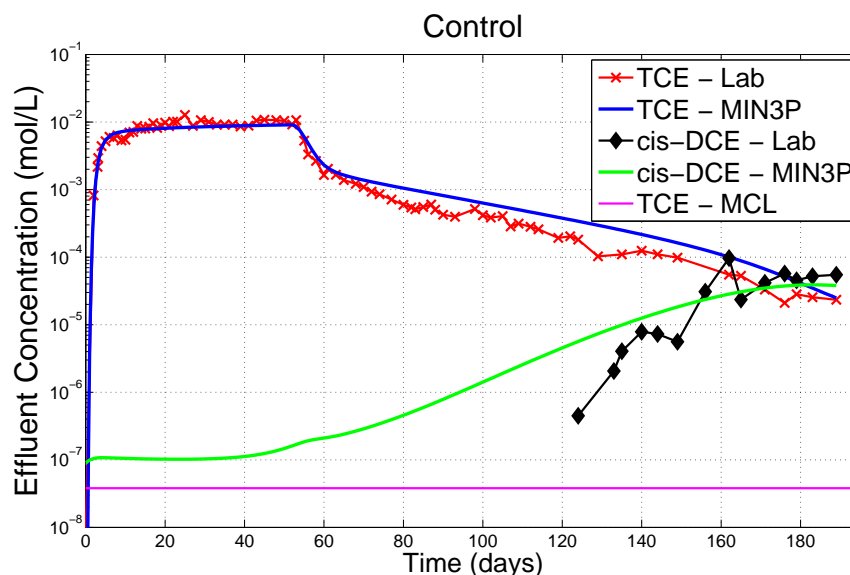
FIGURE 3.5. Laboratory effluent TCE (red) and DCE (black) concentrations through time from the control tank, with model effluent TCE (blue) and cis-DCE (green) breakthrough curves. The green effluent cis-DCE concentrations in the model are from a growing dechlorinating microbial population. Late-time total CVOC fluxes from the tank are seen to approximately match laboratory data.

resulting in effluent TCE concentrations above laboratory data until around day 170. Effluent DCE values during and after treatment were closely approximated by the model. Late-time total molar CVOC flux predicted by the model was close to what was experimentally observed. These findings indicate that this treatment model is effective for determining the specific late-time enhanced flushing and natural attenuation outcomes, but is incomplete in exactly quantifying the observed storage and release capabilities of the soils.

3.5.3. POTASSIUM PERMANGANATE. Utilizing the reactive-transport capabilities of *MIN3P* described in Section 3.4.2, the permanganate treatment produced the effluent TCE and DCE curves shown in Figure 3.7. Before treatment, the model accurately predicted the effluent TCE profile. During treatment, the model shows a significant drop in effluent TCE for the duration of the permanganate flush, which is consistent with laboratory data. After treatment, effluent TCE and DCE concentrations are followed by rebounds consistent with the
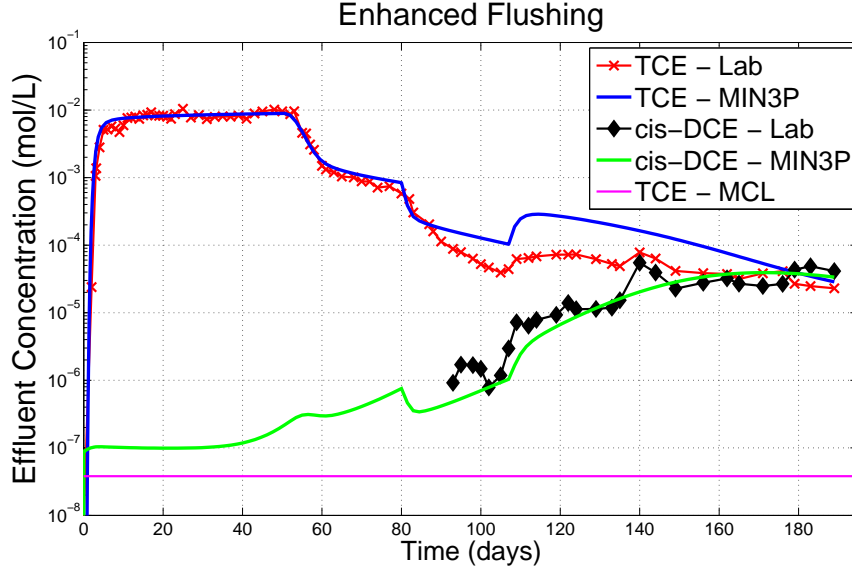
FIGURE 3.6. Enhanced flush effluent laboratory TCE (red) and DCE (black) concentrations, with model effluent TCE (blue) and cis-DCE (green) breakthrough curves. The green effluent cis-DCE concentrations in the model are from a growing dechlorinating microbial population. The divergence between the laboratory and model effluent data during and after treatment indicates that there were other processes occurring in the tank which are not considered in the model.

observed incomplete treatment of the low k zones. Late-time effluent TCE values agreed closely with laboratory data. Porosity (ϕ) and tortuosity (τ) changes in the model from the $MnO_2(am)$ mineral phase reduced chemical diffusion within the low k zones at late time. These minerals are responsible for a flattening of the effluent TCE rebound behavior after treatment. These changes are accomplished in the model using Equations 5 and 6:

$$\phi^{t+\Delta t} = \phi^t - \sum_{i=1}^{N_M} \phi_i^{t+\Delta t} - \phi^t, \tag{5}$$

$$\tau = S_P^{7/3} \phi^{1/3} \tag{6}$$

where S_P is the phase saturation ($S_P=1$ in this case). Effluent DCE values during and after treatment were close to observed results, indicating a good understanding of natural
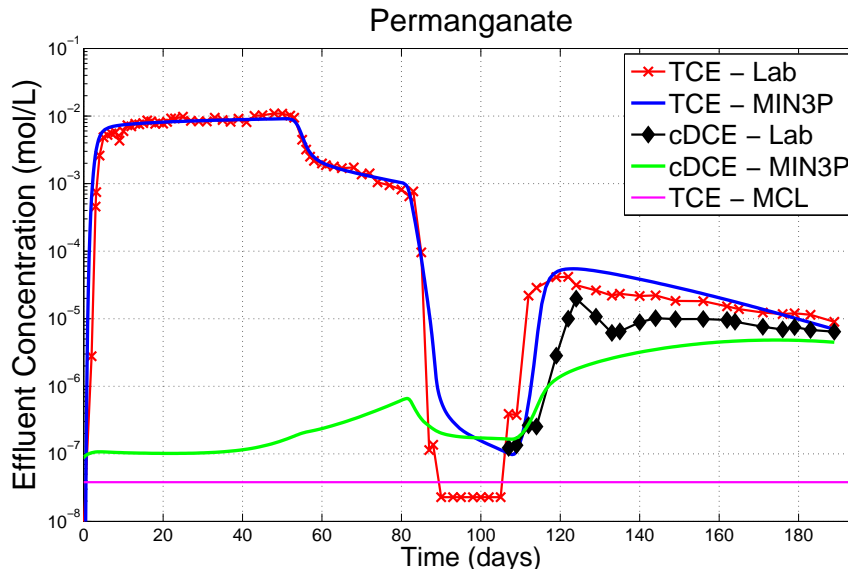
FIGURE 3.7. Permanganate flushing effluent laboratory TCE (red) and DCE (black) concentrations, with model effluent TCE (blue) and cis-DCE (green) breakthrough curves. The green effluent cis-DCE concentrations in the model are from a growing dechlorinating microbial population. The close match in effluent TCE before and during the permanganate flush indicates a good agreement between the model and the laboratory data. The timing and level of rebound in effluent TCE and cis-DCE in the model after treatment agree with laboratory data as well, indicating a good overall understanding of the biogeochemical processes occurring in the tank during treatment. Laboratory effluent cis-DCE concentrations before treatment are unavailable due to detection limits of ECD.

attenuative processes and DCE treatment from the laboratory experiment. Total CVOC fluxes in the model fit well before treatment, and match reasonably well with observed data after treatment. These results suggest an overall near-complete quantification of the low k storage, permanganate treatment and mineralogical processes that occurred in the laboratory.

3.5.4. KB-1 MICROBIAL TREATMENTS. Effluent TCE and DCE flux curves for the two KB-1 biological treatment models are presented in Figures 3.8 and 3.9. Boundary fluxes in the KB-1, lactate and xanthan gum treatment (Figure 3.9) were changed to account for the 23-day shut-in period, which is shown as the absence of effluent data from day 84-107. Before

treatment, the models show a good fit to the observed TCE breakthrough curves. During and immediately after the delivery of lactate within treatment 4 (Figure 3.8), the beginning of significant TCE dechlorination in the model is faster than was experimentally observed, but still captures the overall rate and lower concentration limit of the TCE dechlorination. For the KB-1, lactate and xanthan gum treatment (Figure 3.9), the model shows a good fit to effluent TCE while sufficient lactate was present. The two models both demonstrate good fits to effluent DCE and total CVOC flux data during and after treatment as well. The
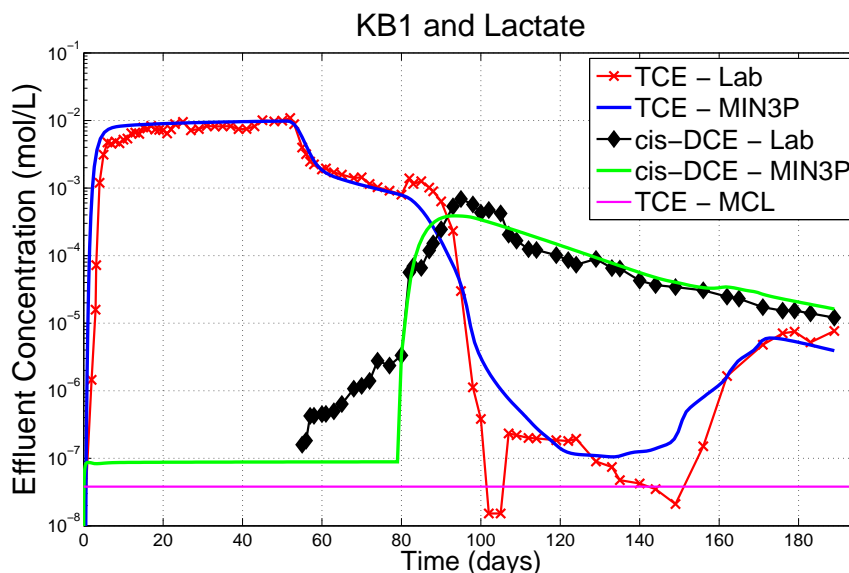
FIGURE 3.8. KB-1 and lactate effluent laboratory TCE (red) and DCE (black) concentrations, with model effluent TCE (blue) and cis-DCE (green) breakthrough curves. The timing and duration of the TCE and cis-DCE dechlorination, as well as the timing and level of the TCE rebound indicate a good overall understanding of the conditions necessary for this microbial treatment to proceed.

shape of the TCE rebounds at the start of the biomass inactivation indicate that the biomass decay process happens much faster than predicted in the models. This discrepancy is most likely because TCE dechlorination in the model is first-order with respect to the biomass population, which is a simplified conception of the overall treatment process. Although the
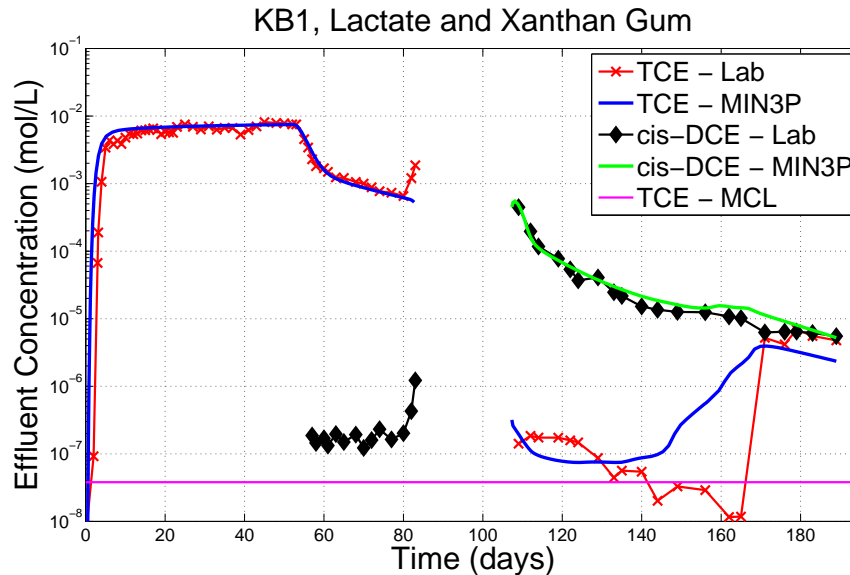
FIGURE 3.9. KB-1, lactate and xanthan gum effluent laboratory TCE (red) and DCE (black) concentrations, with model effluent TCE (blue) and cis-DCE (green) breakthrough curves. As with the previous KB-1 treatment, the overall biogeochemical conditions necessary for this treatment to proceed are acceptably captured in the model.

rebounds happen at a quicker rate than experimentally observed, these rebounds and the late-time effluent TCE and DCE in the models show a good fit to the observed data. These findings indicate a good overall understanding of the processes involved in this biological treatment, which includes the placement, growth and rate of microbially mitigated dechlorination. Although these dechlorination processes could be extended to fit VC and ethene effluent concentrations in future work, it would not be verifiable in this work since the data is not available.

3.5.5. SRB, LACTATE AND MAGNESIUM SULFATE. Although the last treatment of SRB, lactate and sulfate has two potential treatment mechanisms (biological and reactive iron-sulfide minerals), the conceptual model for this treatment assumes that a population of biomass is responsible for TCE dechlorination into DCE. This modeling effort is shown in Figure 3.10. Before and during treatment, the model shows a good fit to effluent TCE data.
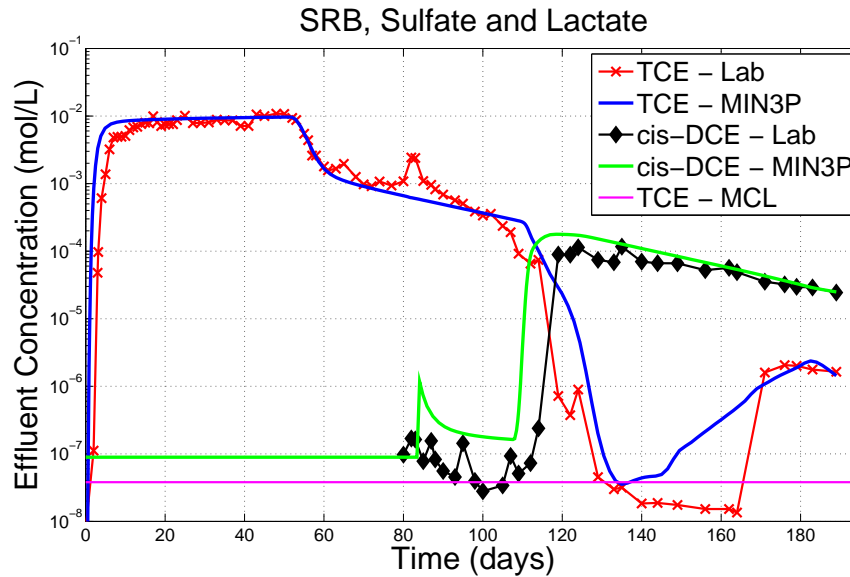
FIGURE 3.10. SRB, lactate and sulfate effluent laboratory TCE (red) and DCE (black) concentrations, with model effluent TCE (blue) and cis-DCE (green) breakthrough curves. The model was assumed to proceed through a microbial dechlorinating population, which did not use TCE for respiration until sulfate concentrations had fallen over 2 OoM from treatment flushing levels. As with the two KB-1 treatments, microbial dechlorinating was stalled once lactate was exhausted, resulting in the observed effluent TCE rebound.

Using a sulfate inhibition term for dechlorination, the model was able to present the delay and slope of the laboratory effluent TCE concentrations during and after treatment, extending until around day 140. As with the two KB-1 treatments, once lactate concentrations depleted, the microbial population in the model began to deactivate, presenting the observed rebound in effluent TCE. At this point, the model predicts that the effluent TCE rebound will be more gradual than was experimentally observed, suggesting that the biogeochemical situation within the model merits further consideration. Late stage effluent values of TCE and DCE concentrations and mass fluxes closely match the observed data, suggesting a good overall understanding of the processes occurring within the tank.

3.5.6. SORPTION ANALYSIS. Further analysis concerning the efficacy of the treatments can be done by exploring total sorbed TCE mass. A plot of total sorbed TCE mass from

the tanks is shown in Figure 3.11. Not surprisingly, the control (red line) provides a baseline which shows a steadily decreasing sorbed TCE mass with time. Although the laboratory and model for the enhanced flushing treatment did not show a significant improvement in effluent TCE at late-time, the amount of sorbed TCE mass within this treatment was 45% lower than the control. Similarly, improvements in the permanganate treatment show a 51% drop in total sorbed TCE at the end of the experiment.

The largest drop in total sorbed TCE occurred in the SRB, lactate and sulfate treatment model, observed around the same experimental time when effluent TCE concentrations fell multiple OoM. This outcome is expected as this treatment had the lowest sustained effluent TCE concentration at day 189, suggesting a lower total system TCE mass. Interestingly, the KB-1, lactate and xanthan gum treatment had the highest mass of sorbed TCE, which is seen diverging above from the control during the treatment window. This is most likely due to the 23-day shut-in period during the treatment. Due to the lack of flushing and an increase in retention time of the TCE, the delay in the desorption processes is seen as a shift in the curve to the right of the other systems. Although effluent TCE data showed relatively acceptable treatment of TCE occurring, this result suggests that the observed effluent TCE rebound may have further increased with time.

3.5.7. TREATMENTS: TIME TO COMPLIANCE. In the interests of providing a metric to compare the relative effectiveness of each treatment, the Time to Compliance (TtC) for each treatment was modeled. This term is defined as the time required to reach MCL after the source has been removed. For instance, the TtC of the tanks was modeled beyond the 189 day treatment window to determine the length of time needed to reach a TCE effluent concentration of 5 ug/L (MCL). Due to the uncertainty of the behavior of this natural attenuation beyond day 189, and for the sake of comparing the base case of the control,
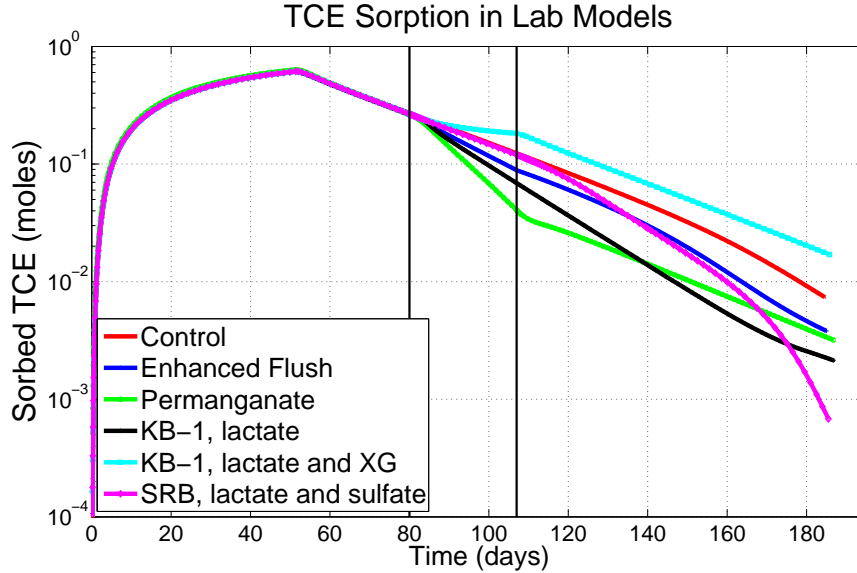
FIGURE 3.11. Laboratory-scale total TCE sorbed mass through time within the six models.

enhanced flushing and permanganate treatments, these 3 treatments were modeled to the TtC assuming that biological growth and decay was absent. An assumption was also made about the biological treatments after day 189 that the effluent cis-DCE and TCE trends after day 170 in the analytical results continue as observed. These 6 results for the TtC are shown in Table 3.7. Interestingly, increasing the source duration time from 52 to 104 days in the control produces only a 6-day increase in the TtC from 391 to 397 days. This absence of a significant increase in TtC suggests that due to the low k architecture of the setup, the soils are already so close to TCE saturation at day 52 that a further 52 days of exposure to the TCE source will not significantly increase the mass of TCE stored in the low k zones.

3.6. Field-Scale Model Development

Using the transport, biological and chemical input parameters from the laboratory-scale models, the efficacy of the treatments are evaluated at the field-scale. The following subsections provide the methods used in the development of the field-scale treatment models. The

TABLE 3.7. Modeled Time to Compliance (TtC) and corresponding reduction in effluent TCE longevity values for each laboratory treatment with respect to the control.

Treatment	TtC (days)	Reduction in longevity w.r.t. control (%)
1. Control	391	NA
2. Enhanced flushing	385	1.6
3. Permanganate	335	14
4. KB-1 and lactate	337	14
5. KB-1, lactate and xanthan gum	330	16
6. SRB, lactate and $MgSO_4$	287	27

field-scale models employ two distinct soil architectures. The first architecture demonstrates long-term treatment outcomes due to the influence of an aquitard. The second architecture demonstrates treatment outcomes in the absence of an aquitard.

3.6.1. FIELD-SCALE MODEL DOMAIN. In the interest of comparison to published work, the geometry of this field scale portion of the research follows the work of Parker et al. (2008). The hydraulic conductivities for the first-scenario where a lower aquitard is present is shown in Figure 3.12a. The field scenario uses the same soil parameters (e.g., hydraulic conductivities, porosities etc.) from the laboratory experiment for the high and low k zones. The layout shows a 10-m thick transmissive zone layered with seven (7) low k lenses. This transmissive high k zone is underlain by a 5-m thick aquitard.

To provide a more complete understanding of the effects that the lower aquitard plays on the long-term down-gradient TCE concentrations, a second field scenario is analyzed. This scenario is identical to the previous in soil parameters, source history and treatments, but the aquitard is replaced with a smaller low k lens and a transmissive layer. Figure 3.12b shows the hydraulic conductivities of the soils within the second, no-aquitard scenario. To mimic the contaminant source history from Parker et al. (2008), five (5) TCE DNAPL pools were placed on top of the left hand side of the low k lenses. These five TCE DNAPL pools are

initially 2-m wide by 1-cm tall, occupy 75% of the available volume fraction (=1 - porosity), and dissolve into the groundwater until fully depleted at year 30.

(A)

(B)
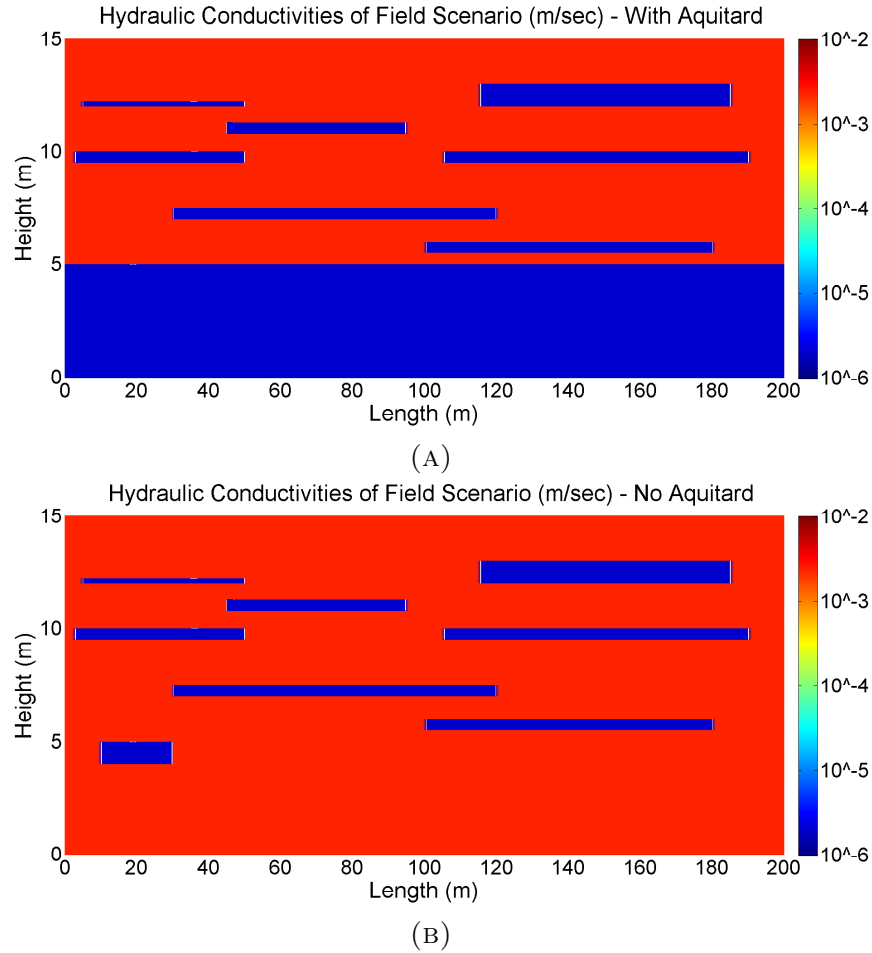
FIGURE 3.12. Following Parker et al. (2008): transmissive and low k zone domain, hydraulic conductivities and geometric layouts of A) aquitard-present and B) no-aquitard scenarios. Red and blue indicate transmissive and low k soils, respectively. In both cases the domain is 200-m long, and 15-m high. The discontinuous low k layers range from 0.25 to 1-m thick, while the larger low k aquitard in A) is 5-m thick. Five, 2-m long TCE DNAPL pools of were placed on top of the low k layers at various points between 20 and 40-m from the left-hand side of the domain.

3.6.2. BOUNDARY CONDITIONS. To simulate a semi-infinite horizontal domain, the entire 15-m height of the left and right-hand side of the aquifer represent the inflow and outflow boundaries, respectively. The left and right-hand boundaries are both represented

as Dirichlet boundaries, with head values of 15.25-m and 15-m, respectively. These boundary conditions create a left to right flow of ≈25 cm/day in the transmissive layers. The right boundary is considered a well-mixed monitoring well which serves as the down-gradient point-of-compliance for the model. Since the bottom of the 5-m thick aquitard is an impenetrable boundary, this can dampen vertical diffusive processes at late time. However, the size of the domain is reasonable given the objectives of this work.

3.6.3. SPATIAL DISCRETIZATION. The model domain contains 196,392 nodal points. The nodes are spaced 0.5-cm vertically within the low k lenses and at the high-low k interfaces, and at 5-cm vertically in the transmissive layers and from 0 to 4-m in the aquitard. Horizontal nodal spacing is set to 5-mm around the DNAPL pools, and at 50-cm elsewhere. Use of finer horizontal discretization did not noticeably affect contaminant storage, transport or treatment within the aquifer. A plot of the nodal points is shown in Figure 3.13a. Herein, all 2-D aquifer profiles outline the locations of the low k zones in black.

3.6.4. TREATMENTS. The model allows for nodal points to be used as injection points for the delivery of treatment fluids. The four (4) treatment injection points used in the field models are seen at the center of the four expanding plumes in Figure 3.13b. These 4 injection points are all located within the transmissive zone of the aquifer. In Figure 3.13b, the treatment solution can be seen spreading about the injection point, while being transported down-gradient with the groundwater flow. These injection points were chosen to best represent field locations where an injection would likely have a significant impact on stored TCE. The treatment durations and injection volumes are shown in Table 3.8. All treatments began at 35 years, which is 5 years after all the TCE DNAPL pools had dissolved completely. The treatment concentrations are the same used in the laboratory experiment

Field-Scale Model Nodes

(A)

Treatment Injection Points - Sample Solution (mol/L)

(B)
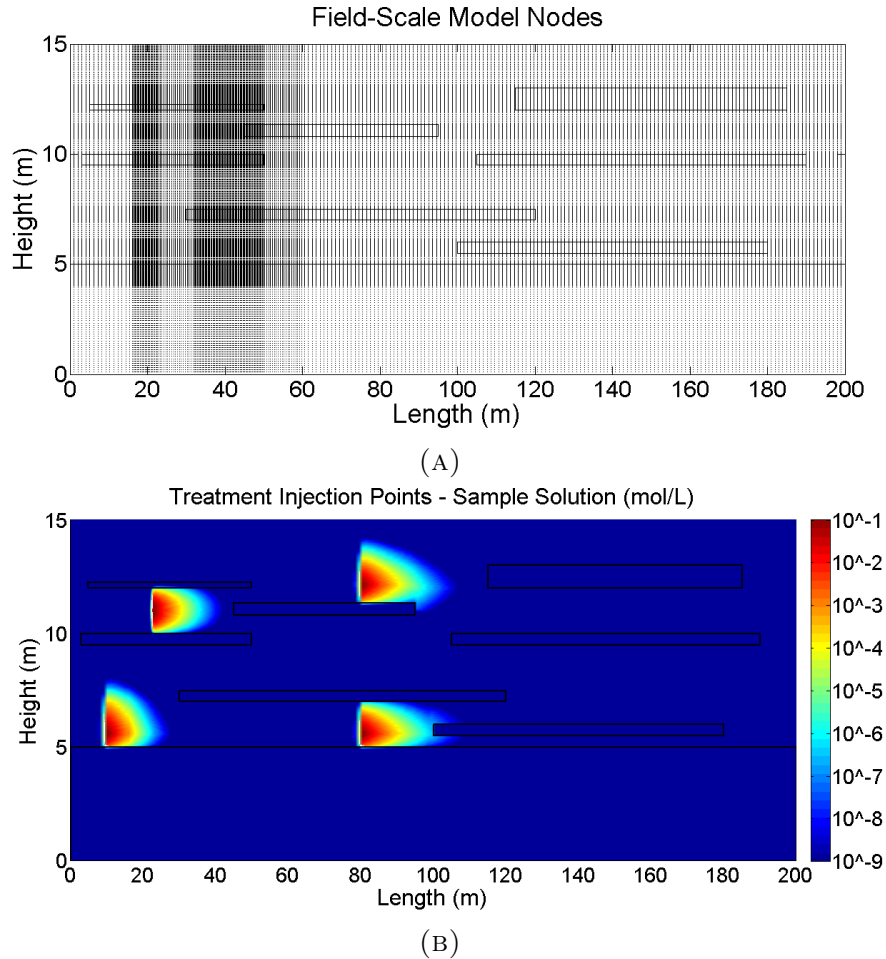
FIGURE 3.13. A) Aquifer nodal discretization (196,392 nodes) and B) injection locations for treatment solutions (2-day sample injection shown). Higher densities of nodes were used in the low k zones, as well as in zones containing the five DNAPL pools. The treatment injection points, seen at the center of the 4 sample plumes in B), were chosen to best represent a field scenario which would impact the largest volume of the aquifer. The right-side boundary is considered as the down-gradient monitoring well (point of compliance), and is screened the entire 15-m of the domain height.

and previous laboratory modeling (Table 3.3). Due to constraints of the code and the similarity of the biological treatment models presented earlier, only treatments 1, 2, 3, and 4 (Section 3.4) are considered for the field-scale models. Due to the lack of long-term data concerning effluent DCE and biological activity within tanks 1-3 (Chapter 2), field-scale models of these treatments will be done without the use of naturally occurring biological dechlorination. Instead, the effects on the aquifer from only the treatments themselves will

TABLE 3.8. Treatment schedules and influent volumes for the two field scenarios. The injection volumes and delay between the injections on treatments 2-4 is usually typical of field activities.

Treatment	Treatment Duration	Delay Between Treatments	Volume
1. Control	N.A.	N.A	N.A.
2. Enhanced flushing	2 instances of: 10 years, 5 years[a]	5 years	20-x transmissive flow
3. Permanganate	3 instances of 120 days	90 days	1/4 transmissive P.V. each injection
4. Lactate	3 instances of 120 days	3 years	1/4 transmissive P.V. each injection

be analyzed. This imposes a limitation on these 3 models because the long-term impact of natural attenuative processes in low k zones may be significant. The time to model each of these treatments ranged from 1 to 10 days on an *Intel(R)* Core i5 2.8 GHz CPU with 4 GB of RAM.

3.7. Field-Scale Models - Results and Discussion

This section describes the treatment results from the two field scenarios. Treatments from the aquitard-present scenario are considered first, followed by the results from treatments within the no-aquitard case. Down-gradient contaminant concentrations through time, the efficacy of the treatments, as well as the total stored TCE for each treatment are discussed for both scenarios.

3.7.1. Aquitard Scenario.

3.7.1.1. *No-Action Control.* The first treatment considered for the aquitard-present case is the no-action control. This model serves as the baseline for the three active treatments. Starting at the time of TCE DNAPL depletion (year 30), Figure 3.14 shows 2-D TCE profiles within the aquifer as it evolves over the course of 400-years thereafter. Stored TCE is shown diffusing out of the low k lenses, with a significant amount of TCE storage and release from

the bottom low k aquitard. The smaller low k lenses are observed to be mostly free of TCE by year 100, while the vast majority of late-time TCE storage and release is due to the aquitard.
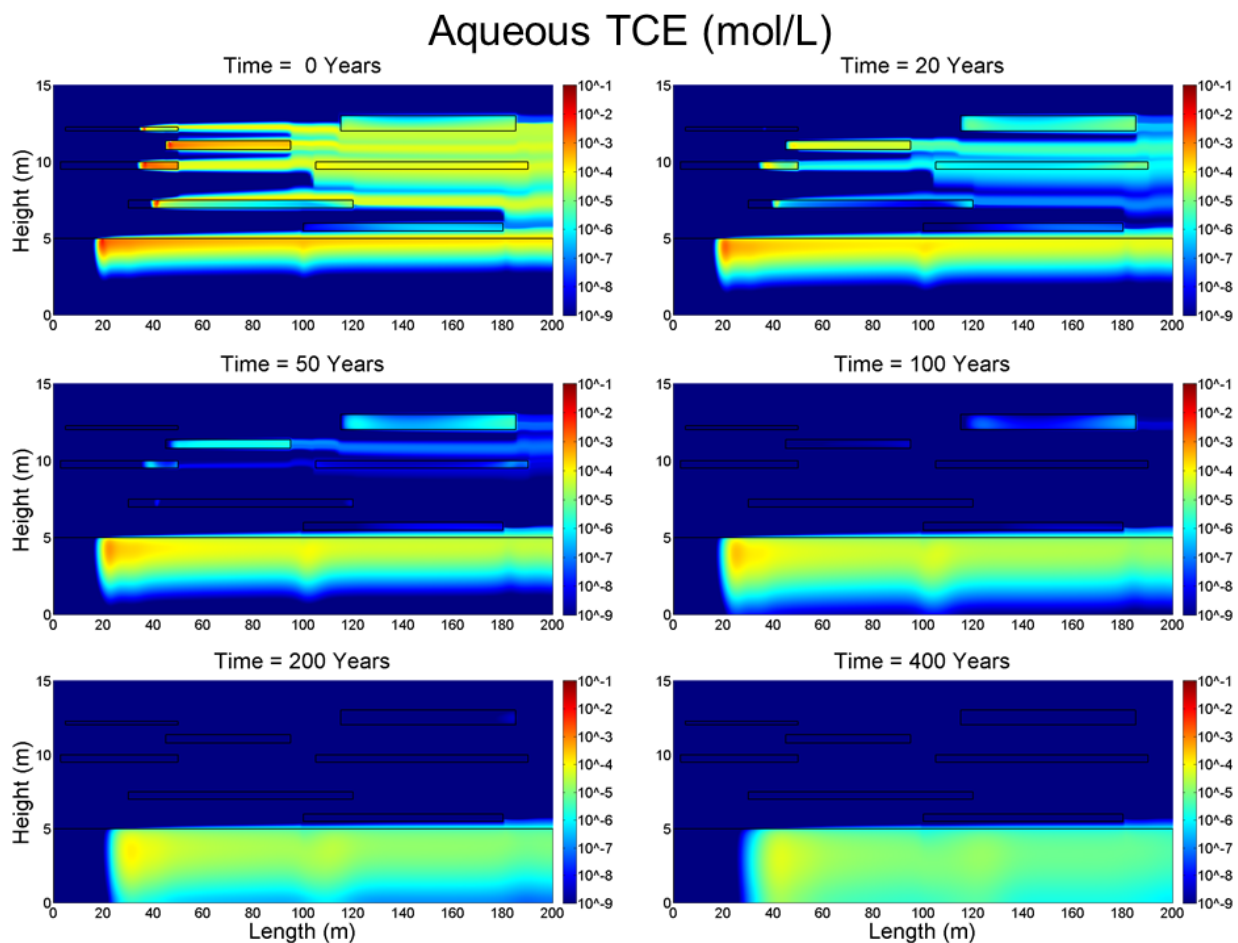
FIGURE 3.14. 2-D aquifer TCE profiles through time for the control, aquitard-present scenario. Note that the times shown are measured from time after full TCE DNAPL dissolution (i.e., year 30 = year 0). The storage and release of TCE in the low k soils is apparent, as well as the impact of the aquitard on late-time releases.

Figure 3.15 presents the TCE concentrations with time in the down-gradient, 15-m screened well on the right-hand side of the model domain. The TtC for this scenario was found to be 429 years, or 394 years from the start of the active treatments. This TtC suggests that in the absence of an active treatment, large low k lenses can sustain down-gradient TCE

compliance issues for centuries. The TtC value is higher than that published by Parker et al. (2008), an expected outcome due to the different biogeochemical parameters in the models. It should be noted that from Figure 3.14 demonstrates that late-time TCE monitoring well concentrations are almost entirely due to releases from the aquitard. That said, a limitation of the boundary conditions in the model is presented here; a more realistic monitoring well should be screened only within the transmissive zones, which would produce a different TtC.

The total TCE mass in the aquifer system through time is shown in Figure 3.16. At year zero, the aquifer contains 889.63 moles of TCE (present as DNAPL). When the three active treatments began at year 35, 826.14 moles out of 889.63 moles (92.8%) of total system TCE has already flushed through the down-gradient well. At 429 years, the aquifer system contains 10.4 moles (1.2%) of TCE, almost all of which is stored in the aquitard. This finding demonstrates that even a relatively small amount of stored TCE mass can sustain down-gradient exceedance of drinking water standards for extended periods of time. A limitation of this particular model setup is the lack of natural attenuative processes occurring in the soils, which were observed in the laboratory treatment studies. These processes may be significant at large time-frames.
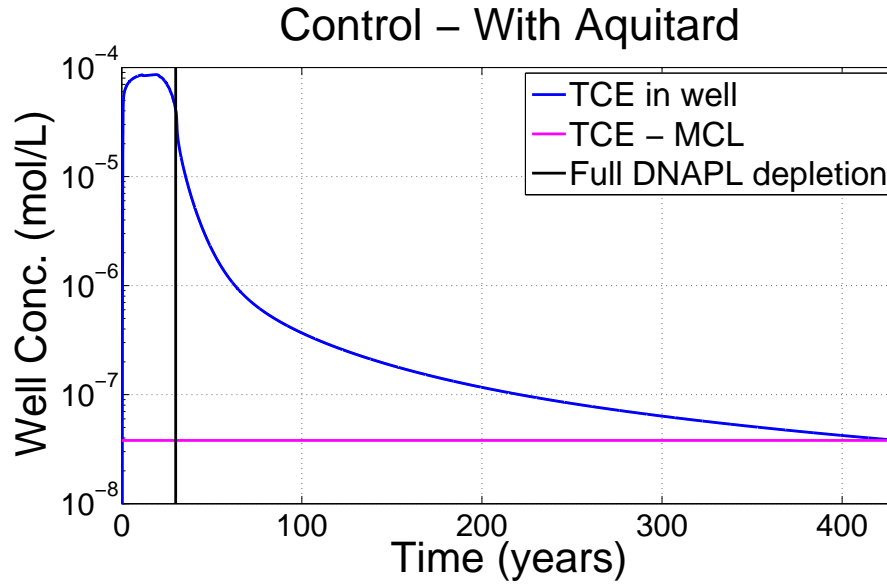
FIGURE 3.15. Control TCE concentrations in a 0 to 15-m screened down-gradient well over a 430-year time-frame, aquitard-present case. Magenta lines represent the MCL for TCE only. DCE and VC MCLs not shown. The vertical black line indicates the time when TCE DNAPL phase is fully depleted, and is typical of all future plots. Note the extended period of time necessary for the down-gradient monitoring well to reach MCL in the absence of natural attenuative processes.
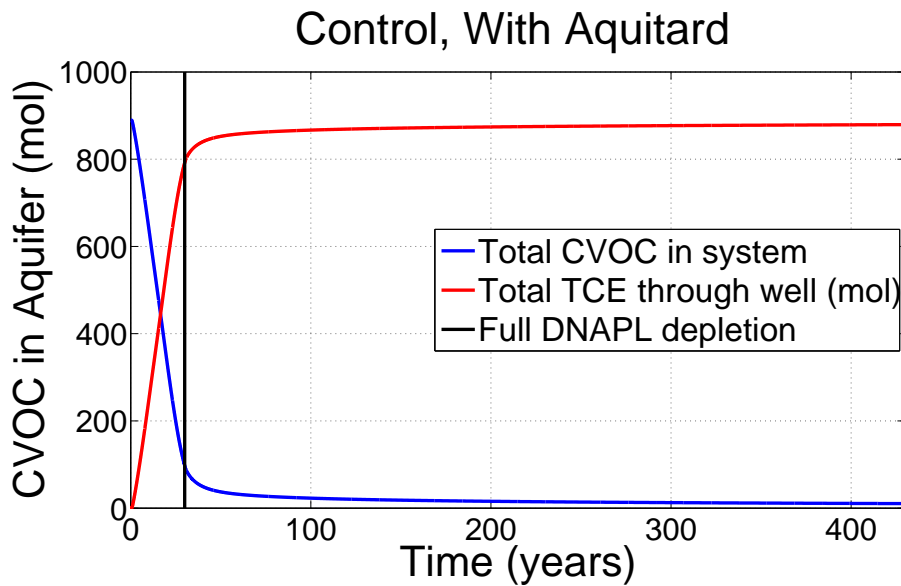
FIGURE 3.16. CVOC mass flux through the down-gradient well from the control, aquitard-present case over a 430-year time-frame. The slow removal of TCE from the aquitard at late-time is apparent.

The migration of the dissolved-phase TCE through the aquitard is of interest. Quantifying this migration can be done by analyzing a vertical slice through the aquitard at the point x=20-m through time. Figures 3.17a and 3.17b show the migration of TCE during and after DNAPL loading for this vertical-slice of the aquitard. As shown, the constant TCE DNAPL source loads the aquitard through diffusion for the first 30 years. After the TCE DNAPL is fully dissolved, TCE is seen diffusing downward farther into the aquitard, migrating to the right with the very small advective flow, and back into the high k zone at the top aquitard boundary. This shape and behavior of TCE evolution through an aquitard has been previously discussed analytically by Johnson and Pankow (1992), Parker et al. (1994) and in Shackelford and Lee (2005).

(A)

(B)
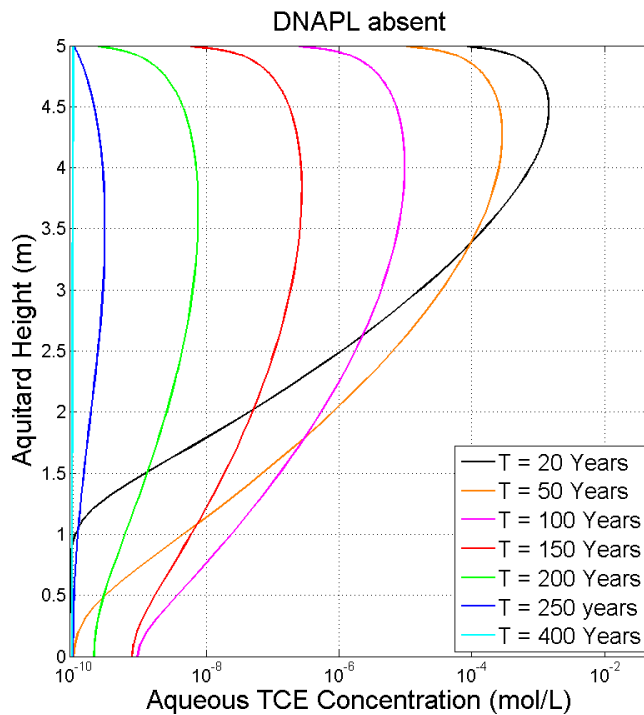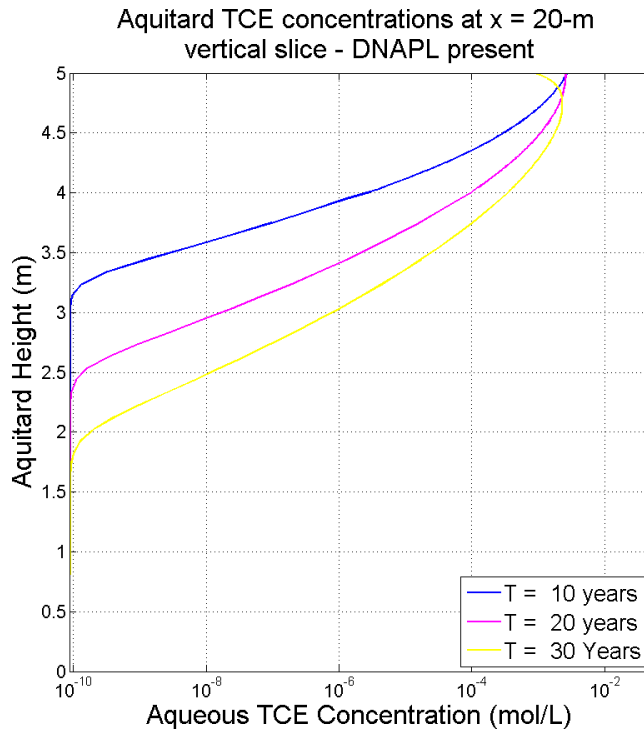
FIGURE 3.17. Aqueous TCE concentrations in the aquitard A) during and B) after DNAPL loading. from a vertical slice at x=20-m below the bottom-leftmost DNAPL pool. The migration of TCE into, out of, and down-gradient with the aquitard is observed.

3.7.1.2. *Enhanced Flushing.* The first active-treatment field scenario considered is an enhanced flushing of contaminant free water at 20-x base seepage velocity, analogous to treatment 2 from the laboratory studies. Figure 3.18 shows the down-gradient TCE monitoring well concentrations with time for the enhanced flush relative to the control scenario. During treatment, down-gradient concentrations can be seen dropping approximately 2 OoM, followed by a rebound after each flushing activity. Measured from the start of treatment, the TtC for this treatment is 391 years, only 3 years (0.7%) earlier than the control. Figure 3.18 suggests that even with 20 total years of 20-x seepage-rate flushing, the mass of TCE removed from the system is not enough to meaningfully reduce the longevity of the TCE plume in the down-gradient well. Since the rebound of TCE was not immediately apparent in the down-gradient well, this outcome also demonstrates that site managers should exercise care when analyzing the outcome of this treatment type.

TCE concentrations in the monitoring well are further explained by Figure 3.19, which shows the mass remaining in the aquifer through time. At year 35, only a very slight decrease in total aquifer TCE mass is observed. The aquifer still contains 10.38 moles at year 430, which is only 0.02 moles less than the control at this time. Again, the vast majority of the late-time TCE mass is stored within the aquitard. Under these conditions, this treatment outcome demonstrates how ineffective an enhanced flushing treatment can be when used with flow parallel to thick low k bedding, and/or when a large low k zone is present.
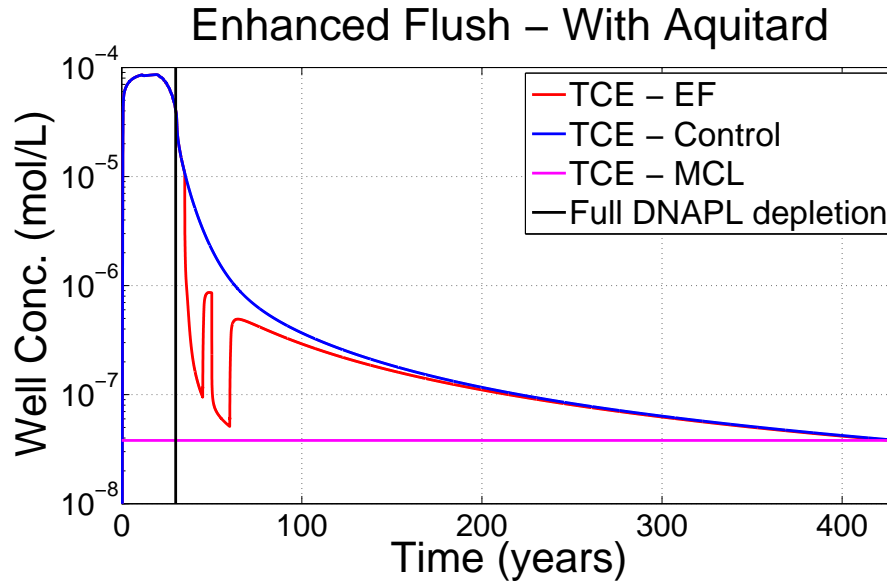
FIGURE 3.18. TCE concentrations in the enhanced flushing treatment for a 0 to 15-m screened down-gradient well over a 430-year time-frame, aquitard-present case. For reference, control TCE values are shown in blue. Magenta lines represent the MCL for TCE only. DCE and VC MCLs not shown. The two drops and rebounds of TCE starting at year 35 in the two, 10-year flushes is apparent. Late-time down-gradient TCE concentrations were not significantly different from the control, indicating little benefit to this treatment scheme.
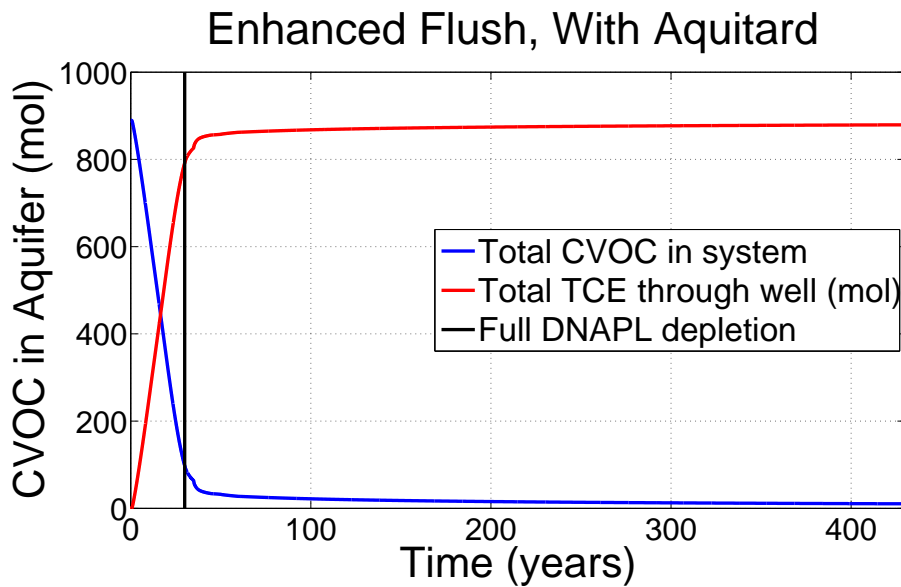
FIGURE 3.19. CVOC mass flux through the down-gradient well from the enhanced flushing, aquitard-present case over a 430-year time-frame.

3.7.1.3. *Permanganate ISCO.* The next active-treatment field scenario considered is 3 instances of 1/4 transmissive P.V. injections of permanganate (see Table 3.8), analogous to treatment 3 from the laboratory studies. Figure 3.20 shows the down-gradient TCE monitoring well concentrations from the permanganate flush relative to the control scenario in the down-gradient well. During treatment, down-gradient concentrations can be seen dropping over 2 OoM, quickly followed by rebound. Measured from the start of treatment, the TtC for this treatment was 389 years, only 5 years (1.2%) earlier than the control. This finding demonstrates that 3 instances of 1/4 P.V. injections of the 2 g/L permanganate solution were not enough to significantly impact long-term down-gradient TCE concentrations. This outcome is again most likely due to the storage and release of TCE from the aquitard at late time. Further modeling of this system with increases in injection volumes had no noticeable effect in the down-gradient monitoring well, as the permanganate was simply not able to penetrate a meaningful distance into the low k layers. Modeling using large increases in the concentration of the permanganate treatment may produce more desirable results.
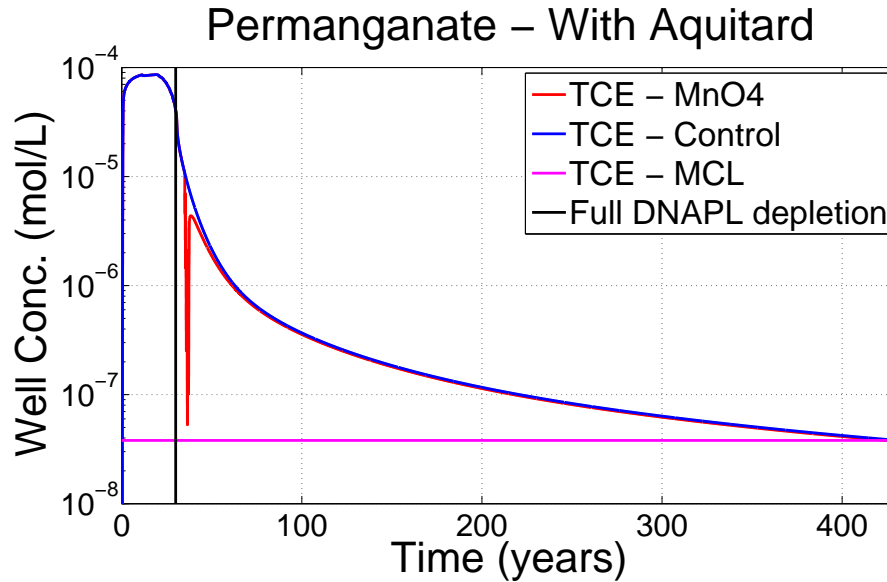
FIGURE 3.20. TCE concentrations in the permanganate flushing treatment for a 0 to 15-m screened down-gradient well over a 430-year time-frame, aquitard-present case. For reference, control TCE values are shown in blue. Magenta lines represent the MCL for TCE only. DCE and VC MCLs not shown. The drop and rebound of down-gradient TCE at year 35 is observed, indicating that the oxidant demand and transport processes within the soils significantly inhibited this treatment.
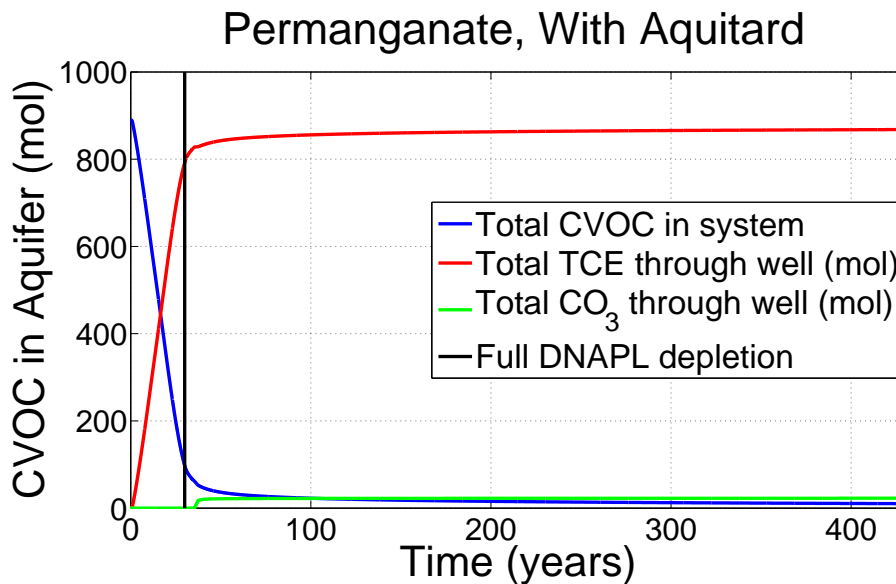
FIGURE 3.21. CVOC mass flux through the down-gradient well from the permanganate flushing, aquitard-present case over a 430-year time-frame. Stoichiometric based mass flux from the degradation product CO_3 is incorporated.

Figure 3.21 shows the mass remaining in the aquifer through time for the permanganate treatment. At year 35, the down-gradient arrival of aqueous CO_3^{-2} (a reaction product of TCE and MnO_4) demonstrates that treatment is indeed occurring. The aquifer contains 10.3 moles of CVOC at year 430, which is only 0.1 moles less than the control at this time. Again, the vast majority of the TCE mass is stored within the aquitard at the end of the simulation. This result demonstrates how ineffective a permanganate treatment can be when flushed through field sites with large low k zones and inhibitory soil oxidant demands.

To more clearly see the extent of the permanganate injections, Figure 3.22 shows the extend of the MnO_2 deposits at 430 years. As shown, even though the permanganate flushed through the most impacted transmissive zones, the treatment was not able to penetrate far enough into the low k zones to have a meaningful impact on the TCE stored within. Instead, the permanganate most likely acted by oxidizing the TCE as it diffused into the transmissive layer. It should be noted that this outcome is specific (but not unique) for the soils used in the laboratory experiment, which imposed a significant oxidant demand on the ISCO treatment. A limitation of this model lies within the constant definition of the soil retardation parameters, which most likely change under real circumstances due to the interaction of the oxidant and soil organic carbon.
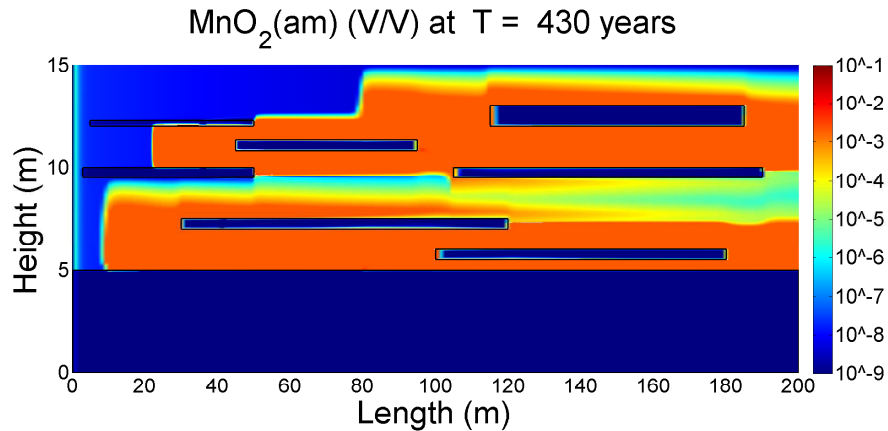
FIGURE 3.22. MnO$_2$ deposits showing the extent reached by the 3, 1/4 P.V. permanganate injections at 430 years, aquitard-present scenario. The transmissive soil domain impacted by the treatment was acceptable. Note the lack of permanganate penetration into the low k lenses and aquitard.

3.7.1.4. *Microbial Growth & Dechlorination with Lactate.* The next active-treatment field scenario considered is 3 instances of 1/4 transmissive P.V. injections of lactate, analogous to treatment 4 from the laboratory studies. Figure 3.23 shows the TCE, DCE and VC down-gradient monitoring well concentrations from the lactate flush relative to the control scenario. During treatment, down-gradient concentrations can be seen dropping 1 OoM, followed by rebound. The TtC for TCE was the longest between down-gradient TCE, DCE and VC. Measured from the start of treatment, the TtC was observed to be 164 years. This represents a 58% decrease in CVOC down-gradient longevity, but would still be considered a treatment failure in need of further refinement.
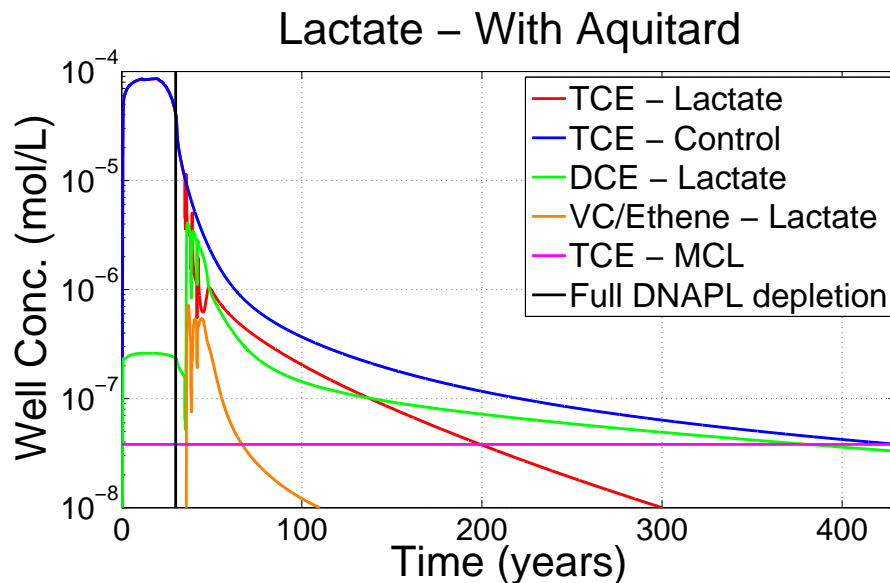
FIGURE 3.23. CVOC concentrations in the lactate flush treatment for a 0 to 15-m screened down-gradient well over a 430-year time-frame, aquitard-present case. For reference, control TCE values are shown in blue. DCE and VC/Ethene concentrations are shown as green and orange, respectively. Magenta lines represent the MCL for TCE only. DCE and VC MCLs not shown. The three lactate injections beginning at year 35 result in an overall decreasing trend in down-gradient TCE concentrations, producing a reduced TtC relative to the control.
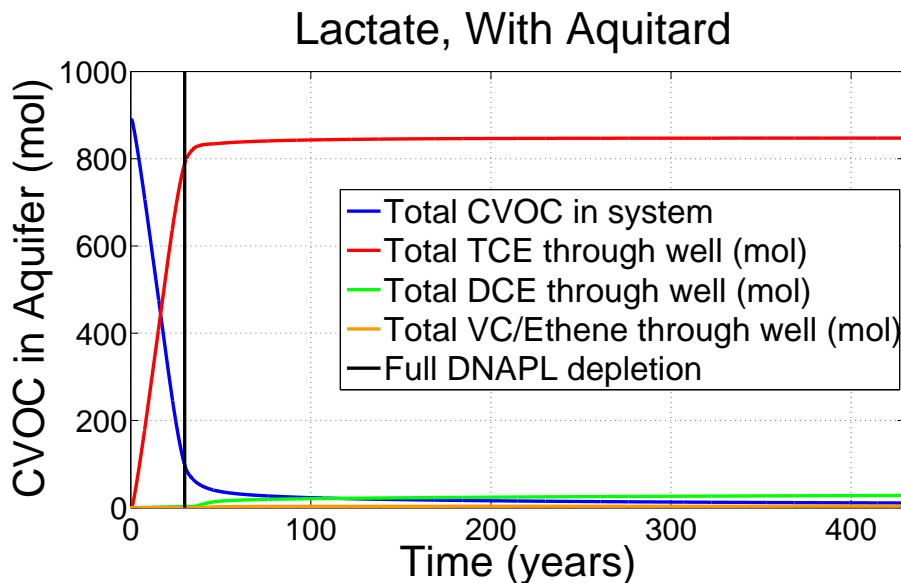
FIGURE 3.24. CVOC mass flux through the down-gradient well from the lactate flush, aquitard-present case over a 430-year time-frame. Note that the dechlorination products VC and ethene are from treatment of cis-DCE (rates calculated in the laboratory modeling study), and are grouped as a single component in the model.

Figure 3.24 shows the mass remaining in the aquifer through time for the lactate treatment. After year 35, the down-gradient arrival of dechlorination products indicate that treatment is occurring. The aquifer contains 10.74 moles of CVOC at year 430, which is 0.34 moles more than the control at this time. This result is interesting because it highlights aquifer assimilative capabilities due to processes such as sorption. In the model, sorption processes limited the releases of treatment daughter products (e.g., DCE) from the aquifer. These result highlights two important points. First, that aquifers can have significant *assimilative capacities* for potential sequestration of contaminants due to sorption and diffusive processes. Secondly, sorption may benefit a treatment by increasing the retention time of the daughter products for microbial dechlorination, which is demonstrated in the significant reductions in the TtC and longevity of down-gradient contaminant concentrations.

Due to the functionality behind the biomass components within *MIN3P*, many simplifications of these types of components have to be made in the model. At field sites, microbial treatments tend to slowly grow outward from injections points at a slower rate than the injected carbon source or the groundwater flow. Due to the model constraints, the model assumes that the microbes are present everywhere within the aquifer at very low populations, and will grow when introduced to lactate. From this, a significant limitation of modeling this type of treatment at the field-scale is the inability of the model to depict the exact migration of an injected microbial inoculum.

3.7.2. No-Aquitard Scenario.

3.7.2.1. *No-Action Control.* The down-gradient monitoring well TCE concentrations for the control in the no-aquitard field-scenario is shown in Figure 3.25. This curve shows a TtC value of 102 years, or 67 years after the three active treatments began. This value is much faster than the aquitard-present case due to the lack of TCE storage and release from an aquitard. The mass of TCE in the aquifer system for this no-aquitard case is shown in Figure 3.26. As with the previous field scenario, the system began with 889.63 moles of TCE in DNAPL form. When the three active treatments began at year 35, 851.4 moles (95.7%) of the total system TCE had already passed through the down-gradient well. This effluent mass is 25.26 moles (2.8%) more than the aquitard-present scenario. At year 35, a portion of the remaining TCE mass is also not stored in the low k zones, but is actively being flushed through the transmissive zones towards the well. Compared to the aquitard-present case, these findings imply that the treatments have to manage a significantly lower amount of stored TCE mass. Finally, only 0.11 moles of TCE remain in the aquifer system at the TtC at year 102. This is a 99.5% decrease compared to the aquitard-present case at the same point in time.
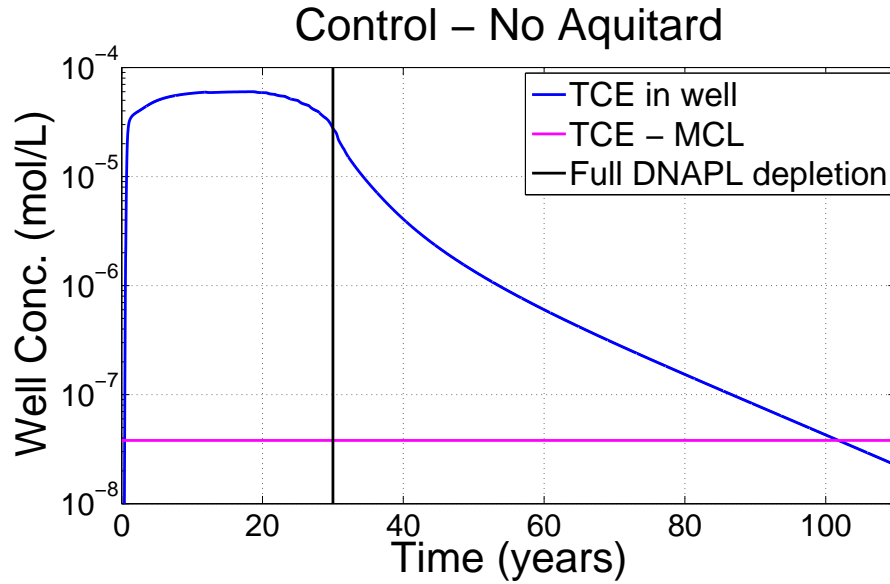
FIGURE 3.25. Control TCE concentrations for a 0 to 15-m screened down-gradient well over a 110-year time-frame, no-aquitard case. Magenta lines represent the MCL for TCE only. DCE and VC MCLs not shown. The vertical black line indicates the time when TCE DNAPL phase is fully depleted. The lack of a lower aquitard has resulted in a 77% reduction in down-gradient TtC from 429 to 102 years. This scenario assumes no natural attenuation is occurring, so actual field outcomes may vary.
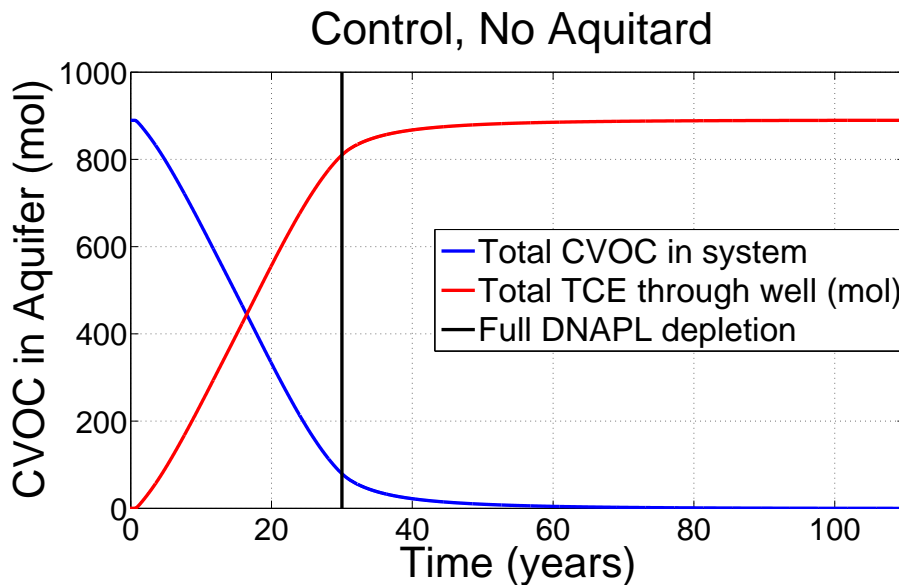
FIGURE 3.26. CVOC mass flux through the down-gradient well from the control, no-aquitard case over a 110-year time-frame.

3.7.2.2. *Enhanced Flushing.* Figure 3.27 shows the monitoring well TCE concentrations for the enhanced flushing, no-aquitard case. The drop in down-gradient TCE at the start of the 5-year flush is obvious, followed by a slight rebound and another large drop once the pumps began again after another 5 years. The second 5-year flush removed enough TCE mass from the aquifer that another rebound afterwards was not observed. Using the pumping scheme shown in Table 3.8, this treatment suggests a TtC value of 44 years, or 9 years after the start of treatment. Measured from the start of treatment, this value represents a 86% decrease in down-gradient TCE longevity. The mass of TCE in the aquifer system through time is shown in Figure 3.28. A large drop in total system TCE after year 35 is observed, which suggests that this type of treatment works well under the no-aquitard scenario.
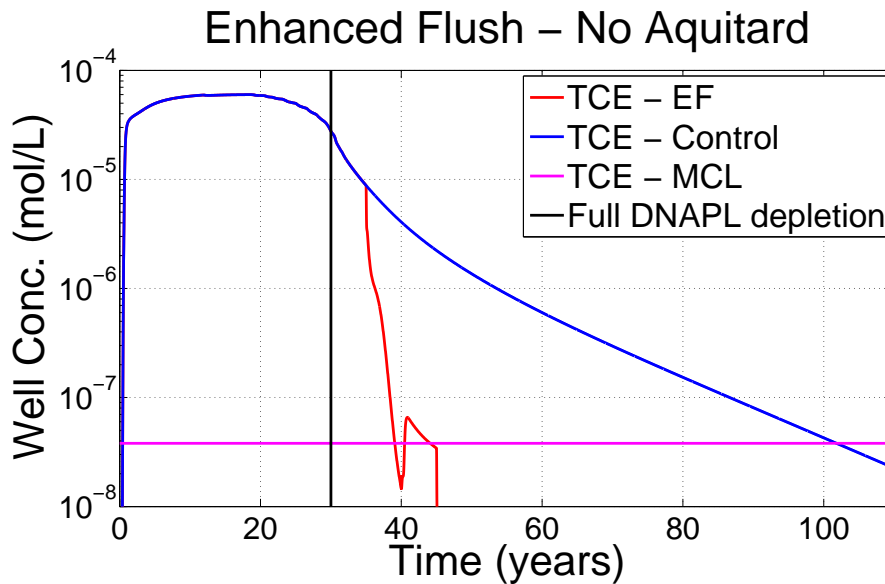
FIGURE 3.27. TCE concentrations in the enhanced flush treatment for a 0 to 15-m screened down-gradient well over a 110-year time-frame, no-aquitard case. The start of the flush at year 35 and end at year 40 are apparent, followed by a further drop from flushing at year 45. For reference, control TCE values are shown in blue. Magenta lines represent the MCL for TCE only. DCE and VC MCLs not shown.
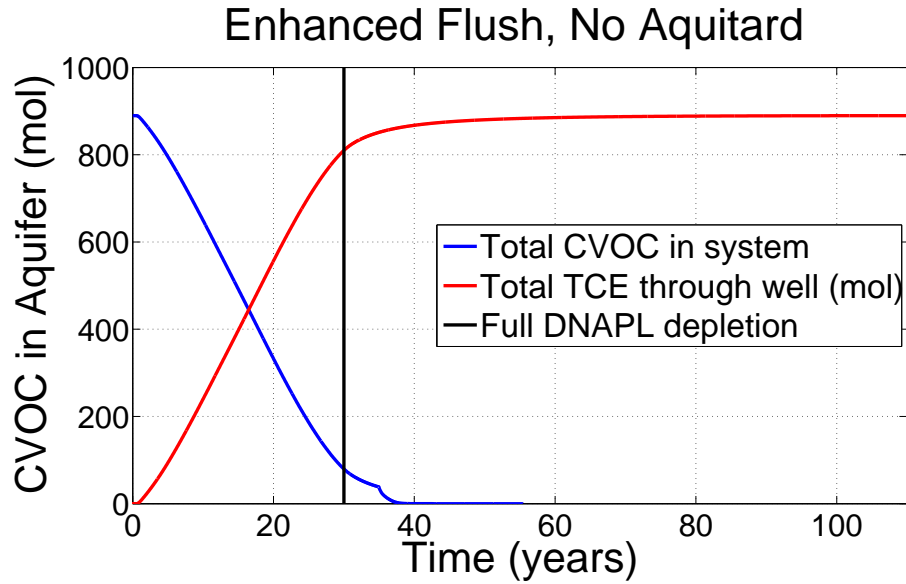
FIGURE 3.28. CVOC mass flux through the down-gradient well from the enhanced flush, no-aquitard case over a 110-year time-frame. The drop in total system CVOC at year 35 from the flushing is apparent.

3.7.2.3. *Permanganate ISCO.* Monitoring well TCE concentrations for the no-aquitard permanganate injection treatment are shown in Figure 3.29. During treatment, concentrations in the down-gradient monitoring well can be seen dropping roughly 1.7 OoM, followed by rebound once the treatment ceased. Measured from the start of treatment, the permanganate injections show a TtC value of 66 years, a 1.5% decrease in down-gradient TCE longevity.
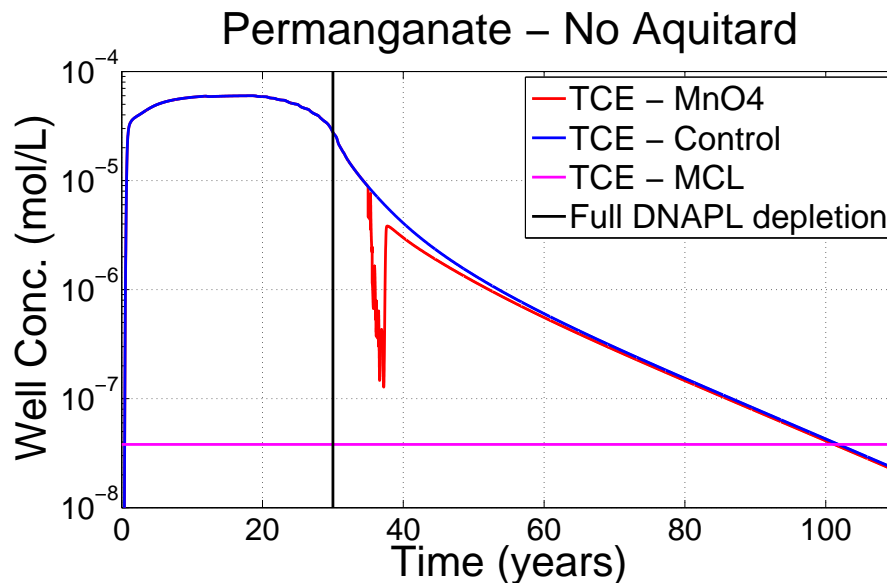
FIGURE 3.29. TCE concentrations in the permanganate treatment for a 0 to 15-m screened down-gradient well over a 110-year time-frame, no-aquitard case. For reference, control TCE values are shown in blue. Magenta lines represent the MCL for TCE only. DCE and VC MCLs not shown. The drop and rebound of down-gradient TCE during and after the permanganate flushing is clear, indicating little advantage to this treatment scheme under these biogeochemical parameters.
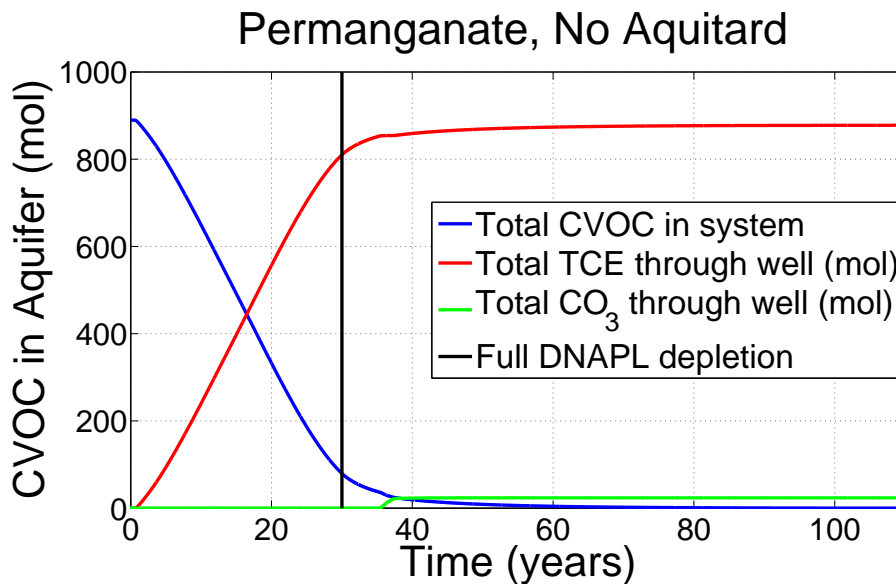
FIGURE 3.30. CVOC mass flux through the down-gradient well from the permanganate flush, no-aquitard case over a 110-year time-frame. Mass flux from the degradation product CO_3 is incorporated.

Figure 3.30 provides the mass of TCE in the aquifer through time. The sharp rise in down-gradient CO_3 after year 35 indicates that oxidation of the TCE is occurring. Overall, results from the permanganate treatments under both scenarios suggest that this treatment will not be very effective at reducing long-term TCE concentrations when these particular low k soils are present. Figure 3.31 shows the MnO_2 deposits left in the wake of the permanganate injections, demonstrating the extent within the aquifer that the permanganate injections impacted. Due to the larger transmissive zone, the volume of these MnO_2 deposits occupies a similar but larger region of the domain compared to the aquitard-present case.
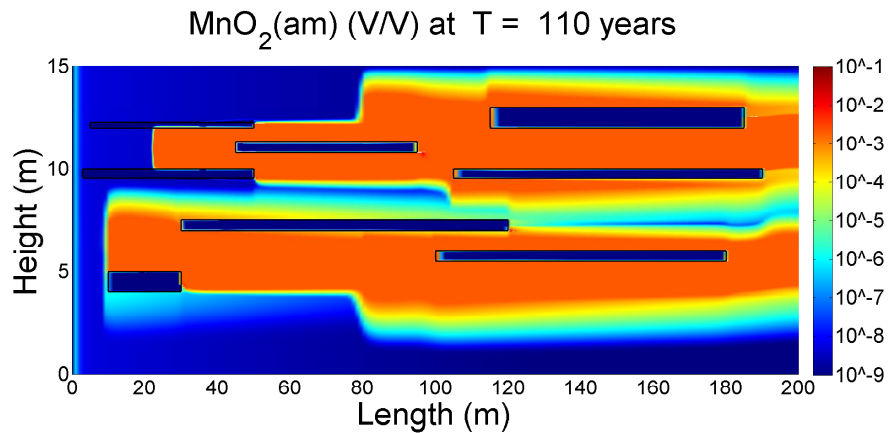
FIGURE 3.31. MnO_2 deposits showing the extent reached by the 3, 1/4 P.V. permanganate injections at 110 years, no-aquitard scenario. The impacted transmissive volume is larger than the aquitard-present scenario, but was still unable to meaningfully impact the low k soils which resulted in a down-gradient TCE rebound after treatment.

3.7.2.4. *Microbial Growth & Dechlorination with Lactate.* Monitoring well TCE concentrations for the lactate injection, no-aquitard field treatment is shown in Figure 3.32. The 3 treatment injections are visually apparent as the sharp changes in down-gradient CVOC concentrations. During each of the 3 injections, dechlorination coupled with increases in flow volume cause down-gradient TCE concentrations to drop roughly 0.25 OoM. Each treatment injection is followed by rebound. Increases in down-gradient DCE and VC/Ethene can be

observed after each injection as the microbes grow in population. Mirroring results from the

laboratory studies, the small spike in down-gradient TCE after the first lactate injection is

indicative of a change in equilibrium sorption conditions within the aquifer. This is likely

due to removal of aqueous TCE resulting in increasing aqueous DCE concentrations.
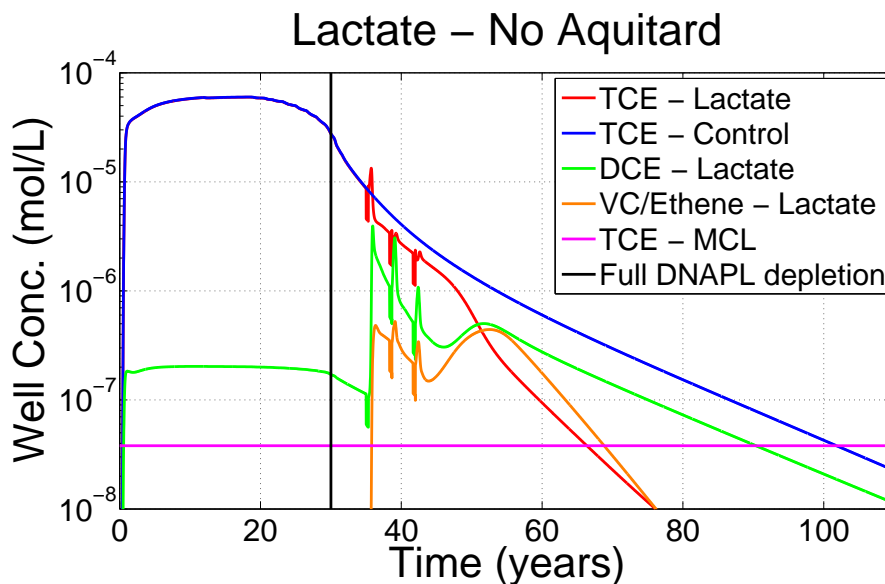
FIGURE 3.32. CVOC concentrations in the lactate flush treatment for a 0
to 15-m screened down-gradient well over a 110-year time-frame, no-aquitard
case. The drops and rebounds in CVOC concentrations during and after each
flushing period are apparent. For reference, control TCE values are shown in
blue. DCE and VC/Ethene concentrations are shown as green and orange,
respectively. Magenta lines represent the MCL for TCE only. DCE and VC
MCLs not shown. The three lactate injections beginning at year 35 are ob-
served, each resulting in an increased biomass population that was able to
impact long-term down-gradient TCE concentrations.

TABLE 3.9. Summary of TtC values and reductions in longevity for the two modeled field-scale scenarios.

Treatment	Aquitard-Present		No-Aquitard	
	TtC (years)	% Reduction	TtC (years)	% Reduction
Control	396	N.A.	102	N.A.
Enhanced Flush	391	0.7	9	86
Permanganate	389	1.2	66	1.5
Lactate	164	58	31.5	53
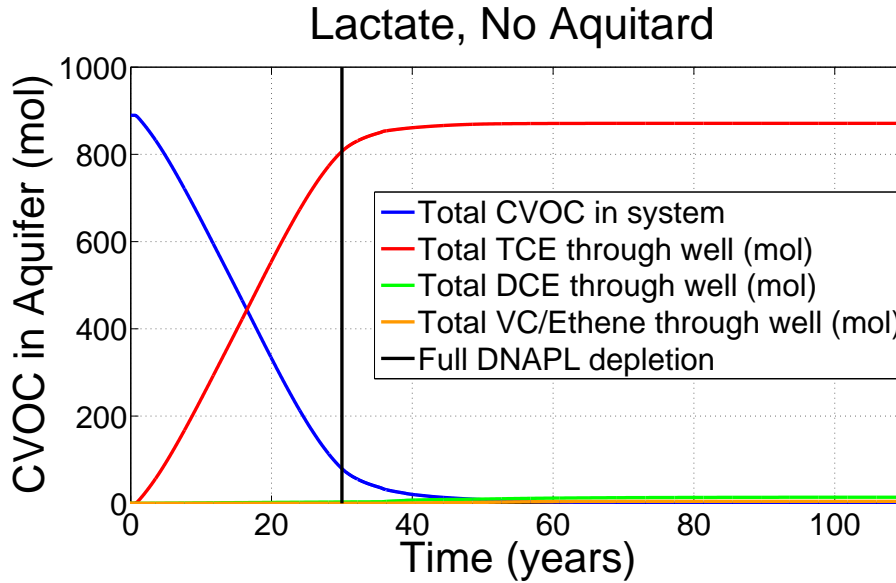
FIGURE 3.33. CVOC mass flux through the down-gradient well from the lactate flush, no-aquitard case over a 110-year time-frame.

Measured from the start of treatment, the lactate injections show a TtC value for TCE of 31.5 years, a 53% decrease in down-gradient TCE longevity. Down-gradient DCE and VC can be seen diminishing as the lactate is flushed down-gradient. CVOC fluxes in the aquifer system through time are shown in Figure 3.33. No large drops in total system TCE are obvious after year 35, indicating a slower treatment as the microbes grow. More concentrated and voluminous injections of lactate may increase the efficacy of this treatment and merits further investigation. Table 3.9 summarizes the modeled TtC values for each treatment for the two field scenarios.

3.7.3. FIELD-SCALE TCE SORPTION. The TCE sorbed mass through time for the field-scale models are shown in Figures 3.34a and 3.34b. By comparing early and late-time sorption data between these two figures, the CVOC storage effects from the aquitard are clear. Within the aquitard-present scenario, Figure 3.34a suggests no meaningful sorbed TCE mass reductions from the enhanced flush or permanganate treatments, but indicates the KB-1 treatment showed promise in reducing sorbed TCE. Observations from Figure 3.34b suggest that there was meaningful removal of sorbed TCE from the enhanced flushing and the lactate treatments, but little advantage to removal of total system TCE through multiple injections of permanganate. Overall, results from these models demonstrate the impacts that aquifer heterogeneities can have on CVOC mass storage, down-gradient longevity, and in constraining the relative performances of common remediation technologies.
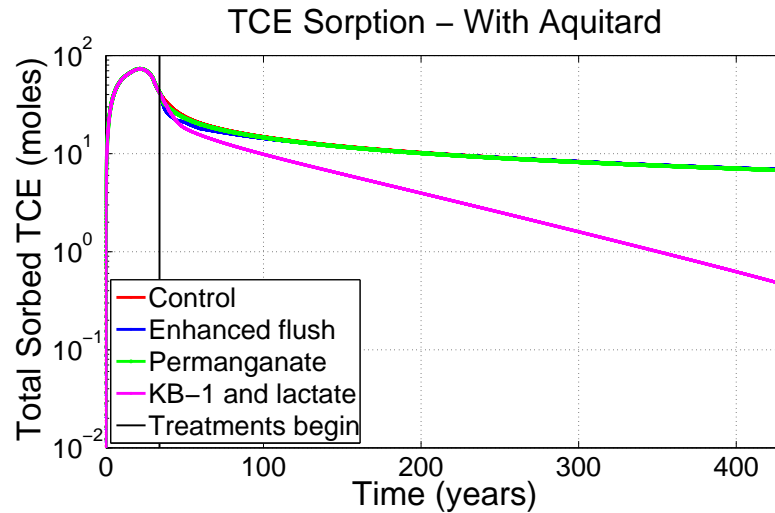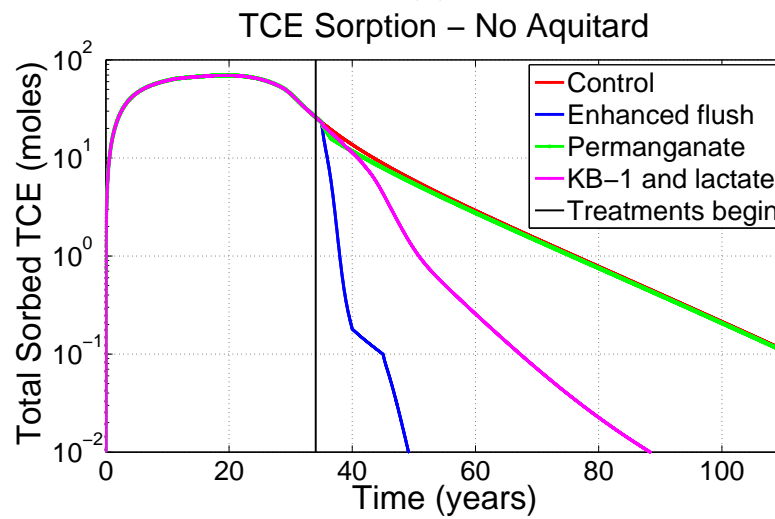
FIGURE 3.34. Modeled field-scale total TCE sorbed mass on the soils through time for A) aquitard-present and B) no-aquitard scenarios. Note the different x-axis values which demonstrate the very distinct amount of storage occurring due to the presence of the low k aquitard.

3.8. SUMMARY AND CONCLUSIONS

Using experimentally and literature derived soil and chemical parameters, numerical simulations using *MIN3P* were able to replicate the evolution of the laboratory treatments TCE and cis-DCE effluent breakthrough curves with varying degrees of accuracy. At both the laboratory and field-scale, the simulations primarily show that even with treatment, the effects

of sorption and chemical diffusion within low k zones can maintain effluent CVOC concentrations above MCLs for extended periods of time. Laboratory-scale modeling of the control tank were close to observed values of effluent TCE over the course of the experiment. The model was also able to produce an increasing effluent DCE concentration due a hypothesized growing microbe population from the impacted the field soils. Modeling a potassium permanganate treatment predicted a significant drop in effluent TCE during treatment. The soil NOD imposed into the model inhibited the penetration of the permanganate into these zones, producing the observed rebound. Precipitation of amorphous MnO_2 was able to reduce the high and low k zone porosity to reduce the slope of effluent TCE after treatment. Modeled DCE values for the enhanced flush and the permanganate treatments were very close to those observed in the laboratory. The model for the KB-1 inoculum and lactate treatment was successful in replicating the drop and subsequent increase of effluent TCE and DCE during and after the lactate injection. The model was also able to account for a deactivation of the microbes once carbon starvation occurred, which resulted in a rebound in effluent TCE. Modeling the last treatment of SRB, lactate and sulfate produced a very good fit to the data during and after the lactate and sulfate flush. By inspecting the timing of the TCE dechlorination, the assumption that the microbes would use sulfate as the preferred electron acceptor to delay TCE dechlorination appears to be justified. Laboratory-scale modeling results suggest that the conceptual models developed as a part of analyzing the laboratory treatments were accurate in the assumptions and insights stated in Chapter 2. These insights include: 1) the natural attenuative capabilities of the soils, 2) the interaction of the permanganate and the oxidant demand of the soils, 3) the location of the KB-1 inoculum for treatment, and 4) the SRB, lactate and sulfate treatment is most likely justified in concluding a biological dechlorination mechanism. Further insights gained

from the lab-scale modeling exercise include chemical and biological reaction rates, mineral-chemical interaction rates, biological growth rates, and maybe most importantly, evidence that *MIN3P* can handle the biogeochemical processes necessary to model these types of treatments in heterogeneous media.

For the aquitard-present field-scale model, five 2-m x 1-cm TCE DNAPL pools caused a down-gradient well to remain above the TCE MCL for over 400 years. At the field-scale, effluent down-gradient monitoring well results showed the relative ineffectiveness of the treatments when an aquitard is present. A second field-scale model was able to quantify the difference on long-term down-gradient concentrations due to the absence of a lower aquitard. Results show that the most likely successful treatment scenario when an aquitard is present is the lactate flushing treatment. In the absence of a lower aquitard, the most successful treatment was an enhanced flushing. These results indicate that the architecture, location and size of the low k zones has an enormous impact on the likely outcome of these considered treatments.

Limitations of the field-scale model include a simplification of field high/low k architecture, as well as the locations and distribution of the dechlorinating microbes. Further limitations of the model include the absence of long-term known (and other unknown) processes that may significantly reduce plume longevity, such as natural microbial or mineralogical attenuation, co-valent bonding, and/or irreversible sorption. These limitations will most likely produce only OoM estimates of treatment outcomes, but are still useful in the determination of *relative* treatment outcomes and highlighting potential problems within treatment schemes. These two contrasting field-scale scenarios highlight the impact that a large low k layer (aquitard) can have on sustaining down-gradient contaminant concentrations, regardless of treatment.

Modeling results indicate that up-scaling the laboratory treatments to the field scale can benefit the user in illuminating unknowns. These unknowns include the scale and locations of contaminants after a prolonged DNAPL release, the distribution of treatment solutions and mineral deposition, or the effects of soil architecture on treatment outcome. Furthermore, field-scale modeling results through time show smaller zones of contamination than down-gradient monitoring wells would suggest. This demonstrates the misleading nature of large-screened monitoring wells for analyzing the extent of subsurface contamination. As a predictive tool, *MIN3P* allows for models to be made significantly more complex in parameters. These parameters include soil architecture, the chemical species present, and the reaction pathways which can help illuminate even more potentially significant biogeochemical processes involved in treatment. Assuming that controlled laboratory experiments are representative of field conditions, the likely OoM outcomes of treatments can be known beforehand. This knowledge can aid in planning better treatment schemes, such as injection locations and the chemical make-up of treatments. These model predictions may provide time and money savings when considering treatments.

CHAPTER 4

THE SIGNIFICANCE OF GROUNDWATER VELOCITY AND SCALE ON HYDRODYNAMIC TRANSVERSE DISPERSION

4.1. CHAPTER SYNOPSIS

The advancement of high-resolution subsurface site-characterization techniques has produced data that demonstrates a potential disconnect between a commonly used definition of transverse hydrodynamic dispersion and field-scale plume evolution. The validity of coupling transverse hydrodynamic dispersion to seepage velocity at the laboratory-scale was investigated in two distinct experiments. The first was an experiment to clarify the validity of using a diffusion-only transverse hydrodynamic dispersion term in a contaminant plane-source model (Bird et al., 1960). Results from this experiment suggest that diffusion alone was unable to account for the observed mass flux emanating from a dissolving gypsum ($CaSO_4$) pool above a flowing transmissive layer. This finding suggests that processes beyond diffusion (e.g., flow-path tortuosity) were at work in transversely spreading the aqueous sulfate. A second experiment developed a method of quantifying the transverse spreading of a fluorescein tracer in a uniform flow field as a function of distance and time. Quantifying the transverse spreading of the fluorescein tracer was accomplished using image-analysis and function minimization techniques provided by *MATLAB*. Results from this second experiment suggest that: 1) the transverse spreading of the fluorescein tracer was non-linear with distance from the source, 2) molecular diffusion alone is not enough to account for the transverse spreading at the chosen seepage velocities, and 3) at a specific time from source, transverse hydrodynamic dispersion within the steady-state plumes seemed to increase as the seepage velocity was increased. Physical explanations regarding this phenomenon are

discussed, and include the presence of non-laminar flow at the microscopic pore-scale due to soil electrostatic forces or flow-path tortuosity. Non-laminar flow at this scale may result in pore-space micro-eddies that can result in enhanced transverse spreading of contaminants perpendicular from the mean flow-path.

4.2. INTRODUCTION

Transverse spreading of miscible solutes in aqueous flow fields has historically been attributed to the effects of transverse hydrodynamic dispersion. Previously used as an explanation for missing contaminant mass or for dilute solute concentrations down-gradient of a source, the recognition of contaminant storage and release from low k zones is driving emerging controversy regarding the magnitude and importance of *transverse* hydrodynamic dispersion in transmissive zones (Chapman et al., 2012). Historically, dispersion has been defined in modeling efforts (e.g., Anderson et al., 1992; Johnson and Pankow, 1992) as the combined effects of molecular diffusion and a mechanical dispersion term. A common formulation of dispersion is shown in Equation 7 (Bear, 1972):

$$(7) \qquad\qquad D_{L,T} = \alpha_{L,T} \cdot v + D^*,$$

where D is dispersion ($L^2 \cdot T^{-1}$), α is the dispersivity coefficient (L), v is the seepage velocity ($L \cdot T^{-1}$), D^* is the molecular diffusion coefficient which accounts for porosity and tortuosity ($L^2 \cdot T^{-1}$), and subscripts L and T represent the longitudinal and transverse directions along the mean flow path, respectively. As Equation 7 demonstrates, mechanical dispersion in modeling studies is mathematically described as a function of the seepage velocity. To account for unknowns in the subsurface, many authors have attempted to estimate both the longitudinal and transverse α as a function of the total travel distance of the solute. It should

be emphasized here that solutes have been repeatedly observed to spread longitudinally with contaminant plumes ahead and behind of the mean groundwater advective front, such as the experiments and mathematical theory proposed in Scheidegger (1957) (and many others). Longitudinal solute spreading has been exhaustively quantified and documented, and will not be addressed in this work.

The phenomenon of *transverse* hydrodynamic dispersion has been historically theorized to cause the solute front to mix into wider and wider transverse offshoots. This includes early work from Slichter (1905), who proposed that variations in pore-space seepage velocities due to surface tension caused a plume front to spread transversely to flow. This concept was advanced with an infiltration study through an unsaturated media done by Danel (1952). This work suggested a tracer expanding with a plume in a 6-degree 'cone'. Figure 4.1 shows the graphical depiction of this work by Danel (1952). Note Figure 4.1 visually portrays a spread of 29-degrees, even though the author was suggesting a 6-degree transverse spread from monitoring well data.

Payne et al. (2008) notes that Bear (1972) rotated Figure 4.1 90 degrees to produce Figure 4.2. Bear (1972) further visually skewed 4.1 to a near 36-degree spread and ignored the idea that 4.1 represented both saturated and unsaturated zone data. As an explanation for the observations of transversely spreading contaminants, Danel (1952) (reproduced by Bear, 1972) presented Figure 4.3. These figures were used thereafter as a qualitative explanation for transverse solute spreading, as important publications and textbooks later used very similar depictions (Freeze and Cherry, 1979; Fetter, 1993).

Using injection and monitoring wells, field data were collected throughout the 1960's, 70's and 80's with the intention of refining the concept of hydrodynamic dispersion. Many of these efforts are summarized in the work of Gelhar et al. (1992), which analyzes the
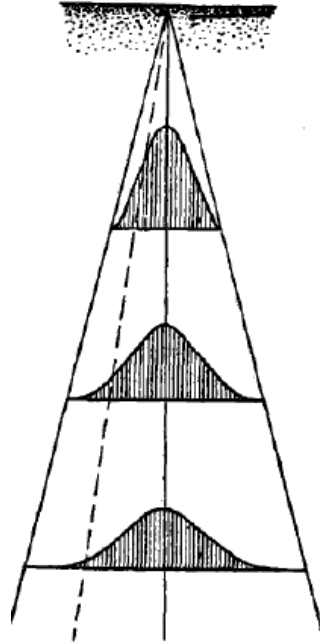
FIGURE 4.1. Pear-shaped solute spreading front in an unsaturated zone as explained by Danel (1952). Danel (1952) states that this type of spreading follows a normal-distribution curve.
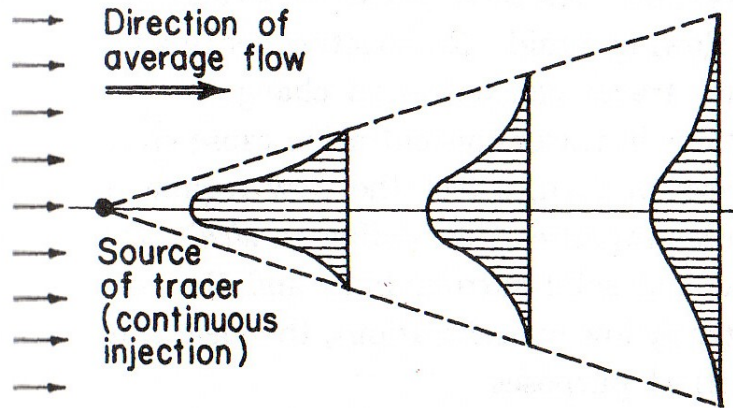
FIGURE 4.2. The evolution of a solute spreading front as explained by Bear (1972), modified from Danel (1952). Reproduced here from Chapter 1 for convenience.

'reliability' of data collected from these field efforts. Gelhar et al. (1992) shows that most of

the data is unreliable. The reasons for this outcome are complex. The primary limitations

appear to be due to the sampling methods used by the investigators. These methods include

artificial spreading and non-uniform flow-fields due to injected reagents, or perceived solute spreading that occurs from mixing in the monitoring wells (Anderson et al., 1992) leading to the perception of dilute concentrations in plumes, not within the formation.
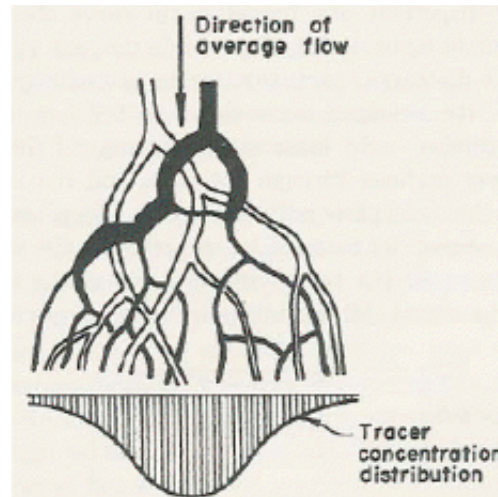
FIGURE 4.3. Bear (1972) showing the bifurcation, mixing and concentration profile of a solute as it advances through a porous media.

Large-scale field studies done by Sudicky et al. (1983), Mackay et al. (1986), Garabedian et al. (1991), Rivett et al. (1994), van der Kamp et al. (1994) and Rivett et al. (2001) in conjunction with the emergence of high-resolution field sampling methods has cast doubt on the linear dependence of transverse contaminant spreading with seepage velocity (Equation 7). For example, in findings from van der Kamp et al. (1994), a chloride plume in a heterogeneous aquifer produced a transverse dispersion of only ≈0.1-m on a 5500-m scale with a groundwater velocity over 1- m/day. This finding is similar to a measured transverse hydrodynamic dispersion value of 0.01-m observed by Rivett et al. (1994) in a field study using an emplaced chlorinated solvent source. Examples of thin plumes measured in field studies are shown in Figure 4.4. Findings such as these highlight the possibility that modeling studies which use Equation 7 as the dispersion parameter may have a flawed conceptualization of governing transport processes. These flaws may have costly real-world consequences. These

consequences include: 1) flawed designs of water quality monitoring wells, 2) a perception of large and dilute plumes where in fact there could be thin plume cores, 3) the selection of a treatment that can fail to achieve anticipated results due to incorrect plume classification, 4) incomplete or improper risk evaluation, and 5) overlooking the concept that thin plumes can cause sufficiently large concentration gradients to exist at large distances from sources, which can drive contaminants into low k zones.

(A)

(B)

(C)
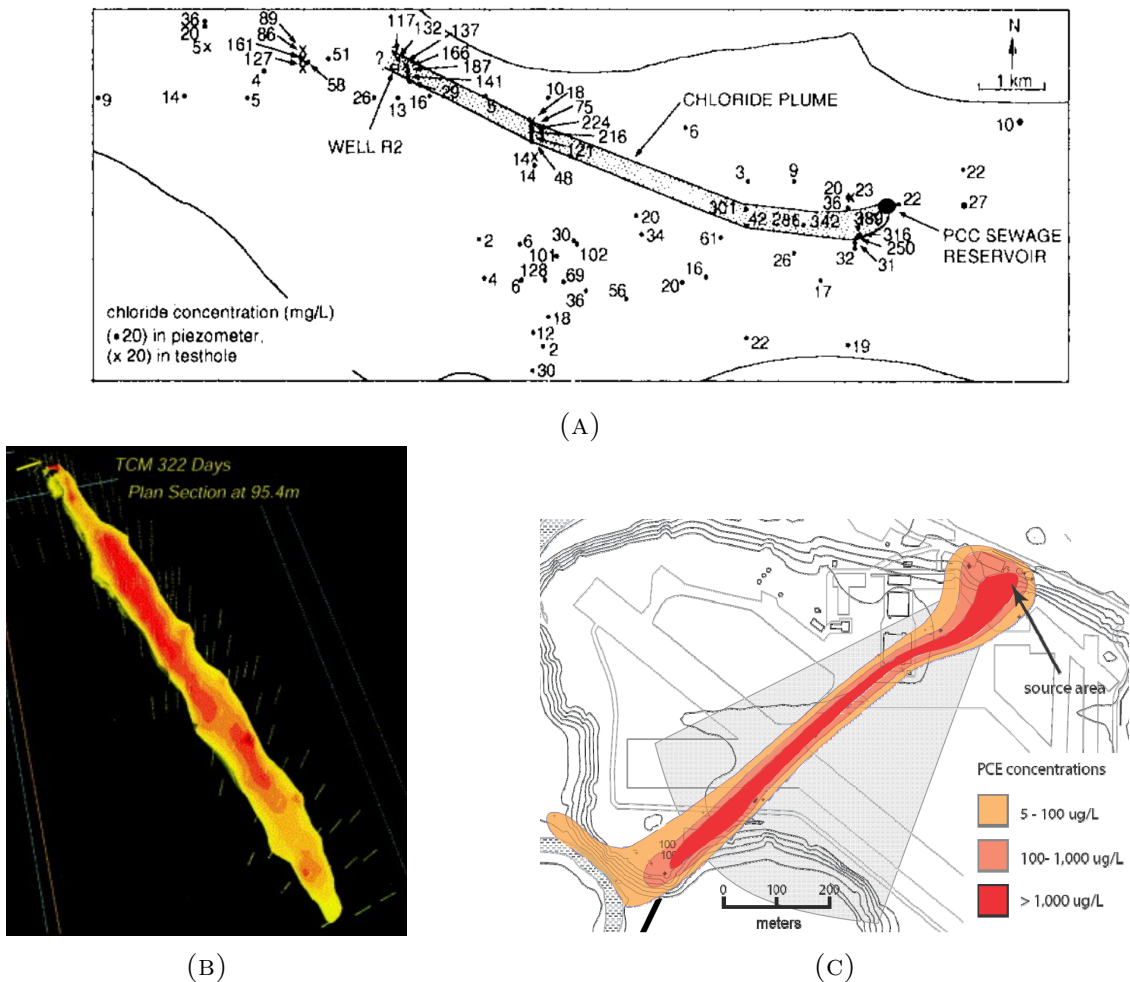
FIGURE 4.4. High-resolution profiling of contaminant plumes from A) van der Kamp et al. (1994), B)Rivett et al. (2001) and from C) a Fort Deven PCE spill (courtesy *Arcadis*). These plumes present a different outcome than would be predicted using the traditional form of Equation 7 in modeling efforts.

Two laboratory experiments to characterize the dependence of transverse hydrodynamic dispersion on seepage velocity were conducted. These studies include: 1) a 1-m long tank experiment that used a range of seepage velocities and source lengths (analogous to NAPL pools) to determine the experimental validity of a model proposed by Bird et al. (1960) and 2) a 1.75-m long tank experiment in conjunction with image analysis software to determine the nature of how a fluorescein tracer in water spread transversely with distance and time from a point-source injection. A limitation of this work is the scale of the laboratory studies, which may dampen the effects of transverse hydrodynamic dispersion when compared to larger domains.

The main objective of this work is to test the hypothesis that diffusion alone is capable of describing how a contaminant will spread transversely when moving through a porous media. This work will furthermore investigate the notion that transverse hydrodynamic dispersion increases with the seepage velocity of the fluid. The vision of this work is that it will aid in advancing efforts currently underway that are addressing the magnitude and importance of transverse hydrodynamic dispersion, which can help support better solutions for managing groundwater contamination at field-sites.

First, a theoretical background on hydrodynamic dispersion and relevant literature is presented. Second, the experimental and analytical methods are discussed. Lastly, the results and discussion from the two laboratory experiments are advanced. Collectively, this work illustrates that the current definition of transverse hydrodynamic dispersion is most likely incomplete, and that the role of dispersion beyond diffusion warrants further consideration. This work also advances a promising non-interfering method of quantifying the transverse spreading of a plume as it evolves through time.

4.3. Theory

The evolution of thinking behind hydrodynamic dispersion is of interest. First, the following subsections provide a brief background and discussion of the historical thinking surrounding miscible solute dispersion, as well as a discussion of current theories and results from large-scale studies done at field sites. Following this background, the theories behind the experimental methods used in this analysis of transverse hydrodynamic dispersion are discussed.

4.3.1. Background. As shown earlier in Equation 7, the phenomenon of hydrodynamic dispersion is traditionally defined by the combined effects of mechanical dispersion and molecular diffusion. Mechanical dispersion refers to *advection* driven spreading of contaminants away from the plume center of mass. In true laminar flow, this behavior could be due to a number of processes which will be discussed shortly. Molecular diffusion is the spreading of solutes due to the random movement of solute molecules from zones of higher to lower concentration.

Broadly speaking, mechanical dispersion can be attributed to mixing due to pore-scale turbulence and velocity gradients resulting from soil heterogeneities (Corey and Auvermann, 2003). Although the exact reasons for solute spreading beyond diffusion are still under debate, Bear (1972), van der Kamp et al. (1994) (and many others) provide some possible explanations: 1) external forces on the fluid, 2) intricate soil geometry, 3) molecular diffusion driven by solute concentration gradients, 4) variations in fluid density and viscosity, 5) chemical and physical processes changing the solute concentrations, 6) interaction of the liquid and solid phases (such as adsorption, deposition and/or ion-exchange), 7) variations

in permeability of the soil structure, 8) the bifurcation of paths tubes at soil particles, 9) pore-space variation in seepage velocities, 10) temperature and density gradients within the fluid, 11) transient flow patterns within the plume, and/or 12) the tortuous nature of flow-paths. Consequently, Bear (1972) suggests that processes such as these can lead to what he termed a 'pear-shaped' solute front (Figure 4.2), which occupies a larger and larger cross-sectional area as it advances with the groundwater.

The theory of a pear-shaped solute-front, however, is not representative of some emerging high-resolution sampling from aged field-sites. Observed thin plumes (see Figure 4.4) could suggest a non-Fickian nature to contaminant transverse spreading, a result suggested in lab work by Levy and Berkowitz (2003). At the pore-scale, steady-state plumes suggest that flow channels in a uniform flow-field tend to transport particles through predefined flow-paths. What is observed at the macro scale is merely the combined interactions of all these geologically distinct paths, as well as a conglomerate of the 12 biogeochemical explanations listed previously. Particles can also transversely spread non-mechanically by 'jumping' between these flow tubes through the Fickian process of diffusion. It should be noted that as a consequence of incomplete knowledge of subsurface biogeochemistry at field sites, dispersion phenomenon has been used as a simple and convenient tool to aid in modeling unknowns. These unknowns include flow paths, complex subsurface geological architectures, and/or source history, location and strength.

4.3.2. EARLY LITERATURE. The concept of dispersion in contaminant hydrology emerged as an explanation for laboratory data collected by Slichter (1905). This work by Slichter (1905) reported transverse spreading of electrolyte tracers in porous media experiments that suggested that diffusion alone was not enough to account for the observed plumes. Slichter (1905) suggests that this phenomenon is attributable to soil particles causing variations in

pore-space seepage velocities, resulting in flow paths that randomly split with the advancing groundwater. Slichter (1905) speculates that the reason for these flow variations is due to surface tension on the soil particles.

Besides having one of the earliest derivations of fluid velocities using Darcy-flow with effective permeabilities, Danel (1952) discusses the dispersion of electrolyte tracers. The author suggests that offshoots of flow-paths in granular media divide the solute tracer into smaller and smaller concentrations. No mention of velocity dependent spreading is discussed at this point. The depiction of this spreading was shown earlier in Figure 4.1, which had been exaggerated in his paper, most likely for illustrative purposes. It is important to note that Figure 4.1 was meant to include data for both a saturated and unsaturated zone, indicating part of the spreading can be attributable to a non-uniform flow field. Danel (1952) proposes an explanation for dispersion behavior beyond diffusion, with what is commonly known as the triangle of Pascal, the Pachinko model, or the random-walk model. This model replaces a porous media with a series of perfect spheres, placed at equal distances from each other. As a particle moves through this field, it has a probabilistic choice of spreading either left or right at each sphere, which after a large number of splits, produces a normal probability curve. It is this type of outcome that has been similarly depicted in other publishings, and is represented by the 3 distribution curves shown in Figure 4.1. This model was later extended to 3-dimensions by Scheidegger (1954). Day (1956) expanded on this model from Scheidegger (1954) to explain laboratory data concerning a salt water injection into a column. The work of Payne et al. (2008) expands on the consequences of the Packinko model with a mathematical analysis of plume size with distance from the source. Findings from Payne et al. (2008) indicate that under the assumptions of the model, which includes no diffusion, it is statistically improbable for a particle to transversely deviate from the mean flow path

(using a two-choice, 2-D system) as far as traditional dispersion would dictate. However, since these types of models require numerous assumptions concerning soil properties and ignore the effects of diffusion, they most likely cannot be considered practical.

Many early studies and modeling efforts concerning dispersion of fluids through flow fields were motivated by studies done with recovery efforts by the oil and gas industry, such as the viscosity-dependent miscible-displacement model developed by Peaceman and Rachford (1962). Many of these early studies were interested on the longitudinal dispersion front observed in laboratory and field sites. These include but are not limited to the work of Yuhara (1954), Rifai et al. (1956) and Scheidegger (1957). Investigators such as Danel (1952) and Taylor (1953) used 1-D flow-tubes to model transport, but due to their overly simplified nature, these models are not considered very useful in complex transport scenarios.

Using conservation of mass, a common 1-D form of the advection-dispersion equation describing a tracer distribution in a flow field is given in Equation 8:

(8)
$$\partial C/\partial t = D_x \cdot \partial^2 C/\partial x^2 - v \cdot \partial C/\partial x,$$

where C is solute concentration (M/L^{-3}), D_x is the dispersion term in the direction of flow (L^2/T), v is seepage velocity (L/T) and x is position (L). Note the Fickian description of the dispersion term 'D', suggesting a concentration driven mechanical dispersion term independent of the numerous explanations described previously. Scheidegger (1957) reasoned that the shape of the 1-D *longitudinal* contaminant front can be represented by an error function (as opposed to a plug flow solution), a finding found by others including Crank (1956) and Ogata and Banks (1961). A particular solution of Equation 8 is presented by

Ogata and Banks (1961) as:

$$\frac{C(x,t)}{C_o} = \frac{1}{2}[erfc(\frac{x-vt}{2\sqrt{D \cdot t}}) + exp(\frac{vx}{D})erfc(\frac{x+vt}{2\sqrt{D \cdot t}})]$$

Scheidegger (1957) was one of the first investigators to look into the possible velocity dependency of longitudinal dispersion. Using a geometric and dynamic approach, Scheidegger (1957) concluded that the magnitude of what was termed the *factor of dispersion* lies between the limits of v and v^2: when there is no molecular diffusion between flow-tubes and when v is small enough for significant solute mixing due to diffusion, respectively. In contrast to later work, Bear (1961) gave mathematical models that could be used to determine what was termed the 'constants' of longitudinal and transverse contaminant spreading through the use of variance in the bivariate normal distribution. Scheidegger (1957) concluded that a dispersion constant, D, could be used which is independent of seepage velocity and depends only on the geometry of the pore channels and on the qualities of the porous media.

Harleman and Rumer (1963) published findings from studies that found an empirical relationship between longitudinal and transverse hydrodynamic dispersion:

$$\frac{D_L}{D_T} = \lambda \cdot Re^n,$$

where Re is the Reynolds numbers, D_L and D_T are the longitudinal and transverse hydrodynamic dispersion (defined previously), respectively, and λ and n are dimensionless coefficients which are dependent on the pore geometry. Blackwell (1962) measured dispersion through sand-packed columns and found that for both longitudinal and transverse hydrodynamic dispersion, 'low' flow-rates were diffusion dominated, and conversely dominated by convection at high flow-rates. As an interesting point to correlate the transverse and longitudinal

dispersion values, Blackwell (1962) furthermore reports a ratio for transverse to longitudinal dispersion of 1:24. This type (not value) of correlation later became common practice in modeling the dispersivity coefficients.

The work of Perkins and Johnston (1963) furthered the idea that dispersion in porous media may be larger than from just diffusion processes. As many investigators before them, results from Perkins and Johnston (1963) also point to the possibility of velocity dependent longitudinal dispersion. Perkins and Johnston (1963) reason that at 'low' flow-rates, interstitial transverse hydrodynamic dispersion is diffusion dominated, but at 'high' flow-rates a transition occurs so that stream-splitting is dominant and diffusion can no longer 'damp-out' concentration variations in the pore-space. As with Bear (1972), Perkins and Johnston (1963) proposed that there are many variables that can influence overall dispersion, such as particle shape and size, heterogeneities and turbulence. Perkins and Johnston (1963) suggest that due to these types of experimental variables, a problem in objective interpretations of literature findings concerning true dispersion values arose.

Bear (1972) provides an extensive literature review of many examples of published tube, cell and statistical-type dispersion models from around this period. Bear (1972) concluded after an extensive mathematical analysis of various approaches and schemes relating dispersion and seepage velocity that the 'D' in Equation 8 is a sum of mechanical dispersion and molecular diffusion. Bear (1972) suggested the overall term for dispersion could be given as Equation 7, reproduced here:

$$D = \alpha \cdot v + D^*$$

Bear (1972) states that α is a numerical constant (defined previously) which may be a function of the porous media and the Reynolds Number. Separate values of 'D' are often applied to the horizontal, transverse and vertical direction to flow. Developments in the literature

of Equation 7 have resulted in some commonly used relationships between dispersion, scale and the dispersivity coefficients. Modifications of the equation for longitudinal dispersion are often used to define transverse hydrodynamic dispersion. These relationships are shown in the following equations:

$$D_L = \alpha_L \cdot v + D^*,$$

$$\alpha_L \approx .1 \cdot L,$$

$$D_T = \alpha_T \cdot v + D^*,$$

$$\alpha_T = \beta \cdot \alpha_L,$$

where α_L and α_T are the hydrodynamic longitudinal and transverse dispersivity coefficients (L), respectively, L is the domain length (L), and β is a constant that has typically been assigned literature values that vary from 0.01 to 0.33 and higher. It is these mathematical descriptions of dispersion used within solutions to Equation 8 that has pervaded modeling and treatment efforts for decades (Gelhar et al., 1992). More papers concerning the mathematical modeling of dispersion were published around this time (such the work of Saffman, 1960; Simpson, 1962, 1969, Gelhar et al., 1979), but the findings and perspectives were similar to those already discussed. The authors wish to simply convey the historical mindset that has guided the research of this phenomena during the decades that followed.

4.3.3. FIELD-SCALE EXPERIMENTS. Beginning with the Stanford-Waterloo experiment at the Canadian Forces Base Borden, Ontario, Mackay et al. (1986) provided a field-scale demonstration of the emergence of a plume with very minimal transverse spreading after a pulse injection. The measured plumes through time are shown in Figure 4.5. After this finding by Mackay et al. (1986), controversy and interest grew around the traditional viewpoint
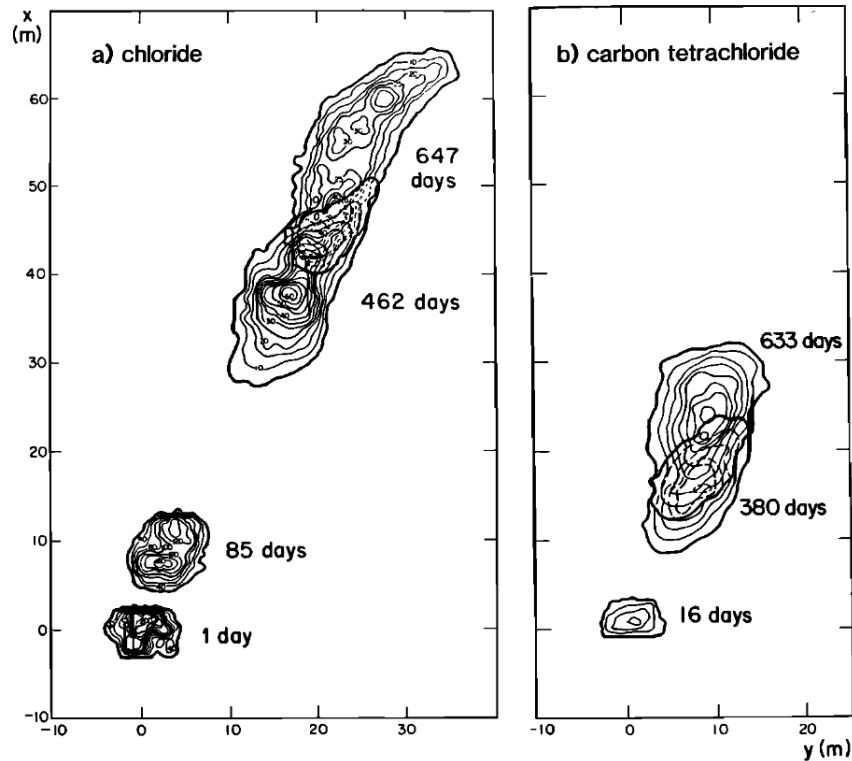
FIGURE 4.5. Concentration profiles through time of chloride and carbon tetra-chloride plumes from Mackay et al. (1986).

that transverse hydrodynamic dispersion will actually lead to the large and dilute plume situation shown in Figure 4.2. Numerous other field studies have been done with similar results showing minimal transverse spreading, such as those by Sudicky et al. (1983), Rivett et al. (1994), van der Kamp et al. (1994) and Rivett et al. (2001). With a groundwater velocity of 40 cm/day in a sand and gravel aquifer, Garabedian et al. (1991) observed a 1.8-cm transverse horizontal dispersion (from the bromide center of mass) over a 280-m sample distance, or roughly 50 times smaller than the observed longitudinal dispersion of 1-m on the same test. One important conclusion drawn from the work of van der Kamp et al. (1994) was that an observed transverse spreading of an emplaced DNAPL source was due to the uniquely steady flow of the aquifer. This conclusion was theorized earlier in the work of Rehfeldt and Gelhar (1992), and suggests that the outside influences from discharge and recharge into

aquifers may have a larger impact on dispersion than had previously been thought. Some investigators have even shown that larger seepage velocities correlate to a decrease in transverse spreading (Delgado and de Carvalho, 2001; Cirpka et al., 2006). Findings such as these should in the least cast a certain level of doubt for the situation shown in Figure 4.2 and the strict use of Equation 7 in modeling the transverse spreading of contaminant plumes.

4.3.3.1. *Field-Scale Data Summary.* Throughout the 1970's, 80's and 90's, numerous papers were devoted to the field measurement, estimation and modeling of dispersion, and a comprehensive review of this work is beyond the scope of this work. Two decades after Bear (1972) was published, Gelhar et al. (1992) produced an extensive review on the *reliability* of 59 published field longitudinal, transverse and vertical dispersivity values. From this review, Gelhar et al. (1992) was able to produce some interesting results. The authors tabulated the data according to parameters such as: aquifer type, hydraulic properties, aquifer saturated thickness, effective porosity, pore velocity, dimensionality of monitoring network, flow and tracer type, scale of observation, longitudinal, transverse and vertical dispersivities (α_L, α_T and α_V), and maybe most importantly, the *method of data acquisition* and interpretation. Scrutinizing the data collection and analysis methods of each paper, Gelhar et al. (1992) were able to classify the published findings and data from these 59 sites into 3 categories of reliability; low, intermediate and high. The mathematical methods for determining this reliability scale is discussed at length in the paper.

Concerning the coefficient of longitudinal dispersivity, one important finding from from Gelhar et al. (1992) was that α_L had an increasing overall trend with plume length, but that all of the reported upper values were determined to be of low reliability, whereas the lower values of α_L tend to be rated at high reliability. Gelhar et al. (1992) note that at a given scale, longitudinal dispersivity ranged from 2 to 3 orders of magnitude. The authors

concluded that although one could apply a linear regression to the α_L data, it would be irresponsible to do so. Rather, a family of curves that are more dependent on the individual aquifer properties should be used. This finding highlights some of the problems with a strict velocity and scale-dependence interpretation of this phenomenon.

Since this research is focused on the role of transverse hydrodynamic dispersion, the data collected by Gelhar et al. (1992) on α_T is of a higher interest. Analyzing the same data from the 59 sites for transverse dispersion, Gelhar et al. (1992) were able to illuminate some interesting behaviors. Figure 4.6 shows the plot of the horizontal transverse dispersivity (α_T) values from the 59 papers, and their respective reliability rating.
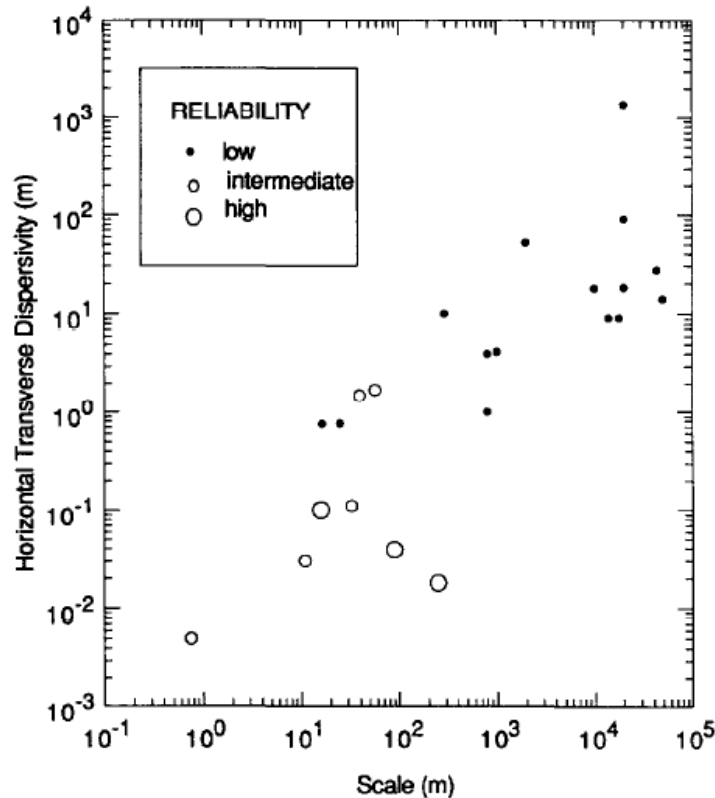
FIGURE 4.6. Horizontal transverse dispersivity versus scale of test, classified by reliability (Gelhar et al., 1992). Note the lack of reliable data at large-scales and transverse dispersivities.

Figure 4.6 demonstrates that data rated as high reliability tends to fall in the lower range

of values for horizontal transverse dispersivity, with the largest scale of data at 250-m with

an α_T value of 0.018 m with a 0.43 m/day groundwater velocity, taken from Garabedian et al.

(1988). Another high reliability data point was taken from the work of Freyberg (1986) in

the Borden aquifer that showed a 0.039 m D_T value for a 90 m long test with a groundwater

velocity of 0.09 m/day. From Figure 4.6, it's also clear that even the intermediately reliable

points for D_T in the analyzed literature tend to stay in the range of <2m for scales near

100-m, which is a drastically smaller solute spread than Figure 4.2 would lead investigators

to believe. Overall, a clear and distinct correlation between seepage velocity, scale and

transverse dispersivities is not observed within the analysis by Gelhar et al. (1992).

Gelhar et al. (1992) also plotted their data (not shown) to demonstrate the limitations

of models that use the simplification of a constant faction of longitudinal dispersivity to

transverse and vertical dispersivity coefficients, which appears to be completely unjustified.

The authors were able to show a vast range of ratios that these dispersivity ratios exhibit at

the 59 field sites, which is understandable once the bigger picture of aquifer characteristics

(e.g. soil type, heterogeneities) are considered.

4.3.4. THEORY OF THE CONTAMINANT PLANE-SOURCE MODEL. The following presents a mathematical model (Bird et al., 1960; Hunt et al., 1988) that will be used in the first experiment to analyze transverse hydrodynamic dispersion. Figure 4.7 presents a 2-D system of a contaminant pool diffusing into a uniformly horizontally moving fluid, along with the assumed boundary conditions. Since dispersion determines the rate at which the contaminant particles will migrate away from the contaminant/water interface (Anderson et al., 1992), laboratory analysis of this model provides a useful tool to analyze the effects of dispersion at this scale. Bird et al. (1960) develop a form of the heat equation as a partial differential equation to arrive at a solution for the contaminant concentration, C_{aq}, for any point in the x-z coordinate system at steady-state. The solution to this PDE is shown in Equation 9.

(9)
$$C_{aq}(x, z) = C_{sol} \left(1 - erf \left(\frac{z}{2} \sqrt{\frac{v_w}{D_T \cdot x}} \right) \right),$$

where C_{sol} (M/L^3) is the aqueous solubility of the contaminant, D_T is transverse dispersion (L^2/T), v_w is the seepage velocity (L/T), and x and z are the spatial coordinate points (L). The complete derivation of this solution is provided in Appendix A at the end of this document.

Equation 9 provides insight into potential concentration profiles for this scenario, which are shown in Figure 4.8. The solute used at z=0 in Figure 4.8 is sulfate (SO_4^{-2}) from a gypsum ($CaSO_4 \cdot 2H_2O$) source. Sulfate has an aqueous solubility of around 2000 mg/L (literature values vary). Low seepage velocity values were used to produce these demonstrative graphs, as higher fluid velocities would not illustrate the dissolution of the sulfate pool into the transmissive zone as well. From Equation 9, the sulfate mass flux off of the gypsum source

127
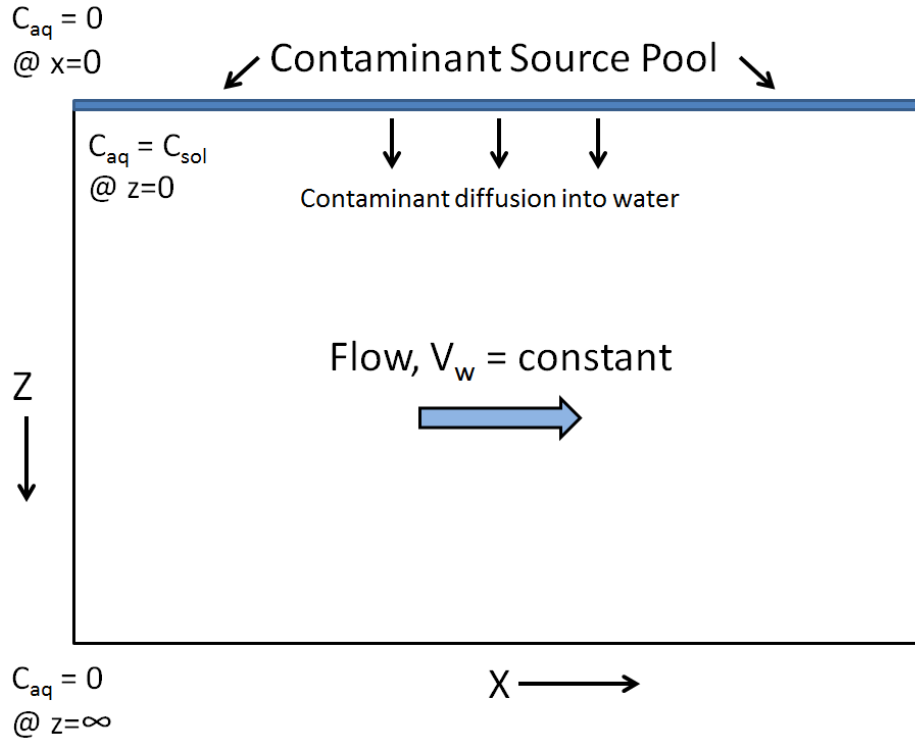
FIGURE 4.7. Conceptual model of solute diffusion from a pool (Bird et al., 1960). The contaminant source pool is dissolving into a homogeneous transmissive flowing soil, resulting in a measurable mass flux from the pool. Note that depth, D, is into page as y-axis.

pool at steady-state (i.e., no retardation) can be calculated using:

$$J_z(x) = \phi \cdot D_T \cdot \frac{\partial C_{aq}(x, z)}{\partial z},$$

where:

$$\frac{\partial (C_{aq}(x, z))}{\partial z} = \frac{\partial}{\partial z} \left(C_{sol} \left(1 - erf \left(\frac{z}{2} \sqrt{\frac{v_w}{D_T \cdot x}} \right) \right) \right) = -\frac{C_{sol} \cdot e^{-\frac{z^2}{4 \cdot D_T \cdot x}{v_w}}}{\sqrt{\frac{D_T \cdot x \cdot \pi}{v_w}}}$$

At the source/soil interface (z=0):

$$\frac{\partial C_{aq}(x, 0)}{\partial z} = -\frac{C_{sol}}{\sqrt{\frac{D_T \cdot x \cdot \pi}{v_w}}}$$
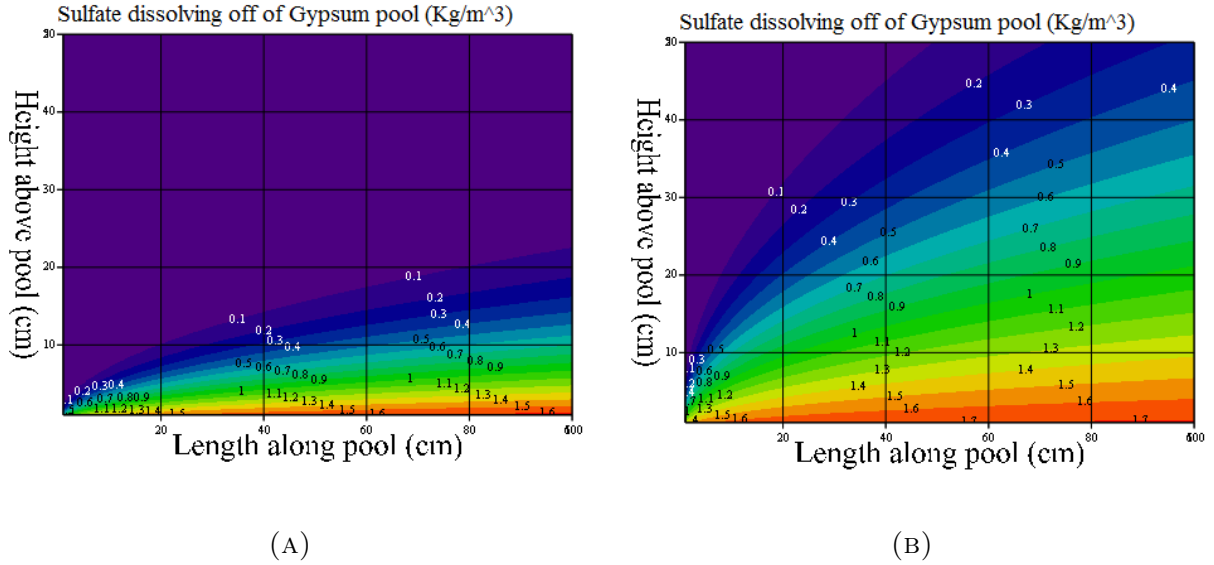
FIGURE 4.8. Concentration profile (kg/m³) of sulfate for Equation 9 with seepage velocities of A) 0.5 and B) 0.05 m/day using a 1-m pool length. Note that the contaminant pool is flipped along the z-axis from Figure 4.7. B) represents a violation of the a boundary condition, and is shown only for the purpose of illustrating the theoretical sulfate plume.

The flux of contaminant off the pool into the transmissive zone at any position x becomes:

$$(10) \qquad J_z(x) = \phi \cdot C_{sol} \cdot \sqrt{\frac{D_T \cdot v_w}{\pi \cdot x}}$$

Equation 10 produces Figure 4.9, which displays the flux of SO_4^{-2} for various groundwater velocites relative to distance along the pool. Notice how the mass flux rate decreases as the x-position along the pool increases due to the decreasing concentration gradient.

From an experimental perspective, this model can be tested by measuring the total mass leaving the source pool over a given time-frame. The total mass leaving the pool into the transmissive zones is derived by taking the area integral of the flux (Equation 10) off the source pool (for generic source pool depth, D):

$$Q_{mass} = \int_0^L \int_0^D \phi \cdot C_{sol} \sqrt{\frac{D_T \cdot v_w}{\pi \cdot x}} \, dy dx,$$

129
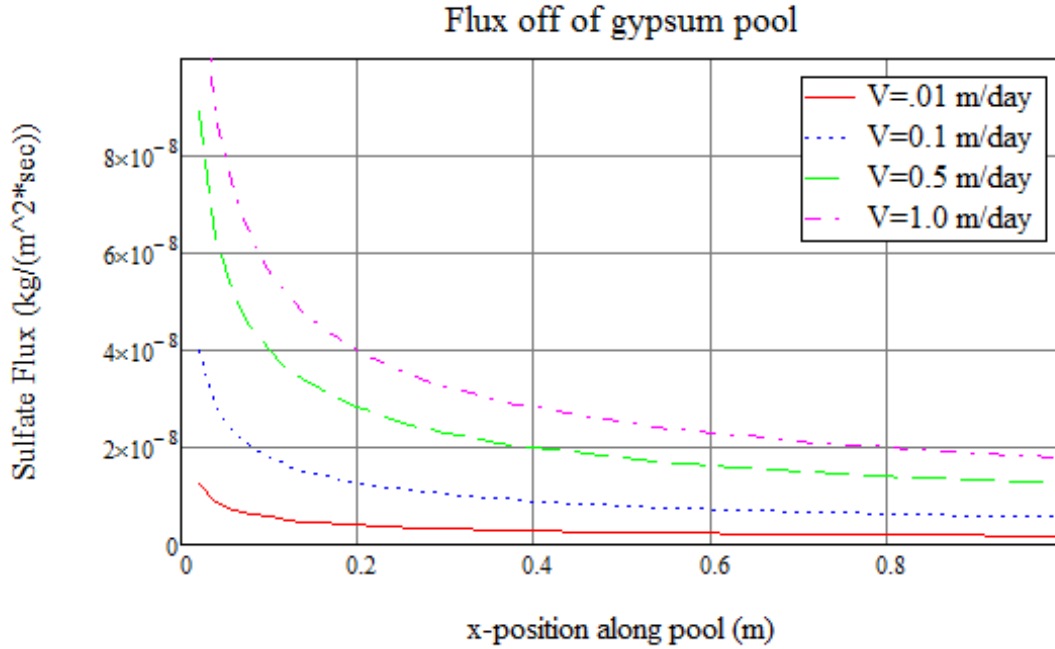
FIGURE 4.9. Sulfate flux $(kg/(m^2*sec))$ off of a 5-cm long, 2.54-cm wide gypsum pool. 4 sample velocities are shown (ϕ=0.38, D_T=5.6E-10·$(\phi)^{1/3}$ m^2/sec). This formulation for D_T is from (Millington and Quirk, 1959). Note the change in sulfate flux off of the gypsum pool with distance along pool due to a decreasing concentration gradient, which is shown visually in Figure 4.8.

$$(11) \qquad Q_{mass} = 2 \cdot D \cdot \phi \cdot C_{sol}\sqrt{\frac{L \cdot D_T \cdot v_w}{\pi}},$$

where L (L) is the pool length along the x-axis. For illustration, Equation 11 produces Figure 4.10. This figure shows the rate of sulfate mass dissolving from the gypsum pool for 4 different gypsum pool lengths, with the groundwater velocity ranging from 0 to 2.5 m/day. The experimental validity of this theory will be tested by comparing the experimental results to Equation 11 using a diffusion-only transverse dispersion term. This diffusion-only dispersion term is shown in Equation 12 (Millington and Quirk, 1959):

$$(12) \qquad D_T = D_m \cdot \phi^{\frac{1}{3}},$$
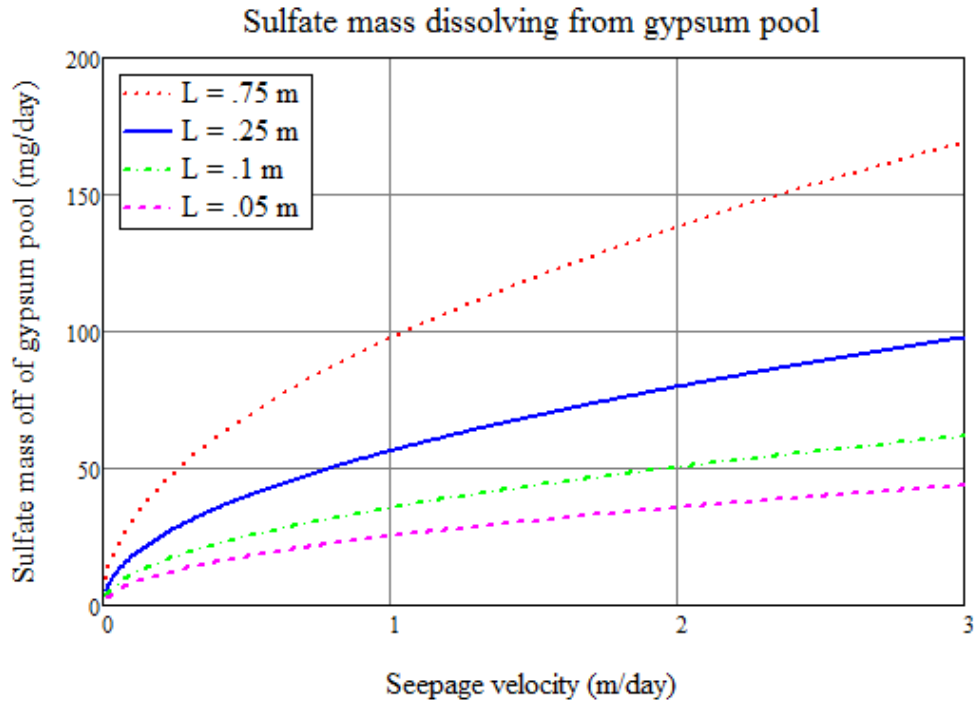
FIGURE 4.10. Mass of sulfate (mg/day) off of 4-different gypsum pool lengths (L) over 0 to 2.5 m/day groundwater velocities. Notice the non-linear increasing trend in mass off of the gypsum pool with increasing seepage velocity.

where D_m is the coeffecient of molecular diffusion ($L^2 \cdot T^{-1}$). Depending on the model's fit to the experimental data, conclusions can be drawn about the nature of D_T at this scale.

4.3.5. THEORY OF QUALITATIVE ANALYSIS OF TRANSVERSE DISPERSION USING FLUORESCEIN. The visual characteristics of a fluorescein tracer under ultra-violet light in conjunction with the visual-analysis software provided in *MATLAB* offers a unique way to measure transverse spreading through a saturated porous media. After a sufficiently large number of interactions with the soil media, steady-state solutions of the advection-dispersion equation (Equation 8) suggest that the transverse spreading of a point-source contaminant should have the characteristics of a normal-distribution curve (Danel, 1952; Bear, 1961, 1972). This behavior suggests a Fickian nature to transverse contaminant spreading. To

131

test the experimental validity of this theory, the transverse spreading of fluorescein plumes can be quantified using image analysis and function-minimization techniques.

Using *MATLAB*, pixel data from the images taken of a steady-state fluorescein plume can be separated into red, green and blue-intensity matrices. Using the green-intensity values in conjunction with function-minimization algorithms, a normal-distribution curve can be fit to the intensity data for each of the transverse cross-sections of the plume. The normal-distribution function used in this analysis is of the form:

$$(13) \qquad f(x) = \frac{1}{\sigma} \cdot \exp(-\frac{(x-\mu)^2}{2\sigma^2}),$$

where μ is the mean and σ is the standard deviation. The intensity data is minimized against Equation 13 by iterating the values of μ and σ until a minimum threshold is reached. A comparison of the σ values at each vertical-section in the plumes allows for an analysis of transverse hydrodynamic dispersion through various seepage velocities.

Lastly, since the seepage velocities are known, each transverse section in the plumes can be put in terms of time and distance from the point-source. This allows a better determination of (any) differences in transverse spreading at any given time, eliminating the element of time-dependent diffusion. Differences in transverse spreading of the fluorescein between the different seepage velocities, therefore, would need to be accounted for elsewhere in other spreading processes. The exact details of the experimental methods used to analyze the transverse hydrodynamic dispersion of fluorescein in a flow-field is explained in more detail in Sections 4.4.2.1 and 4.4.2.3.

4.3.6. FURTHER EXPLANATIONS FOR DISPERSION: SURFACE-TENSION INDUCED FLOW.

Gradients in surface tension can cause what is known as the Marangoni effect, which transfers mass along interfaces between physical mediums. A commonly observed example of this phenomenon is the swirling particle movements within an inhomogeneous solution of alcohol and water due to the lower surface tension of alcohol. At the micro-scale, particles circulating in micro-eddys have been observed at interfaces of varying surface tension in the work of Wang et al. (1993) and Xu and Luo (2007). As an explanation for dispersion beyond the historical theories identified in Section 4.3.1, gradients in surface tension between the water, solute and soil particles could result in what could be described as pore-scale micro-eddys. Theoretically, these micro-eddys could increase solute mixing throughout a pore-space, resulting in a 'stepping' of the transverse concentration profile as the particles move between pores. The scale of these micro-eddys can furthermore be enhanced by the effects of tortuosity experienced by the particles as they moves through complex pore-channels. At the pore-scale, investigations into the validity of this phenomenon could be captured using specialized cameras and lighting equipment. Lastly, micro-eddys (or fluid rotation) can theoretically also result from gradients in viscous shear forces due to fluid heterogeneities at the edges of plumes (Corey and Auvermann, 2003), an idea that deserves further experimental consideration.

4.4. EXPERIMENTAL METHODS

This section describes the experimental and modeling methods used in the setup, execution and analysis of the two laboratory dispersion experiments.

4.4.1. SETUP OF PLANE-SOURCE MODEL.

4.4.1.1. *Laboratory Tank Setup.* The plane source model proposed by Bird et al. (1960) was tested using 1-m x 0.5-m x 2.54-cm sized laboratory tanks filled with washed 20-40 silica sand (Carmeuse Natural Chemicals, Colorado silica sand). Soil classification tests showed that these sands have a porosity of 0.38 and a hydraulic conductivity of 0.2 cm/sec. The tank is made of a stainless steel backplate and a reinforced glass frontplate. The sands were placed into the tank saturated, and are kept in place between the back and frontplates using 3 aluminum gasketed sidewalls. The top of the tank was sealed during the flushing phase to minimize evaporative losses through the exposed portion of the sand. Following the precedent set by Schwille and Pankow (1988) and Whelan et al. (1994), Figure 4.11 depicts the setup used in this first experiment.
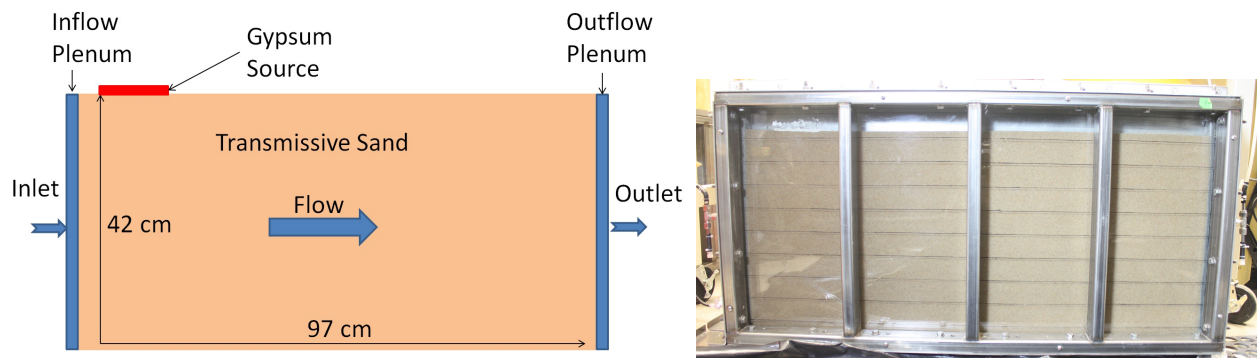
FIGURE 4.11. Laboratory setup of the water flushing through a transmissive sand under a gypsum source pool (setup following Schwille and Pankow (1988) and Whelan et al. (1994)) to test the Bird et al. (1960) plane-source model. The gypsum pool is shown in red (length will vary), and water will flush left to right through the tank. The right-hand side is the effluent and serves as the sampling point to determine the sulfate mass flux off of the gypsum source pool.

The actual emplaced sand dimensions are 97-cm x 42-cm x 2.54-cm, with 1-cm tall x 2.54-cm deep stainless steel screens at each end to maintain the influent and effluent plenums that spanned from the bottom to top of the tank. The tank is placed such that de-gassed, de-ionized tap water (Fort Collins, Colorado) was flushed through the tank from

left to right. The inlet was kept at a constant head by means of a carboy using a mariotte syphon. The outlet was attached to a positive-displacement pump (Fluid Metering Inc., Model RHSY), which controlled the seepage velocity through the sand. A saturated gypsum source pool ($CaSO_4 \cdot 2H_2O$, Alfa Aesar, 99%) was placed on top of the sands at 4 different lengths throughout the experiment: 5, 10, 25, and 75-cm. The seepage velocity through the tank was changed 4 times for each pool length: 25, 50, 100 and 250 cm/day. This created a set of 16 data points for analysis of sulfate dissolution for fit to the plane-source model. Figure 4.12 shows a top-view of a sample gypsum pool (10-cm shown).
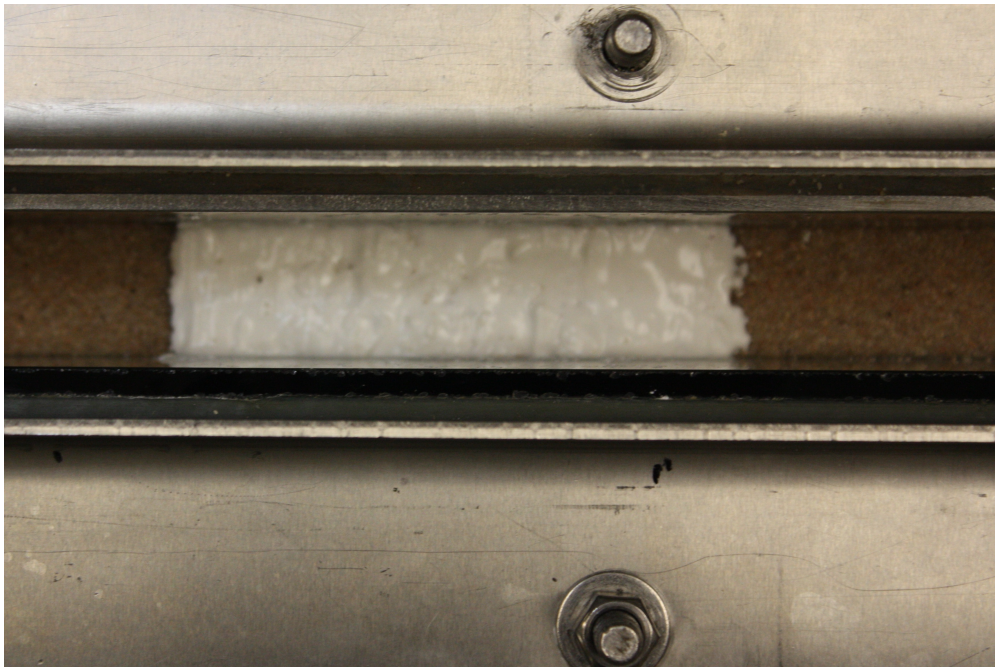
FIGURE 4.12. Setup of a sample gypsum pool (0.1-m) atop the sands (viewed from above, looking downward).

Effluent steady-state conditions were determined by modeling the system using the reactive-transport code *MIN3P*. Using a diffusion coefficient of 5.6e-10 m^2/sec (Mullin and Nienow (2002)), in conjunction with known soil parameters, down-gradient sulfate concentration profiles are shown in Figure 4.13. This figure uses a 10-cm long gypsum pool. All

model runs of the other 3 pool lengths (5, 25 and 75-cm) showed nearly identical steady-state behavior. This plot suggests that effluent sulfate concentrations are not predicted to significantly change after 2.5 P.V.s, so effluent samples were taken only after 3.5 P.V.s had elapsed through the tank. Once steady-state had been reached (≥ 3 pore volumes), aqueous sampling to measure the dissolution of SO_4^{-2} from this pool was done using flow-through sample vials located down-stream of the positive-displacement pumps. These samples were stored at 4°C until analysis.
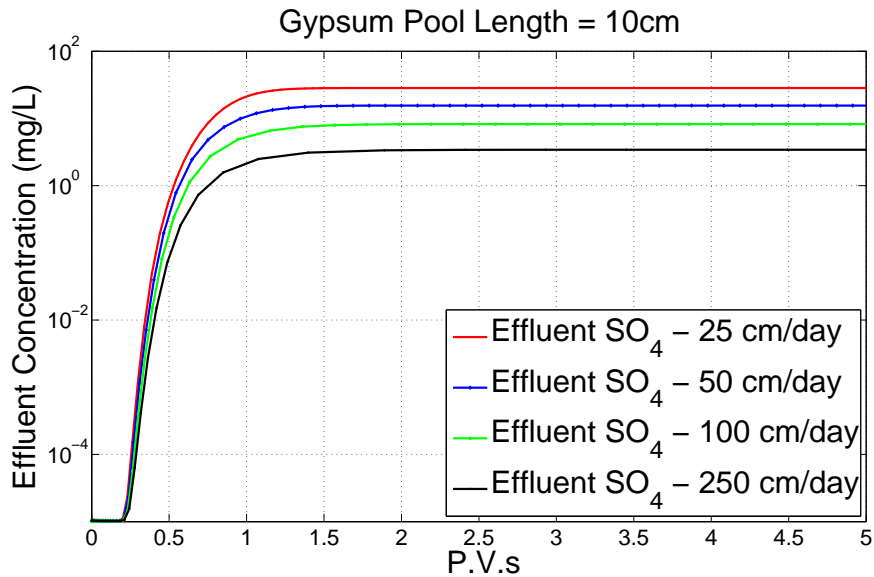
FIGURE 4.13. Modeled down-gradient sulfate concentrations in relation to P.V.s of flow through the effluent. Note that steady-state is predicted after approximately 2.5 P.V.s of flow. This indicates that, to determine the true sulfate mass flux off of the gypsum pool, down-gradient samples should only be taken after this point in time.

4.4.1.2. *Analytical Method for Sulfate Detection.* Effluent sulfate water sample concentrations from this first sulfate plane-source experiment were determined by running the effluent aqueous samples through a Metrohm Advanced Compact Ion Chromatograph 861 with an A Supp5 250 column. Calibration samples with sulfate values ranging from 100 mg/L to 1

mg/L were used with each run. The data from these experimental and analytical methods were stored and analyzed using *Microsoft Excel*, *MATLAB* and *Mathcad.*

4.4.2. Setup of Transverse Dispersion Analysis From a Point-Source Using Fluorescein.

4.4.2.1. *Sand Tank Setup.* Measuring laboratory-scale fluorescein spreading due to transverse hydrodynamic dispersion was done in a 1.75-m long, 39-cm tall, 5.3-cm deep glass tank. The tank was filled with a washed 10-20 silica sand (Carmeuse Natural Chemicals, Colorado silica sand). The sand was emplaced saturated and mixed thoroughly in the tank to ensure minimal gas phase. Figure 4.14 shows the basic setup used for this second experiment and a picture of the filled tank.

During the experiment, de-gassed tap water (Fort Collins, Colorado) was flushed through the sand tank from left to right. The top of the tank was sealed during the flushing phase to minimize evaporative losses through the exposed portion of the sand. The inlet was kept at a constant head by means of a mariotte syphon attached to a sealed 50-L glass carboy with nitrogen gas headspace. The outlet was connected to a positive-displacement pump (Fluid Metering Inc., Model RHSY), which controlled the seepage velocity through the sand.
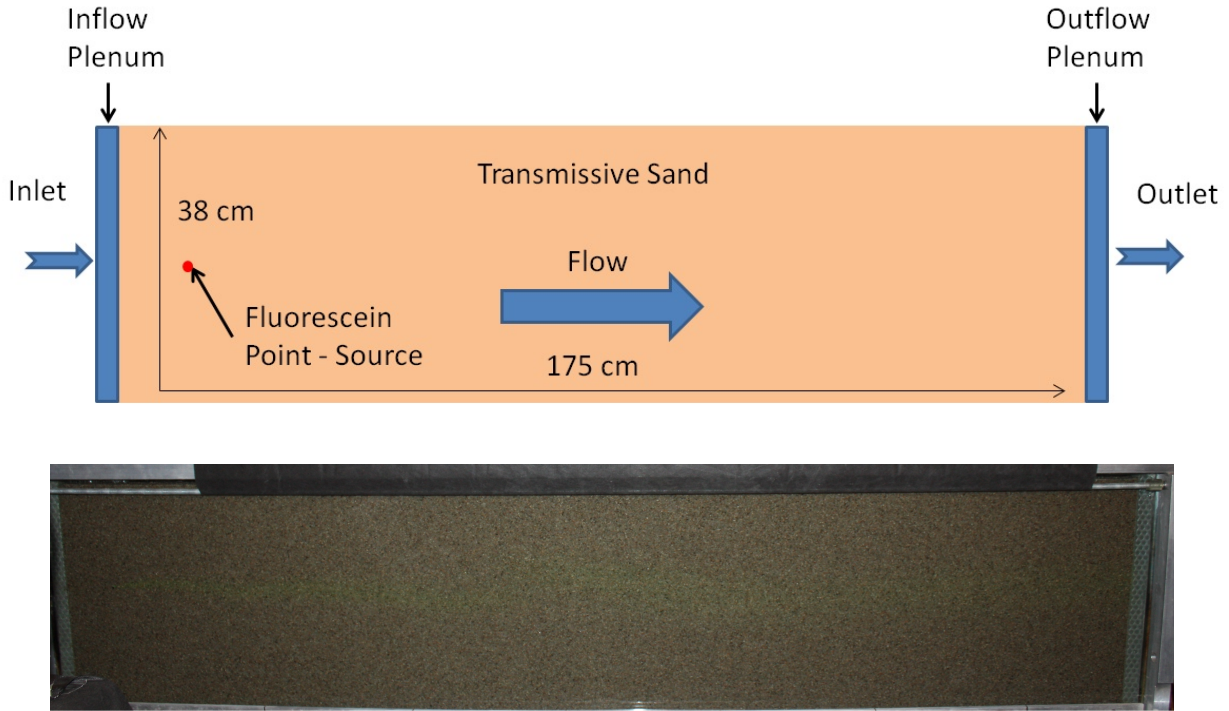
FIGURE 4.14. Setup of the water flushing through a transmissive sand with a fluorescein point-source (red dot) to achieve steady-state plumes at various seepage velocities for image analysis. These steady-state fluorescein plumes will provide a basis for subsequent computational comparison of the transverse dispersion of the plumes at steady-state.

A 1-mm tall, 5.3-cm wide source of 150 mg/L fluorescein (ScienceLab.com, 99%, Houston, TX) was injected into the sand as a point-source using the molded, 2-mm thick stainless-steel tubing device shown in Figure 4.15. This device was emplaced into the tank at the same time as the sands, and the effluent end of the device is located at approximately half the height of the sands (Figure 4.14). From the view shown in Figure 4.14, this injector acts as a point-source delivery mechanism. This injection device was constructed to: 1) minimize the advective disturbance of the flow-field due to the fluorescein injection, and 2) ensure that the experimental transverse-spreading remained as 1-dimensional as possible by delivering a uniform fluorescein pulse over the depth of the tank. This injection device was attached to a syringe pump (Chemvx Inc., model #Fusion 100) with 60-mL plastic syringes (Becton,

Dickinson and Company). The syringe pump flushed the de-gassed fluorescein at 1/380th the flow rate rate of the fluid flow. This value was chosen because the sand layer was 380-mm tall. This flow rate ensured that the advective disturbance transverse-to-flow from the fluorescein injection was approximately 1-mm. This injection scheme also ensured minimum disturbance of the horizontal flow-field, both up and down-gradient of the injection point.
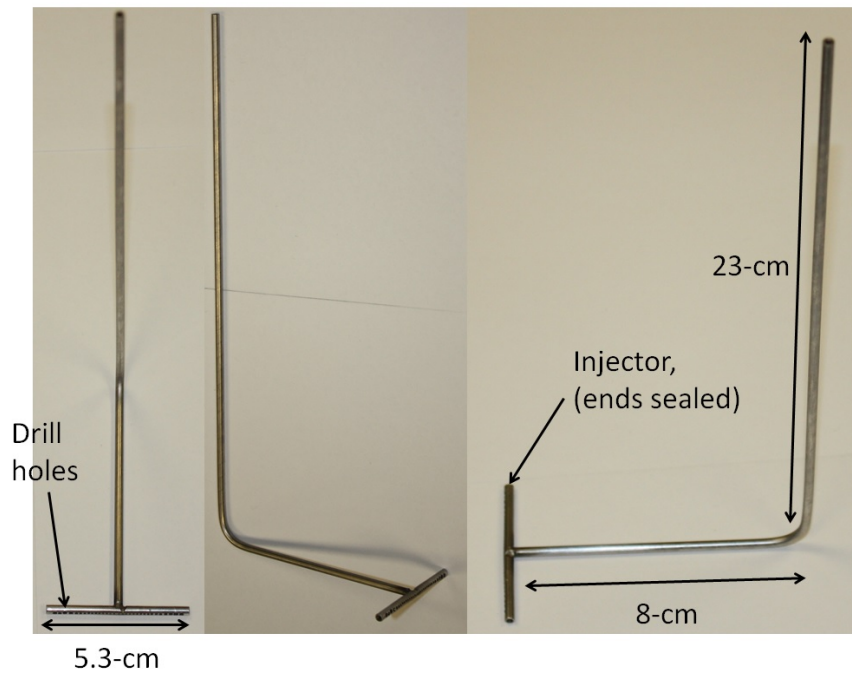
FIGURE 4.15. Dimensions with 3 views of the fluorescein injector: front, isometric and side. Front of injector had 20, 1.0-mm holes to distribute fluorescein.

4.4.2.2. *Determination of Influent Fluorescein Concentration.* Tests were done to investigate the maximum fluorescein influent concentrations that can be used for this experiment. These tests ensure that the captured green intensity values from the red, green and blue (RGB) intensity matrices stay below the asymptotic range for fluorescein. Using a range of fluorescein concentrations, these tests are shown in Figures 4.16a and 4.16b. Using 20 mL glass vials, Figure 4.16a demonstrates the green channel intensity that the fluorescein

exhibits in the absence of a porous media. All images taken for this experiment were from a *Canon* Rebel XSI camera. The maximum value of RGB values that the camera records is 255, which is apparent in Figure 4.16a. This no-soil setup shows a maximum quantifiable intensity value corresponds to a fluorescein concentration between 0.78 and 1.56 mg/L. Another test was run that shows a much different result for fluorescein when in the presence of the sand used in the experiment. Figure 4.16b demonstrates that the green intensity values asymptote at much higher fluorescein concentrations when soil is present in the vials. Figure 4.16b shows that an influent fluorescein concentration of 100 mg/L would be sufficient to avoid this intensity asymptote, because the left hand boundary of the plume photographs are 25-cm from the fluorescein point-source. This distance provides the plume sufficient distance to transversely disperse to concentrations below 100 mg/L.
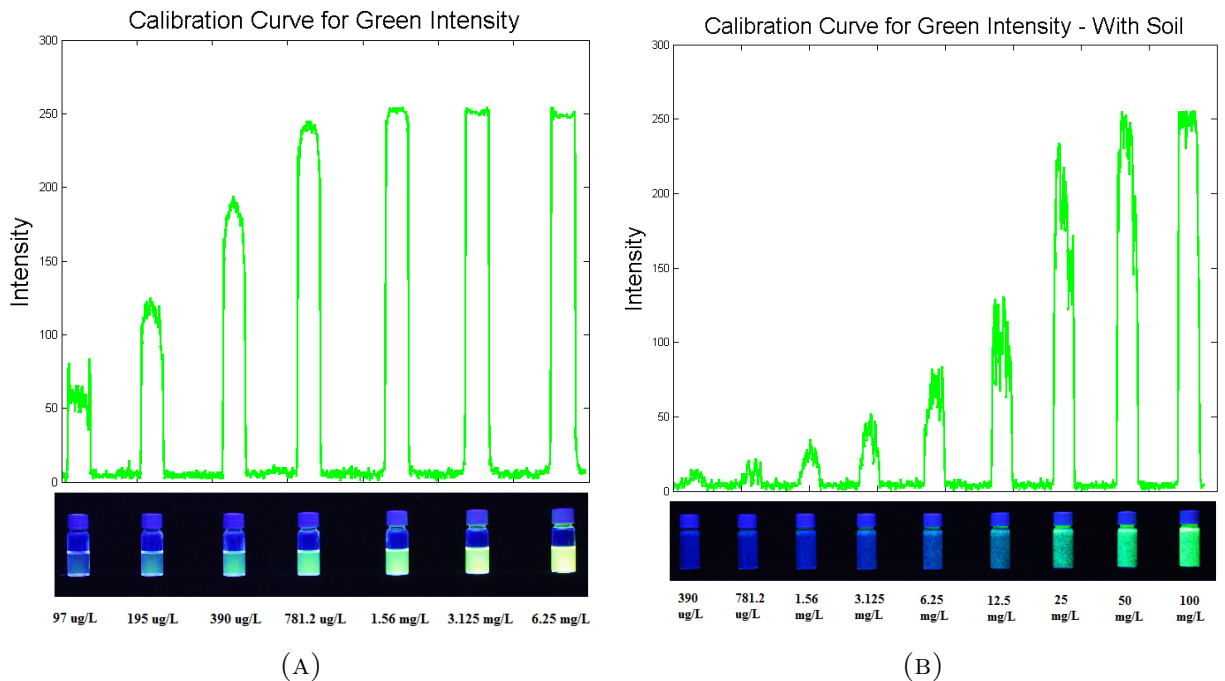
FIGURE 4.16. Green 'intensity' tests for various fluorescein concentrations in the A) absence and B) presence of a porous media. Intensity values correspond to the value assigned to the pixel by the camera, where higher intensity denotes higher brightness and thus a higher fluorescein concentration at that point. Note the saturation of the intensity data at lower fluorescein concentrations in A) due to the increased depth of field relative to when soil is present in B).

4.4.2.3. *Method for Fluorescein Plume Analysis.* The quality of the fluorescein-plume photographs would be crucial for mathematical analysis, so the tank itself was located in a black room. Photos were taken with the highest capable resolution of 4272-horizontal and 2848-vertical pixels. After the lens was focused to the front sand layers, the photos were taken with the lights off with a fluorescent black-light illuminating the plume. To create uniform lighting conditions, the fluorescent black-light spanned the length of the plume. A sample photo (vertically cropped) of the steady-state, 100-cm/day seepage velocity plume is shown in Figure 4.17.
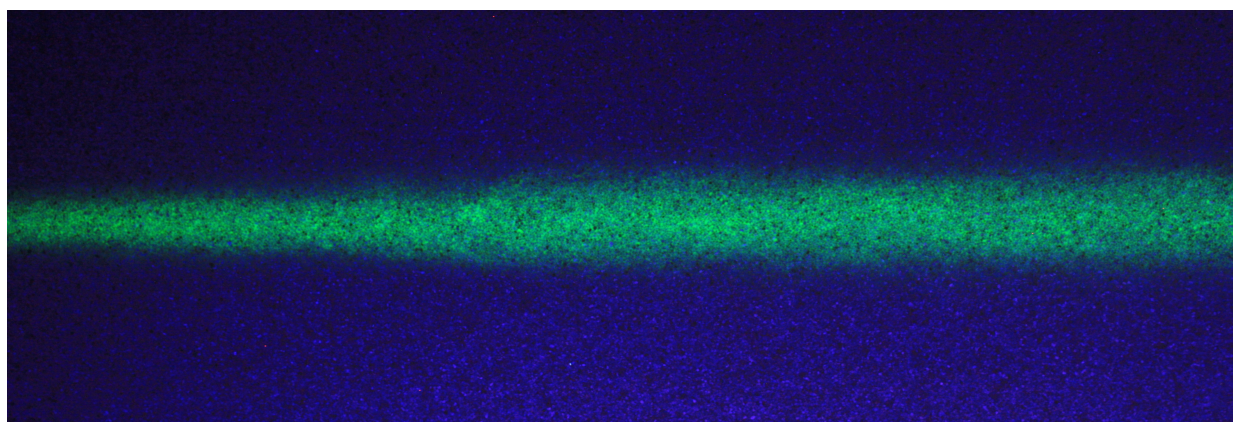
FIGURE 4.17. Image of the steady-state, 100-cm/day seepage velocity fluorescein plume under only UV light. Image shows front-view of 25 to 88-cm distance along the plume from the point-source. Note the increased spreading observed with distance (left to right) from the source.

After acquiring the plume photos, the 3 pixel-color matrices are separated, producing Figure 4.18. Using the 2-D matrix of green-channel data from the photo, *MATLAB* image analysis provides a useful tool for finding vertical intensity (analogous to concentration) values. This is shown graphically in Figure 4.19, which shows the first vertical column of the green values from Figure 4.18.
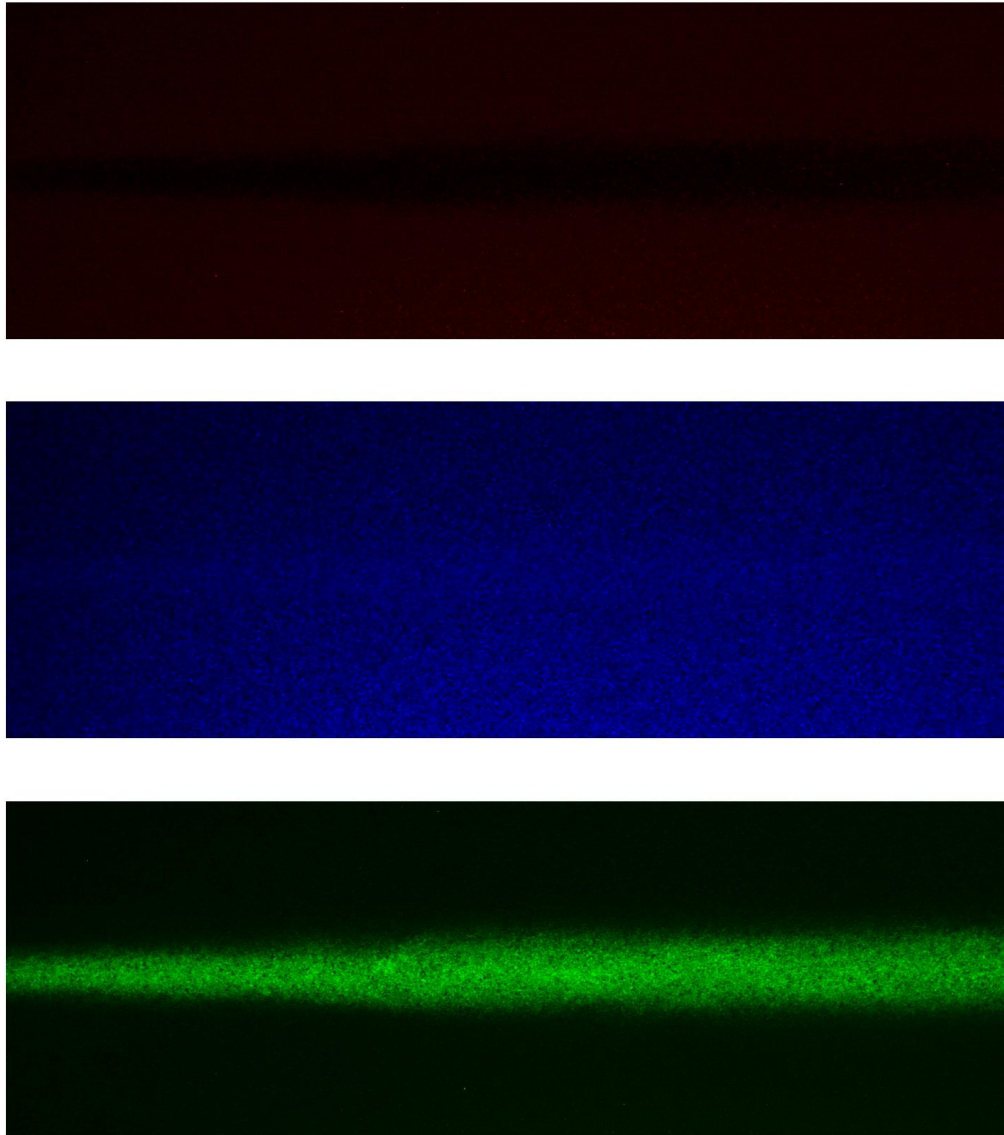
FIGURE 4.18. Separated red, blue and green color matrices from the fluorescein plume in Figure 4.17 using *MATLAB*. The green color matrix will be isolated and used for subsequent computational transverse dispersion analysis.
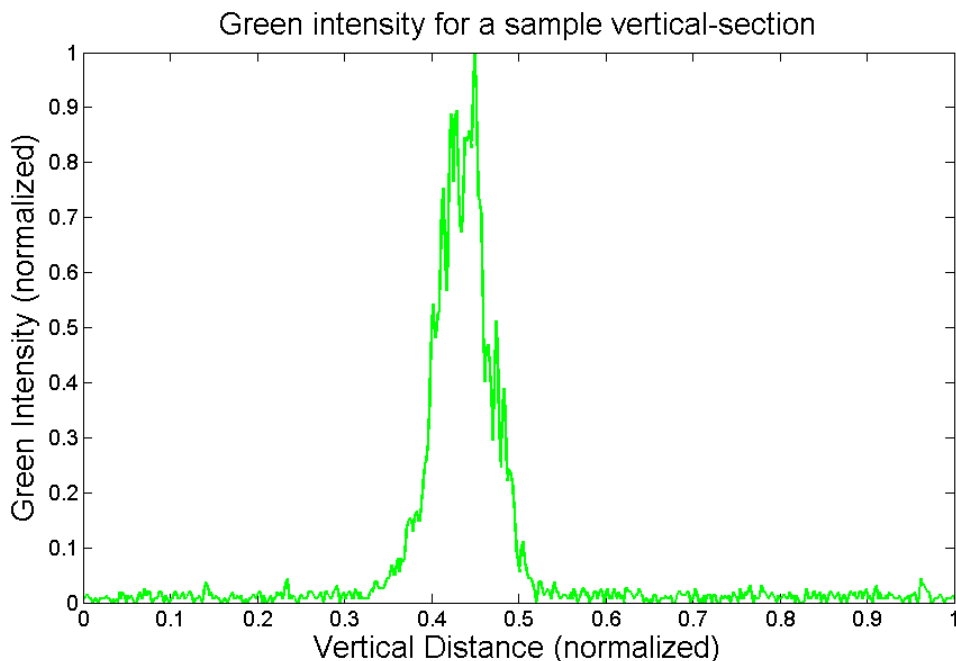
FIGURE 4.19. Normalized green 'intensity' values from a sample vertical cross-section of Figure 4.18. Again, intensity refers to the matrix value assigned for that pixel (0-255), where a higher value corresponds to higher fluorescein concentrations. The shape of this figure can be 'fit' to a number of probabilistic distributions (e.g., normal) or analyzed independently of predefined curves (e.g., area-moment).

A normalized distribution curve can now be fit to the data using Equation 13 by minimizing μ and σ within the function against the green-intensity values shown in Figure 4.19. The minimization function used in *MATLAB* is *fminsearch*, an unconstrained nonlinear optimization tool. An initial guess input into *MATLAB* for μ was given as the x value of the highest green-intensity, and the initial σ guess was 0.05. For the first cross section, this fitting exercise will produce Figure 4.20. Fitting to the normal curve function, *MATLAB* produced values of 0.5155 for μ and 0.03 for σ in this cross-section. This procedure will be repeated for all 4272 cross-sections for each plume photo to determine the growth of the transverse spreading along the plume.
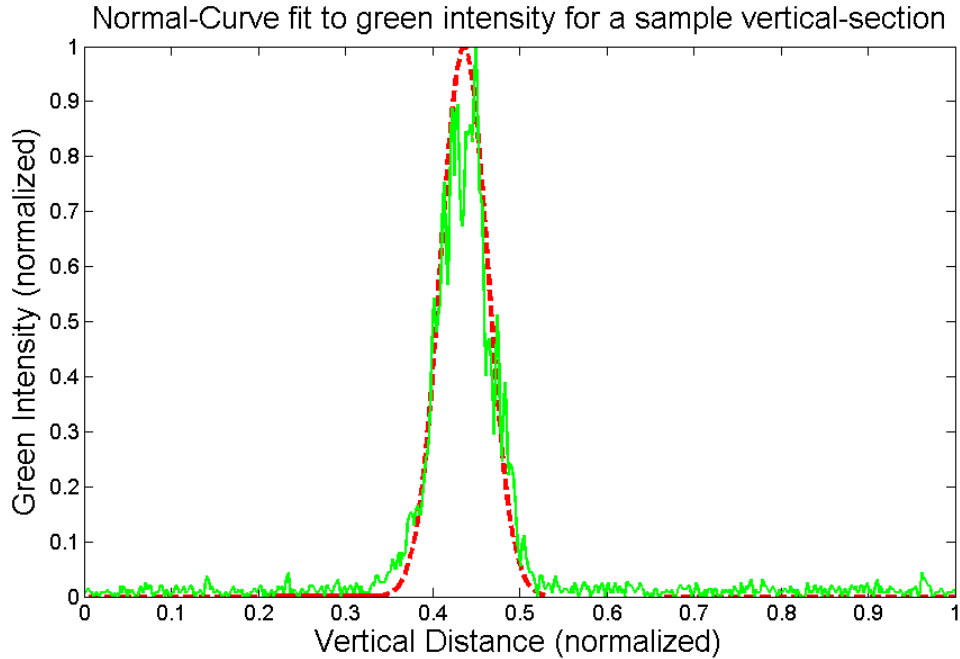
FIGURE 4.20. Sample normal curve fit in *MATLAB* to the green intensity values from Figure 4.19. This fitting procedure provides the σ value needed for plume comparison and analysis.

4.5. PLANE-SOURCE EXPERIMENT: RESULTS AND DISCUSSION

The following subsections present the results from the sulfate flushing experiment to test a proposed plane-source model from Bird et al. (1960).

4.5.1. SULFATE MASS FLUX FROM GYPSUM POOL. Using the analytical techniques discussed in Section 4.4.1.1, Figure 4.21 shows the steady-state effluent sulfate mass fluxes from the tanks. Each data point represents a seepage velocity and gypsum pool-length pairing. Using a diffusion-only dispersion term (D_T), the solid lines represent the analytical predictions of the mass flux from the model (Equation 11). The parameters used in fitting these lines are given in Table 4.1.

TABLE 4.1. Fitting parameters used in modeling predicted sulfate mass flux values of the Bird et al. (1960) plane-source model in Figure 4.21 (solid lines).

Parameter	Value	Units
Porosity, ϕ	0.38	/
D_T	5.6E-10^a $\cdot$ $(\phi)^{1/3}$	m^2/sec
C_{sol}	1750^b	mg/L
D	0.0254	m
v_w	varies	m/day
L_{pool}	varies	m

---

[a]Mullin and Nienow (2002)

[b]Laboratory derived
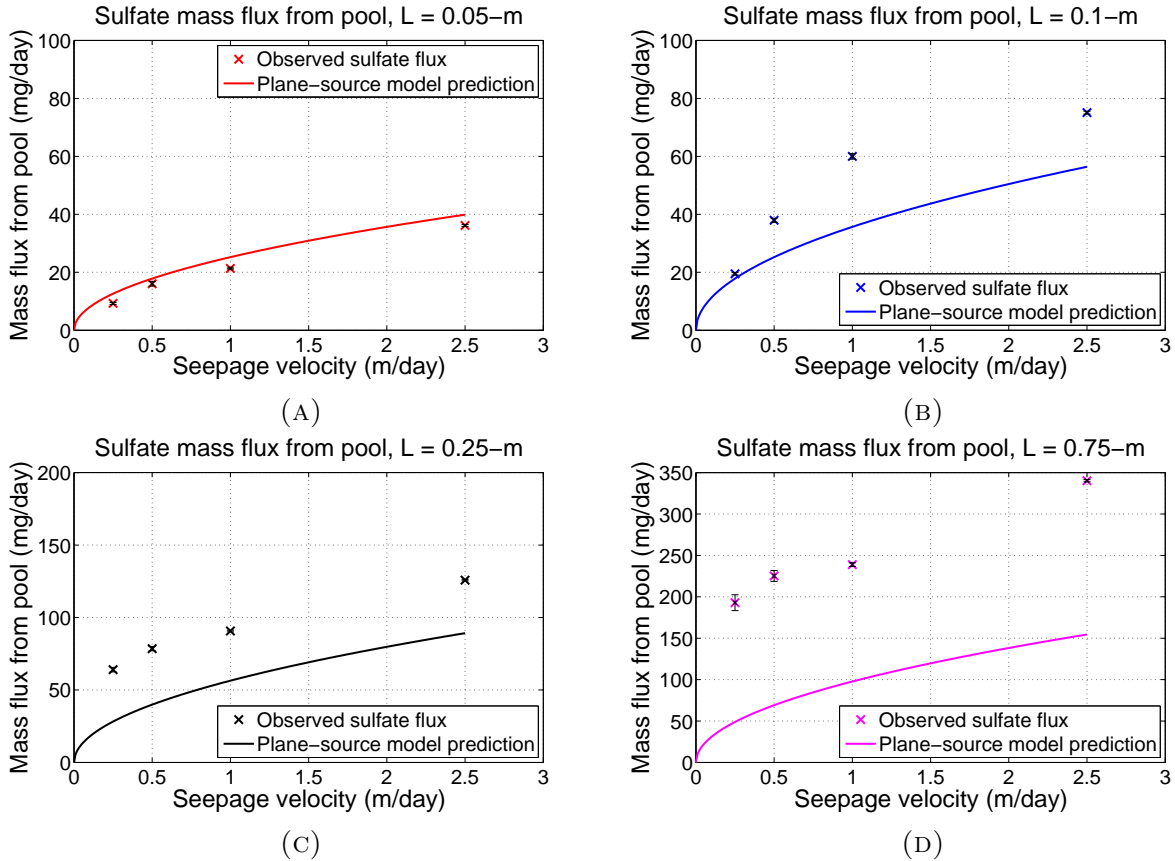
FIGURE 4.21. Plot of experimental sulfate mass fluxes (points) vs. Bird et al. (1960) predicted results (solid lines). The predicted model lines use only an effective diffusion coefficient in place of the 'D_T' term in the model (Equation 11). Note: y-axis values change with pool size, 'L'. 'L' is the length of the gypsum source pool. Standard error is shown.

The observed non-linear shape of the mass flux with respect to seepage velocity is consistent with the model from Bird et al. (1960). Figure 4.21 suggests that the laboratory data and the analytical curves provide a better match at smaller gypsum pool sizes, but diverge as the gypsum pool size increases. However, the amount of divergence between the experiment and model does not seem to to have a strong correlation to increases in seepage velocity. These findings suggest that in addition to molecular diffusion, the presence of a porous media is resulting in contaminant transverse mechanical dispersion. This mechanical dispersion could be responsible for increasing the rate at which the sulfate spreads vertically away from the gypsum pool, thereby explaining the observed increasing sulfate mass flux. This result is likely due in part to the numerous reasons discussed in Section 4.3.

Further explanations for discrepancies between the data and model include: 1) problems intrinsic to the model assumptions and/or formulation, and/or 2) artifacts of the experimental setup. Potential problems associated with the formulation of the plane-source model from Bird et al. (1960) are detailed in Corey and Auvermann (2003). These problems include: 1) the assumption that diffusion flux is measured with respect to the changing center of mass, which results in a constantly changing frame of reference, and 2) the assumption that density gradients have no effect on particle velocity. One artifact in the experimental setup includes the possibility of density driven flow of the sulfate plume downwards from the source, thereby increasing the sulfate mass flux. This effect would be more apparent at larger source pools, which was observed. This same characteristic of the experiment would be present even with the use of a DNAPL located at the bottom of the tank, which would thereby *decrease* or underestimate the sulfate mass flux from the pool due to density effects. Other artifacts of the setup include potential boundary effects due to the presence

of the down-gradient seepage face, and/or consequential changes in fluid viscosity due to incorporation of sulfate (which are assumed to be negligible in the model).

For comparison, applying the dispersion equation (Equation 7) to the Bird et al. (1960) model's 'D_T' term results in the plots shown in Figure 4.22. For this figure, α was set to 0.00003 · L, where 'L' is the gypsum pool length. Figure 4.22 shows how implanting Equation 7 into the model produces a roughly linear increase in sulfate mass flux with seepage velocity, which contrasts with observed results. Figure 4.22 also demonstrates that even when using Equation 7 in the Bird et al. (1960) model, a good fit to the experimental data is not observed. The experimental data diverges with seepage velocity from the smaller pools, and has a poor fit to observed data as the gypsum pool size increases, and over the range of seepage velocities. A further consideration of Figure 4.22 could be that dispersion simply cannot be described within the Bird et al. (1960) model at this scale using the simplified formulation of dispersion from Bear (1972). This concludes the results from the first experiment.
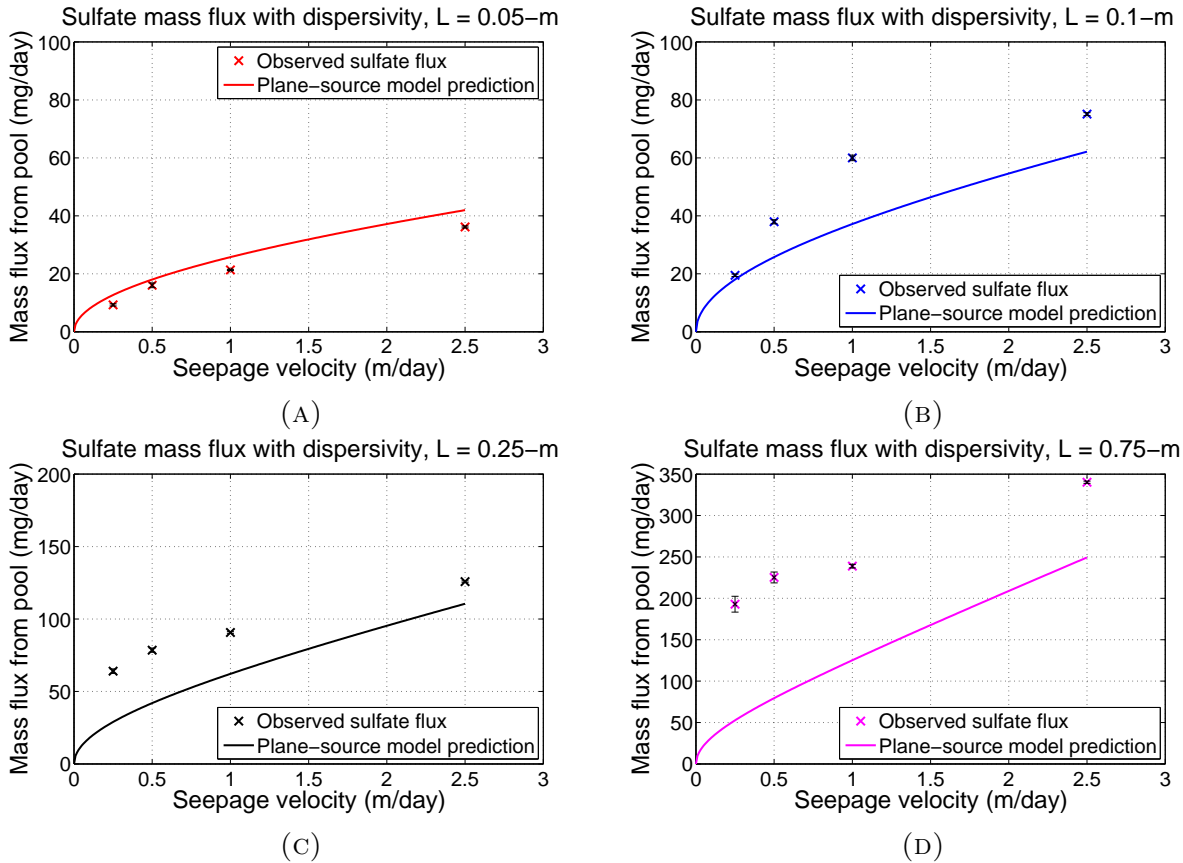
FIGURE 4.22. Plot of experimental sulfate mass fluxes (points) vs. Bird et al. (1960) predicted results (solid lines). Equation 7 is used as the 'D_T' term in the model (Equation 11), where the coefficient of transverse dispersivity, α_T, is defined as 0.00003·L. Note: y-axis values change with pool size, 'L'. 'L' is the length of the gypsum source pool. Standard error is shown.

4.6. FLUORESCEIN PLUME: RESULTS AND DISCUSSION

The following subsections present the results from the second experiment to quantify the transverse hydrodynamic dispersion of a fluorescein tracer from a point-source in a uniform flow field.

4.6.1. FLUORESCEIN POINT-INJECTION RESULTS. After using *MATLAB* to fit each of the green-intensity vertical-sections from the plume photographs to a normal curve (procedure outlined in Section 4.4.2.3), the normalized values of the green intensities for each

cross-section along the plume can be illustrated. As an example, the normal curves from the 250 and 175-cm/day plumes are plotted in Figure 4.23. These curves are in the 25-cm to 150-cm range from the point-source, which is typical of all plots in this experiment.

(A)   (B)
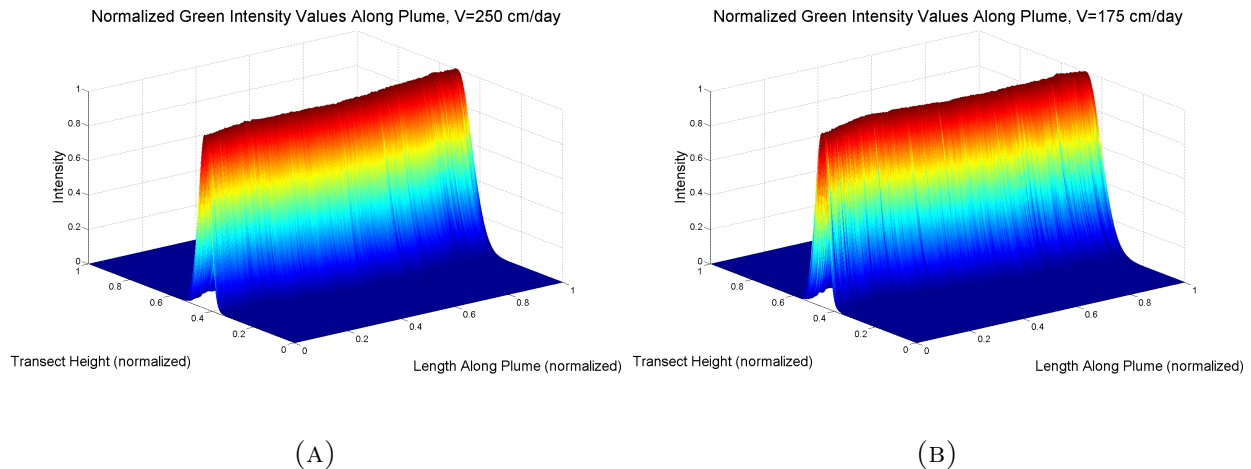
FIGURE 4.23. Isometric view of the normalized green intensity values along plume for V= A) 250 and B) 175-cm/day plumes. Green intensity values are shown as the z-axis. Redder colors indicate more brighter areas of the images, showing the evolution of the plume as it transversely spreads through the tank with distance from the point-source.

Using this data, every σ for each vertical-section for the 5 seepage velocities is shown in Figure 4.24. The utility of this figure is that it provides the fitted σ value for each vertical cross-section relative to the *time* from the point-source. This provides the opportunity to distinguish the effect on dispersion by diffusion, a time-dependent phenomenon. Theoretically, if diffusion was the only process involved in transverse solute spreading, these σ values would overlap each other. This is because the initial contaminant concentrations were equal, and diffusion has had the same amount of time to spread the contaminant. However, at any given time, the plot shows a decrease in transverse spreading with lower seepage velocities. Since these plots do not overlap relative to time from the source, there must be other physical processes (discussed previous; in addition to diffusion) that are transversely spreading the fluorescein.
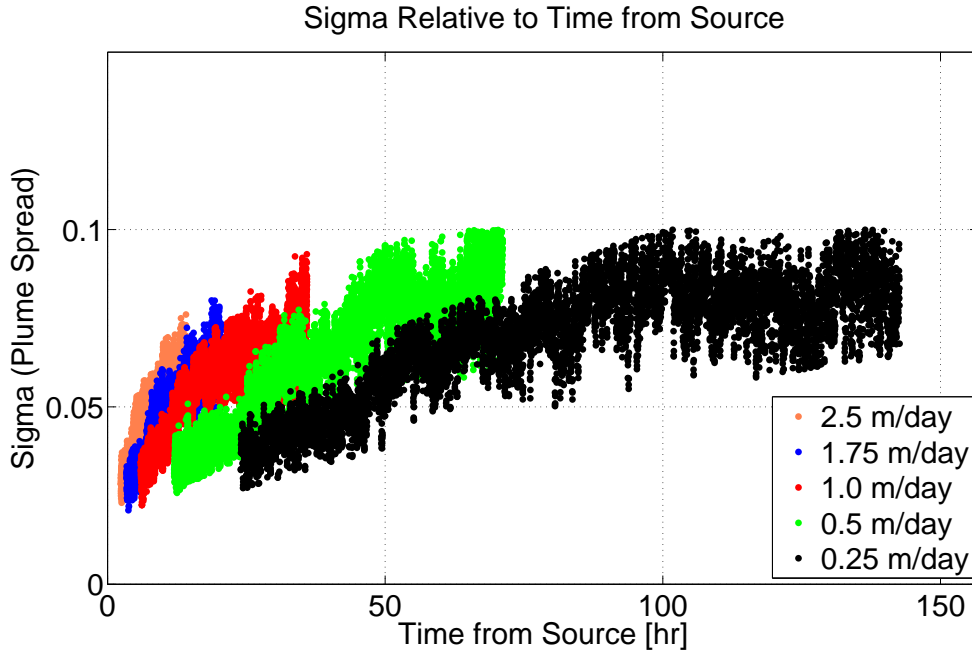
FIGURE 4.24. Computed transverse σ (plume spread) values (from Equation 13) relative to their *time* from the point-source. Each of the five tested seepage velocities are shown. Each point represents a fitted σ value for a vertical cross-section of the plume (see Figure 4.20). Larger σ values correspond to a wider normal distribution curve, indicating a wider plume cross-section at that point in time. Theoretically, if diffusion were the only process transversely spreading the fluorescein in these plumes, the overall trend of these 5 plumes would overlap, which is not observed.

Noticing the non-linear trending of the transverse spreading with distance from the source, *MATLAB* offers a way to fit the σ data to a function using the same minimization techniques used earlier. By analyzing the shape of the σ spreading with time, the fitting equation was chosen in this particular case to follow the form of a solution to the A-D equation (Equation 8) (Aris, 1956):

(14) $$\sigma = \sqrt{2 \cdot D \cdot t}$$

where D is the dispersion coefficient ($L^2 \cdot T^{-1}$), and t is the known time from the source (T). In this case, when given an initial guess, the 'D' term is iterated inside of the *MATLAB*

151

fitting (minimization) function. Presumably, this 'D' term changes with aquifer parameters such as the soil type and architecture. Plotting the σ values with their respective fitted lines from Equation 14 results in Figure 4.25.
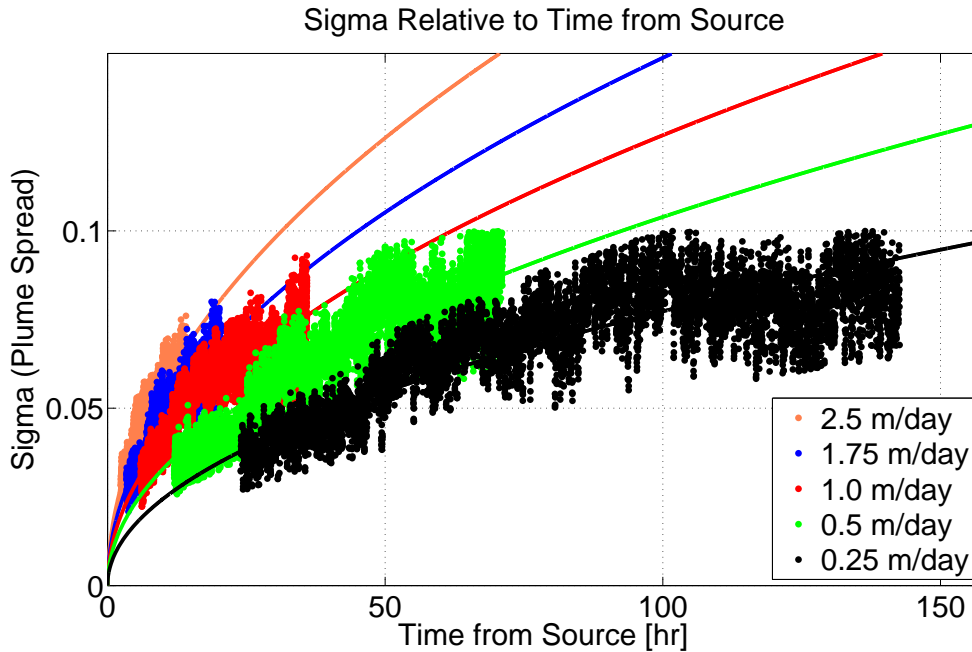
FIGURE 4.25. σ values and fitted curves from Equation 14 for each seepage velocity relative to the time from the point-source. These fitted curves represent a good agreement with the concept of dispersion in this particular solution of D_T in the A-D equation.

When using this solution to model the σ spread relative to time, plotting the values of 'D' from equation 14 produces an interesting result: the values of 'D' appear to increase linearly with increasing seepage velocity, as shown in Figure 4.26. Table 4.2 shows these calculated 'D' values for the fitted curves shown in Figure 4.25. The linear increase in 'D' with seepage velocity (assuming constant D^*) lends credence to Equation 7. If the dimensions of σ were known, the observed values of α could be computed. This further disproves the hypothesis that diffusion alone can account for transverse plume spreading at this scale. This concludes the results from these two laboratory experiments.
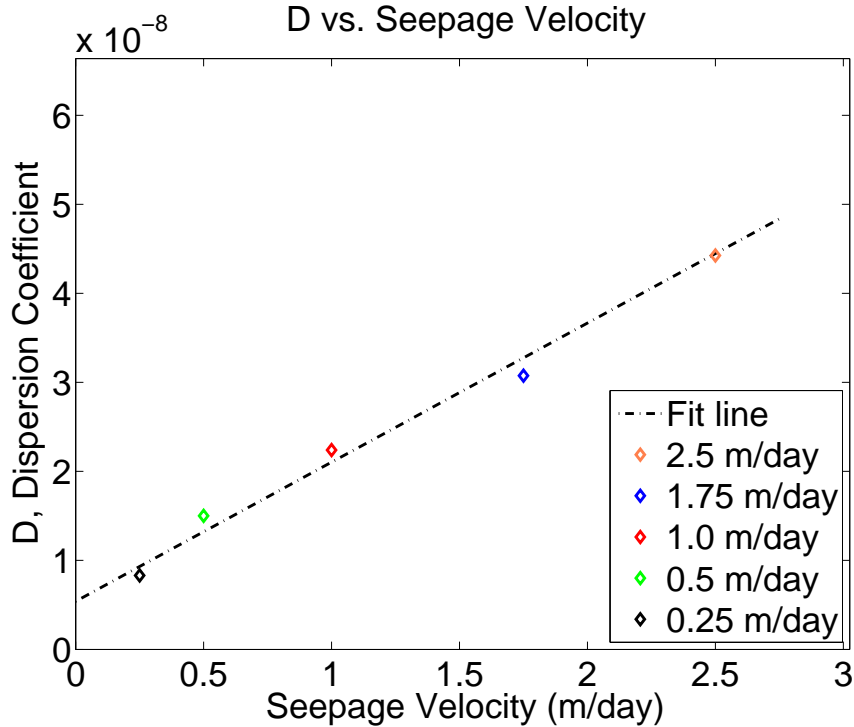
FIGURE 4.26. The five computed 'D' values for each seepage velocity, with a fitted line. This linearly increasing behavior in 'D' with increasing seepage velocity agrees with Equation 7, suggesting that diffusion alone cannot account for transverse plume spreading at this scale.

TABLE 4.2. Computed values of 'D' from iterating Equation 14 to the σ data. The visual representation of this these values are shown in Figures 4.25 and 4.26.

Velocity (m/day)	D
2.5	4.42E-8
1.75	3.07E-8
1.0	2.24E-8
0.5	1.50E-8
0.25	8.3E-9

4.7. SUMMARY AND CONCLUSIONS

The two laboratory experiments conducted to analyze dispersion in a homogeneous media provided a number of interesting results. The first experiment involving a gypsum pool dissolving into a transmissive layer showed a good fit to the plane source model (Bird et al., 1960; Hunt et al., 1988) with smaller pool sizes over a range of 25 to 250 cm/day seepage

velocities, but laboratory data increasing diverged from the model with increasing pool size. This divergence did not necessarily grow with increases in seepage velocity. Findings from this experiment suggest that: 1) the formulation of the model might be incomplete due to the assumptions necessary for an analytical solution, 2) there are forces other than diffusion at work in transversely spreading contaminant plumes, 3) dispersion may be a partly scale-dependency process, 4) velocity does not appear to correlate linearly with mass flux off a contaminant pool, implying incomplete formulation of dispersion (at this scale) in the formulation from Bear (1972), and/or 5) experimental errors such as density-driven flow might account for the observed discrepancies. Further work with larger pool lengths, seepage velocities, experimental scales and/or different soil types is warranted to clarify these findings.

The method developed to measure the behavior of a fluorescein tracer was able to differentiate between the effects of chemical diffusion from mechanical dispersion. At the laboratory scale, results suggest that: 1) using imaging analysis techniques provides a useful tool in the analysis of plumes, and 2) diffusion alone was not enough to account for the transverse spreading observed. This observation suggests that a physical process in addition to diffusion is enhancing transverse hydrodynamic dispersion. Furthermore, the observed transverse spreading exhibited non-linear growth with distance and time from the point-source, which agrees with a solution to the advection-dispersion equation. Further analysis of dispersion at larger scales and time-frames is needed for more accurate plume descriptions. These laboratory results, in conjunction with emerging field data, suggest that the theory of linearly-velocity dependence of transverse hydrodynamic dispersion is incomplete, and warrants further investigation.

CHAPTER 5

Results and Recommendations

This Chapter presents a summary of the results and recommendations for further work drawn from this body of research. Hypotheses introduced in Chapter 1 are presented, followed by a brief summary of relevant results and the outcome of testing each hypothesis. Results include both quantitative analyses of data and the broader implications of the work. One of the primary outcomes from this work is a realization that more needs to be done to resolve the quandary of managing the risks associated with contaminants in low k zones. Given this, the last portion of this Chapter presents recommendations for further work.

5.1. Results from Laboratory Treatment Studies - Chapter 2

Chapter 2 tested a hypothesis involving the use of laboratory treatment studies on low k zones. This hypothesis is stated as:

Laboratory-scale tank studies can be used to evaluate the relative efficacy of common treatments for chlorinated solvents in low k zones.

The six laboratory treatment studies from Chapter 2 demonstrated a range of outcomes and treatment mechanisms that provided the option to analyze the relative performance and limitations of each treatment option. Bottom to top flushing of an aqueous TCE solution at solubility for 52-days produced an asymmetrical effluent breakthrough curve. Once the source was removed, 'tailing' behavior commonly seen in laboratory experiments and heterogeneous field sites was observed due to releases from the low k zones. For the control scenario, effluent TCE from the control tank was still 3.1 mg/L (2.3E-05 mol/L) at 137 days after source removal. This effluent TCE concentration is still almost 3 orders of magnitude above drinking water standards (5μg/L, U.S. E.P.A.). This effluent TCE behavior agrees

with previous studies that have demonstrated long periods of time may be needed to deplete low k zones of contaminants. Effluent cis-DCE concentrations increased between non-detect and 5.3 mg/L (5.4E-05 mol/L) by the end of the experiment. This unexpected finding illuminates the scale that natural attenuative processes can play in aquifer restoration.

During treatment, an enhanced flushing of clean water (analogous to a pump and treat system) reduced effluent TCE concentrations relative to the control. Over the remainder of the experiment, however, this behavior was not sustained. At the end of the experiment, effluent TCE concentrations from this treatment tank were 3.0 mg/L (2.3E-05 mol/L), almost equal to the levels from the control. As with the control, increasing levels of effluent cis-DCE concentrations were observed as the experiment progressed. Results from this specific enhanced flushing scenario demonstrates the limited effectiveness of the treatment relative to a no-action control when flushing occurs parallel to low k bedding.

During a treatment of permanganate, effluent TCE concentrations fell to non-detection levels, but rebounded afterwards to within an OoM of the control due to incomplete penetration of the permanganate into the low k zones. Effluent TCE concentrations were 1.2 mg/L (9.0E-06 mol/L) at the end of the experiment, a roughly 62% drop compared to the control. The deposition of MnO_2 was obvious, indicating a potential for reducing diffusion of contaminant fluxes from low k zones due to the fouling of pore-spaces. As with the control and enhanced flushing tanks, increasing levels of effluent cis-DCE concentrations were observed as the experiment progressed. The permanganate ISCO treatment quantitatively and qualitatively demonstrated the limiting effects that soil oxidant demand and diffusion into low k zones can play in the success or failure of this treatment type.

Results from the two KB-1 microbial inoculum treatments indicate that this treatment can be very effective at dechlorinating TCE while sufficient amounts of a carbon substrate

is present for metabolism. During and for a roughly two month period after treatment, the two KB-1 inoculum treatments dropped effluent TCE concentrations between non-detection levels and 40μg/L. Effluent cis-DCE and VC concentrations were observed to fluctuate during this period as well, indicating that microbial ERD dechlorination is occurring. Nearing the end of the experiment, effluent TCE concentrations from the KB-1 and lactate treatment had rebounded, and ended the experiment at 1.0 mg/L (7.6E-06 mol/L). This rebound behavior was replicated in the KB-1, lactate and xanthan gum treatment. The effluent TCE concentration from the KB-1, lactate and xanthan gum treatment at the end of the experiment was 0.82 mg/L (6.2E-06 mol/L). Effluent concentrations of daughter-products of the dechlorination process were shown to increase in both KB-1 tanks, a finding which may be due in part to the relatively small retention time and scale of the experiment.

Interestingly, although effluent TCE levels during and after treatment were reduced relative to the control, late-stage CVOC fluxes from the two KB-1 injections suggest that these two treatments did not substantially deplete total CVOC mass within the tanks. Although MCLs have been defined, this type of finding highlights a type of unclear definition as to what would constitute a successful treatment scheme. Further observations from the two KB-1 tanks suggest that the microbes preferred to inhabit the interfaces between soil layers. This indicates that this treatment type may also be limited by diffusive processes. This finding furthermore suggests that the effects from the xanthan gum portion of the KB-1, lactate and xanthan gum treatment are not obvious in increasing the volume of low k soils occupied by the microbes. These observations suggest that this treatment functions in much the same way as an enhanced flush; by relying on diffusion of contaminants (and carbon substrate) from low k layers. Results from these two treatments suggest that without multiple injections of a carbon substrate, treatments utilizing a microbial ERD will most likely

become relatively inactive due to metabolic constraints from carbon starvation of the dechlorinating microbes. Overall, this observation suggests that the success of the treatment in reducing overall CVOC releases is restricted by the availability of a carbon substrate. These results suggest that using this technology at the field-scale may require large time-frames for repeated carbon substrate injections to ensure that the microbial system is active during the prolonged contaminant releases from the low k zones. This has implications concerning treatment and monitoring time-frames at field-sites, which greatly impact overall treatment costs for sites that utilize this technology.

Effluent CVOC concentrations from the SRB, lactate and sulfate treatment produced some very unexpected results. During treatment, effluent TCE concentrations were not observed to deviate significantly from the control. This effluent TCE behavior was observed even though the black mineral deposition was visually obvious through the majority of the transmissive and low k zones. After the treatment ceased, effluent TCE concentrations dropped over 3 OoM to MCL levels, which remained for a roughly 40-day period. At this point in time, effluent cis-DCE levels increased to nearly the same molar concentrations as the TCE from the control. The experiment ended with the overall lowest effluent TCE concentration of the treatments at 0.21 mg/L (1.6E-06 mol/L), but a cis-DCE concentration of 2.7 mg/L (2.4E-05 mol/L).

Since dechlorination of TCE by reactive iron-sulfides has been shown to proceed through chloroacetylene to acetylene, these findings suggest a microbial treatment pathway for the TCE which was inhibited by the presence of sulfate. This finding is reinforced by the rebound of TCE near the same point in time as the two KB-1 treatments, suggesting carbon starvation. A further line of evidence for this behavior is in effluent ORP measurements. These measurements showed very reducing conditions while effluent TCE concentrations were

at their lowest, while TCE rebounds in the KB-1 and SRB treatments correspond to large increases in effluent ORP levels towards more oxidizing conditions. Results from this SRB, lactate and sulfate treatment also suggest that the precipitated iron sulfide minerals had little effect on treating TCE. This finding is reinforced by previous studies which showed little to no reactivity of iron-sulfides at a pH of formation ≤ 8. Again, while the effluent TCE data from this treatment may point to a successful remediation strategy, total CVOC flux from the tank was not substantially different from the control to declare a successful treatment scheme. Field-scale considerations from this treatment include the lack of complete treatment of the CVOCs to ethene, as well as the lack of reactivity of the deposited black minerals under these conditions.

Overall, relative to the no-action control, these treatment technologies were limited to 0.01 to 1.16 OoM (2.1% to 93%) improvements in down-gradient TCE water quality. With respect to depleting contaminants in low k zones, results from this experiment suggest that common treatments may have very limited benefits in depleting contaminant levels needed to achieve the MCLs in transmissive zones. These findings indicate that the strategies and expectations for these treatments at field sites need to be re-evaluated. Since the time-frame of care could be on the order of decades or even centuries, results indicate that there exists a need within the hydrogeology profession to manage our expectations of treatment outcomes at field-sites where soil heterogeneities may have stored a significant amount of contaminants. *These experimental results from Chapter 2 confirm the hypothesis that laboratory-scale tank studies can be used to evaluate the relative efficacy of common treatments for chlorinated solvents in low k zones.*

Chapter 3 explored two hypotheses involving the use of reactive-transport models to predict treatment outcomes at lab and field-scales. The first hypothesis tested was:

1. *It is possible to develop laboratory-scale models using the reactive-transport code* MIN3P *to accurately capture the complex biogeochemical processes occurring in each of the treatments presented in Chapter 2.*

Using the laboratory-derived biogeochemical parameters (e.g., hydraulic conductivity, retardation) and soil layout described in detail in Chapter 2, conceptual models for each of the six treatments were developed using the reactive-transport code *MIN3P*. Untested parameters (e.g., diffusion coefficients, TCE-MnO_4 reaction-rate) were taken from published literature. At the laboratory-scale, the model for the control scenario was able to provide a close match to experimental effluent TCE data over the 189 day time-frame. Because these soils are field impacted with TCE, the model assumes a dechlorinating microbial population with second-order growth coupled to TCE and the microbial population itself. This assumption led to a cis-DCE breakthrough curve that was able to capture the behavior of the natural attenuative processes occurring within the soils. Modeling the control scenario demonstrates that the basic transport and natural attenuative processes within these soils can be captured and may be applied to more complex models.

The enhanced flushing treatment model fit the data before and for a short period after treatment, but then overestimated effluent TCE levels afterwards. Late-time effluent TCE concentrations, however, matched well with observed data. As with the control, this model assumed a growing microbial population to account for the observed effluent cis-DCE behavior, which presented a very good fit to effluent cis-DCE data.

Using a reaction network that included the interaction of: 1) permanganate and soil oxidant demand, 2) permanganate and TCE, 3) permanganate and cis-DCE, 4) dechlorination of TCE into cis-DCE via microbes, and 5) deposition of and porosity changes from a MnO_2 mineral phase, the permanganate treatment model was able to simulate the effluent behavior of the TCE before and after the permanganate flush. This includes the observed drop in effluent CVOCs at the start of treatment, as well as the lack of permanganate penetration into the low k zones resulting in CVOC rebounds afterwards. Late-stage effluent CVOC concentrations were a very close match to the observed data, indicating a good overall understanding of the processes occurring during this treatment. This includes an understanding of the overwhelming importance that the soil oxidant demand plays in the treatment outcome.

The two models for the KB-1 inoculum treatments were successful in predicting the observed decreases in effluent TCE during and after the treatment flushes, as well as the subsequent increases in cis-DCE. The reaction network for these models includes a growing microbial population coupled to the TCE and lactate concentration, as well as the microbial population itself. Due to the shape of the modeled effluent CVOC curves, this assumption about the microbial growth appears to be justified. Importantly, the models were able to account for a deactivation of the microbes once carbon starvation occurred, which resulted in rebounds in effluent TCE that closely matched observed data.

Lab-scale modeling the last treatment of SRB, lactate and sulfate produced a very good fit to the observed data during and after the treatment flush. The model assumes a microbial treatment mechanism through reductive dechlorination of TCE to cis-DCE, similar to the KB-1 treatments. The timing of the large drop in effluent TCE suggests that the assumption that the microbes would use sulfate as the preferred electron acceptor to delay TCE dechlorination appears to be justified within the model. As with the KB-1 treatments,

the model was able to predict the same late-time rebound of TCE, suggesting a similar treatment mechanism.

These modeling outcomes indicate a relatively accurate understanding of the treatment mechanisms present in the laboratory treatment studies. The laboratory modeling study furthermore verified that the biogeochemical complexities of low k zones can inhibit these common treatment technologies, resulting in treatment failures. As with the laboratory studies, modeling shows that the considered remediation methods are ineffective at significant OoM reductions in effluent CVOCs with this setup. Further insights gained from the lab-scale modeling include quantifying the scale of the natural attenuative capabilities of the soils, the chemical and biological reaction rates, mineral-chemical interaction rates, and the microbial growth rates. *These modeling studies help confirm the hypothesis that* MIN3P *laboratory-scale models can capture the complex biogeochemical processes occurring in each of the treatments, but further refinement of the model parameters is needed to more accurately quantify the treatments.*

The second hypothesis tested was:

2. *Laboratory-scale calibrated treatment models can be used to explore and compare the relative efficacy of the laboratory treatments from Chapter 2 at the field-scale.*

Up-scaling the laboratory-scale models to the field scale provides some interesting results which highlight the scale of potential problems these treatments may encounter. Overall, the field-scale modeling studies highlight that: 1) in the absence of natural attenuative processes, large low k lenses can sustain long-term down-gradient CVOC concentrations for centuries, 2) treatments that rely on diffusive processes may be considered impractical under these biogeochemical conditions, and 3) that an aquitard can inhibit the considered treatments producing a meaningful impact on long-term aquifer restoration. These results are obvious in

the failures presented by each of the four considered field treatments. These failures include similar down-gradient CVOC behaviors witnessed in the laboratory treatments, such as the rebound of TCE after a permanganate or enhanced flushing treatment.

Due to a large change in the volume of low k storage, a field scenario without an aquitard presented large reductions in down-gradient Time to Compliance values. Results indicate that technologies like the enhanced flushing or lactate injections may be relatively effective for this scenario, but that a permanganate treatment similar to the one use in the laboratory would have little effect on long-term down-gradient TCE concentrations.

A limitation of these field-scale models was the lack of natural attenuative processes occurring within the aquifer. At these large-scales and long time-frames, these processes may be responsible for large reductions in Time to Compliance values. To gain a more complete understanding of the necessary scope of a field treatment, further laboratory and modeling studies are needed to better quantify and incorporate these processes into the treatment models. Further increases in soil architecture and reaction pathway complexity in the models may provide further insights to aid in the selection of a treatment for a contaminated field site. Another limitation of the field-scale model was apparent in the screening interval of the down-gradient monitoring well, which is a limitation imposed by the boundary conditions within the model at present. However, this limitation highlights the theory that smaller zones of subsurface contamination exist that are in need of more direct targeting by treatments. Maybe more importantly, this modeling limitation also demonstrates the misleading nature of large-screened monitoring wells for analyzing the extent of subsurface contamination. *Results from upscaling laboratory treatment models suggest that the hypothesis that the laboratory-scale models can be used to explore and compare*

the relative efficacy of the laboratory treatments at the field-scale is correct, but further work
is needed.

5.3. Results from Laboratory Studies on Transverse Hydrodynamic Dispersion - Chapter 4

Chapter 4 explored three hypotheses involving the phenomenon of transverse hydrodynamic dispersion. The first hypothesis tested was:

1. *The contaminant plane-source model presented by Bird et al. (1960) can be used with a purely diffusive dispersion term to explain laboratory data of a gypsum pool dissolving into a transmissive layer.*

To experimentally test the first hypothesis, a series of homogeneous saturated sand tanks with a dissolving gypsum pool were employed. The tanks had deionized water flow through at 4 seepage velocities, with 4 unique gypsum pool lengths for each seepage velocity. Aqueous effluent samples provided sulfate mass flux data due to the dissolving gypsum source which were compared to the model presented by Bird et al. (1960). This first experiment showed a good fit to the model (using a diffusion-only dispersion term) at smaller pool sizes (i.e., 5-cm), but laboratory mass flux data increasingly diverged from model predictions as the pool size increased (i.e., 25 and 75-cm). This divergence between the experiment and model did not necessarily increase as seepage velocity was increased. These outcomes could be due to experimental artifacts, incomplete model formulation and/or the presence of a porous media causing enhanced mechanical dispersion effects.

Primary findings from this experiment suggest that: 1) the model formulation from Bird et al. (1960) is incomplete when applied to a porous media, 2) there are forces other than diffusion at work in transversely spreading contaminants, 3) dispersion may be a partly

scale-dependency process, and 4) velocity does not appear to correlate linearly with mass flux off a contaminant pool, implying incomplete formulation of dispersion (at this scale) in the formulation from Bear (1972). Limitations of this experiment include potential problems with density-driven flow due to the placement of the gypsum pool, as well as the presence of a down-gradient seepage-face which may have influenced flow-paths into the sampling system. *Overall, the first hypothesis that the contaminant plane-source model can explain mass flux data from a dissolving gypsum pool using a purely diffusion-based dispersion term is not supported by laboratory data from this experiment for all the contaminant pool sizes tested.*

The second and third hypotheses tested were:

2. *The phenomenon of transverse hydrodynamic dispersion in a porous media can be explained at the laboratory-scale by the processes of diffusion.*

3. *The current prevailing definition of transverse hydrodynamic dispersion is in need of further study and consideration.*

To test the second hypothesis, a 1.75-m long saturated homogeneous sand tank and a fluorescein point-source was employed. This setup was used to capture the steady-state plume that develops when a uniform flow-field is introduced to a small point-source contaminant. This experiment was run at 5 seepage velocities, resulting in 5 distinct steady-state plumes. These plumes were illuminated using UV-lights and captured at high-resolution for analysis. A computational method was developed in *MATLAB* to measure the transverse spreading of the fluorescein tracer. This computational method was able to separate the effects of chemical diffusion from mechanical dispersion in the 5 plumes.

In this second laboratory experiment, results suggest that: 1) imaging analysis techniques provides a useful tool in the analysis of plume evolution, and 2) as the seepage velocity

was increased, diffusion alone was not able to fully account for the observed transverse plume spreading. These results indicate that another physical process is at work in the porous media that is transversely spreading contaminant plumes. *Results from this laboratory experiment to test the second hypothesis that transverse hydrodynamic dispersion in a porous media can be explained at the laboratory scale by the processes of diffusion suggest that this hypothesis is incorrect.* The observed transverse plume spreading, however, exhibited non-linear growth with distance and time from the point-source. *In conjunction with emerging field-data, these findings suggest that the third hypothesis is correct in stating that the current prevailing definition of transverse hydrodynamic dispersion is in need of further study and consideration.* Further postulated explanations for the process of transverse contaminant spreading in porous media (described in detail in Chapter 4) include the presence of non-laminar flow, viscosity-gradient induced fluid rotation, and surface tension forces at the very small scale, resulting in micro-eddys which may result in enhanced transverse spreading as contaminants move through the pore-space network.

5.4. Recommendations for Future Work

The diversity of observed effluent CVOC evolution from the six laboratory treatments suggest complex biogeochemical processes taking place. Unexpected results from the control scenario highlight a number of unquantified processes in low k zones that deserve further consideration. The emergence of late-time effluent cis-DCE suggests that further laboratory and field studies are needed to better analyze the scale of potential natural attenuative capabilities in low k soils, such as potentially very slow processes taking place that may become significant at longer time-frames. Since this first treatment study was limited in scale and time, studies would need to be conducted for much longer time-frames and larger

scales to better quantify these processes. These studies would need to analyze the effects of larger domains on the natural assimilative capacities of aquifers, which may consequentially lessen the burdens of treatment activities.

To improve our ability to quantify the effects from incremental changes to the biological and ISCO treatments specifically, more laboratory studies using similar controls but different treatment schemes are recommended. These changes include: 1) larger scope of collected data, 2) increases in permanganate concentration, 3) increasing treatment solution concentrations of sodium hexametaphosphate to determine effects from formation of MnO_2 minerals, 4) the use of a lactate-only control on field soils, 5) further injections of lactate within the KB-1 treatments to quantify benefits of multiple reactivations of the treatment, 6) further consideration of xanthan gum to increase the sweep efficiency of injected treatment solutions, 7) increases in the scale of the experiment to better represent field conditions where microbial dechlorination of TCE daughter-products has sufficient time to occur, 8) implementation of pH≥8 conditions during the formation of iron sulfides to determine potential increases in the long-term efficacy of the treatment, and 9) longer time-frames to determine long-term effects from the treatments. In tandem with the considerations discussed previously, results from the treatment studies highlight an important point: we may be effectively stuck with some of these unwanted subsurface releases, and patience is encouraged when seeking a solution for highly heterogeneous or complex field-sites.

Overall, to better understand field-scale treatment outcomes, modeling studies using *MIN3P* at both the laboratory and field-scale indicate that the further study is needed with increased biogeochemical complexity. This includes the discovery and incorporation of previously unknown chemical processes into the models, such as the natural attenuative processes discussed previously. Discrepancies within the modeling studies highlight some important

gaps in our ability to quantify the scope of our problems. In short, modeling software and real-world validation activities need to improve to the point that hydrogeologists are confident that we have reactive-transport modeling accurate enough to handle the incredibly complex nature of most aged field-sites. This will require extensive and careful work to acquire field-scale characterization data from treatment activities to verify the results from advanced field-scale modeling studies. That said, the impressive capabilities of *MIN3P* to handle the lab and field-scale treatments implies that we should continue to push *MIN3P* as a foundation for future reactive-transport modeling. Furthermore, the code writers for *MIN3P* remain incredibly adaptive at adding new abilities to improve the functionality of the code, suggesting that our only future limitation in modeling treatment activities may be in our own ignorance of subsurface biogeochemical complexities.

To improve our overall understanding of transverse hydrodynamic dispersion at any scale, further investigations into the phenomenon should be conducted at the pore-scale. Laboratory-scale experiments which use advances in sampling and imaging analysis tools could provide improved mathematical quantification of this process. Further experiments measuring transverse plume spreading using quantifiable gradients in fluid viscosities as well as heterogeneous soil geometries are needed to prove the conjectures discussed earlier. Overall, this research supports the theory that flaws exist in our understanding of transverse hydrodynamic dispersion, but a new mathematical formulation is not advanced. A faulty conceptual model may equate to potentially large sums of wasted money during failed treatments. A new and modern approach to heterogeneous transport is needed that allows hydrogeologists to move beyond the current conception of dispersion. Until this happens, our profession will most likely use the theory proposed by Bear (1972), which may continue

to mischaracterize the scope of the subsurface problems we encounter; resulting in wasted time, effort, reputations and money.

BIBLIOGRAPHY

M.R. Anderson, R.L. Johnson, and J.F. Pankow. Dissolution of dense chlorinated solvents into groundwater. 3. modeling contaminant plumes from fingers and pools of solvent. *Environ. Sci. Technol.*, 26:901–908, 1992.

R. Aris. On the dispersion of a solute in a fluid flowing through a tube. *Proc. R. Soc. London*, 235:67–78, 1956.

D.M. Bagley and J.M. Gossett. Tetrachloroethene transformation to trichloroethene and cis-1,2-dichloroethene by sulfate-reducing enrichment cultures. *Appl. Environ. Microbiol.*, 56(8):2511–2516, 1990.

J. Bear. On the tensor form of dispersion in porous media. *Journal of Geophysical Research*, 66(4):1185–1197, 1961.

J. Bear. *Dynamics of Fluids in Porous Media*. Courier Dover Publications, 1972.

R.B. Bird, W.E. Stewart, and E.N. Lightfoot. *Transport Phenomena*. John Wiley & Sons, New York, NY, 1960.

R. J. Blackwell. Laboratory studies of microscopic dispersion phenomena. *Society of Petroleum Engineers Journal*, pages 1–8, 1962.

E.J. Bouwer and P.L. McCarty. Transformations of 1- and 2-carbon halogenated aliphatic organic compounds under methanogenic conditions. *Appl. Environ. Microbiol.*, 45(4): 1286–94, 1983.

R.A. Brown, J.T. Wilson, and M. Ferrey. Monitored natural attenuation forum: the case for abiotic (mna). *Remediation Journal*, pages 127–137, 2007.

E.C. Butler and K.F. Hayes. Kinetics of the transformation of trichloroethylene and tetrachloroethylene by iron sulfide. *Environ. Sci. Technol.*, 33:2021–27, 1999.

E.C. Butler and K.F. Hayes. Kinetics of the transformation of halogenated aliphatic compounds by iron sulfide. *Environ. Sci. Technol.*, 34:422–429, 2000.

E.C. Butler and K.F. Hayes. Factors influencing rates and products in the transformation of trichloroethylene by iron sulfide and iron metal. *Environ. Sci. Technol.*, 35:3884–3891, 2001.

J.C. Chambon, M.M. Broholm, P.J. Binning, and P.L. Bjergr. Modeling multi-component transport and enhanced anaerobic dechlorination processes in a single fractureclay matrix system. *Journal of Contaminant Hydrology*, 112(1-4):77–90, 2010.

S.W. Chapman and B.L. Parker. Plume persistence due to aquitard back diffusion following dense nonaqueous phase liquid source removal or isolation. *Water Resources Research*, 41 (12):16, 2005. ISSN 1944-7973. URL `http://dx.doi.org/10.1029/2005WR004224`.

S.W. Chapman, B.L. Parker, T.C. Sale, and L.A. Doner. Testing high resolution numerical models for analysis of contaminant storage and release from low permeability zones. *Journal of Cont. Hydrology*, 136-137, 2012.

O.A. Cirpka, A. Olsson, Q. Ju, Md. A. Rahman, and P. Grathwohl. Determination of transverse dispersion coefficients from reactive plume lengths. *Ground Water*, 44(2):212–221, 2006.

A.T. Corey and B.W. Auvermann. Transport by advection and diffusion revisited. *Vadose Zone Journal*, 2:655–663, 2003.

J. Crank. *Mathematics of Diffusion*. Oxford University Press, New York, 1956.

A.M. Cupples, A.M. Spormann, and P.L. McCarty. Comparative evaluation of chloroethene dechlorination to ethene by dehalococcoides-like microorganisms. *Environ. Sci. Technol.*, 38(18):4768–4774, 2004b.

I. Damgaard, P.L. Bjerg, C.S. Jacobsen, A. Tsitonaki, H. Kerrn-Jespersen, and M.M. Broholm. Performance of full-scale enhanced reductive dechlorination in clay till. *Groundwater Monitoring & Remediation*, 33(1):48–61, 2012.

P. Danel. The measurement of ground water flow. *Arid Zone Hydroglogy, Proc. UNESCO*, (2):99–107, 1952.

P.R. Day. Dispersion of a moving salt-water boundary advancing through saturated sand. *American Geophysical Union*, 37(5):595–601, 1956.

T.J. Dekker and L.M. Abriola. The influence of field-scale heterogeneity on the infiltration and entrapment of dense nonaqueous phase liquids in saturated formation. *Journal of Contaminant Hydrology*, 42:187–218, 2000.

J.M.P.Q. Delgado and J.R.F.G. de Carvalho. Measurement of the coefficient of transverse dispersion in flow through packed beds for a wide range of values of the schmidt number. *Transport in Porous Media*, 44(1):165–180, 2001.

D.E. Ellis, E.J. Lutz, J.M Odom, R.J. Buchanan, C.L. Bartlett, M.D. Lee, M.R. Harkness, and K.A. Deweerd. Bioaugmentation for accelerated in situ anaerobic bioremediation. *Environ. Sci. Technol.*, 31(11):2254–60, 2000.

S. Feenstra, J.A. Cherry, and B.L. Parker. *Conceptual Models for the Behavior of Dense Nonaqueous Phase Liquids (DNAPLs) in the Subsurface; Chapter 2 in Dense Chlorinated Solvents and Other DNAPLs in Groundwater*. Waterloo Press, Portland, Oregon, 1996.

D.E. Fennell, A.B. Carroll, J.M. Gossett, and S.H. Zinder. Assessment of indigenous reductive dechlorinating potential at a tce-contaminated site using microcosms, polymerase chain reaction analysis, and site data. *Environ. Sci. Technol.*, 35:1830–39, 2001.

C.W. Fetter. *Applied Hydrogeology*. Macmillan, 1993.

J.A. Field and R. Sierra-Alvarez. Biodegradability of chlorinated solvents and related chlorinated aliphatic compounds. *Reviews in Environmental Science and Bio/Technology*, 3 (3):185–254, 2004.

D.L. Freedman and J.M. Gossett. Biological reductive dechlorination of tetrachloroethylene and trichloroethylene to ethylene under methanogenic conditions. *Appl. Environ. Microbiol.*, 55(9):2144–2151, 1989.

R.A. Freeze and J.A. Cherry. *Groundwater*. Prentice-Hall, 1979.

D.L. Freyberg. A natural gradient experiment on solute transport in a sand aquifer, 2, spatial moments and the advection and dispersion of nonreactive tracers. *Water Resources Research*, 22(13):2031–2046, 1986.

S.P. Garabedian, L.W. Gelhar, and M.A. Celia. Large-scale dispersive transport in aquifers: Field experiments and reactive transport theory. *Ralph M. Parsons Lab. for Water Resources and Hydrodynamics*, 1988.

S.P. Garabedian, D.R. LeBlanc, L.W. Gelhar, and M.A. Celia. Large-scale natural gradient tracer test in sand and gravel, cape cod, massachusetts 2. analysis of spatial moments for a nonreactive tracer. *Water Resources Research*, (5):911–924, 1991.

L.W. Gelhar, A.L. Gutjahr, and R.L. Naff. Stochastic analysis of macrodispersion in a stratified aquifer. *Water Resources Research*, 15(6):1387–1397, 1979.

L.W. Gelhar, C. Welty, and K.R. Rehfeldt. A critical review of data on field-scale dispersion in aquifers. *Water Resources Research*, 28(7):1955–1974, 1992.

R.W. Gillham, E.A. Sudicky, J.A. Cherry, and E.O. Frind. An advection-diffusion concept for solute transport in heterogeneous unconsolidated geological deposits. *Water Resources Research*, 20(3):369–378, 1984.

M.B. Goldhaber and I.R. Kaplan. *The sulfur cycle. In the Sea.* Goldberg, E. D, Wiley-Interscience, New York, 1974.

A. Grostern and E.A. Edwards. Growth of dehalobacter and dehalococcoides spp. during degradation of chlorinated ethanes. *Appl. Environ. Microbiol.*, 72(1):428–436, 2006.

D. R. F. Harleman and R. R. Rumer. Longitudinal and lateral dispersion in an isotropic porous medium. *Journal of Fluid Mechanics*, 16(3):385–394, 1963.

Z.C. Haston and P.L. McCarty. Chlorinated ethene half-velocity coefficients (ks) for reductive dehalogenation. *Environ. Sci. Technol.*, 33(2):223–226, 1999.

Y.T. He, J.T. Wilson, and R.T. Wilkin. Transformation of reactive iron minerals in a permeable reactive barrier (biowall) used to treat tce in groundwater. *Environ. Sci. Technol.*, 42:6690–6696, 2008.

T.H. Henderson, K.U. Mayer, B.L. Parker, and T.A. Al. Three-dimensional density-dependent flow and multicomponent reactive transport modeling of chlorinated solvent oxidation by potassium permanganate. *Journal of Contaminant Hydrology*, 106(3-4):195–211, 2009.

E.R. Hendrickson, J.A. Payne, R.M. Young, M.G. Starr, M.P. Perry, S. Fahnestock, D.E. Ellis, and R.C. Ebersole. Molecular analysis of dehalococcoides 16s ribosomal dna from chloroethene-contaminated sites throughout north america and europe. *Appl. Environ. Microbiol.*, 68(2):485–495, 2002.

J. Hønning, M.M. Broholm, and P.L. Bjerg. Role of diffusion in chemical oxidation of pce in a dual permeability system. *Environ. Sci. Technol.*, 41(24):8426–32, 2007.

K.C. Huang, G.E. Hoag, P. Chheda, B.A. Woody, and G.M. Dobbs. Oxidation of chlorinated ethenes by potassium permanganate: a kinetics study. *Journal of Hazardous Materials*, 87(1-3):155–169, 2001.

J.R. Hunt, M. Sitar, and K.S. Udell. Nonaqueous phase liquid transport and cleanup 1. analysis of mechanisms. *Water Res. Research*, 24(8):1247–1259, 1988.

S.P. Hyun and K.F. Hayes. Feasibility of using in situ fes precipitation for tce degradation. *Journal of Environ. Eng.*, pages 1009–1014, 2009.

H.Y. Jeong and K.F. Hayes. Impact of transition metals on reductive dechlorination rate of hexachloroethane by mackinawite. *Environ. Sci. Technol.*, 37:4650–4655, 2003.

H.Y. Jeong and K.F. Hayes. Reductive dechlorination of tetrachloroethylene and trichloroethylene by mackinawite (fes) in the presence of metals: Reaction rates. *Environ. Sci. Technol.*, 41:6390–96, 2007.

H.Y. Jeong, H. Kim, and K.F. Hayes. Reductive dechlorination pathways of tetrachloroethylene and trichloroethylene and subsequent transformation of their dechlorination products by mackinawite (fes) in the presence of metals. *Environ. Sci. Technol.*, 41:7736–7743, 2007.

R.L. Johnson and J.F. Pankow. Dissolution of dense chlorinated solvents into groundwater. 2. source functions for pools of solvent. *Environ. Sci. Technol.*, 26(5):896–901, 1992.

G.R. Kassenga, J.H. Parduea, S. Blairb, and T. Ferrarob. Treatment of chlorinated volatile organic compounds in upflow wetland mesocosms. *Ecological Engineering*, 19(5):305–323, 2003.

A.C. Lasaga. *Kinetic Theory in the Earth Sciences*. Princeton Univ. Press, 1998.

M.D. Lee, J.M Odom, and R.J. Buchanan. New perspectives on microbial dehalogenation of chlorinated solvents: Insights from the field. *Annual Review of Microbiology*, 52:423–452, 1998.

P.K.H. Lee, D. Cheng, K.A. West, L. Alvarez-Cohen, and J. He. Isolation of two new dehalococcoides mccartyi strains with dissimilar dechlorination functions and their characterization by comparative genomics via microarray analysis. *Environmental Microbiology*, 15(8):2293–2305, 2013.

M. Levy and B. Berkowitz. Measurement and analysis of non-fickian dispersion in heterogeneous porous media. *Journal of Cont. Hydrology*, 64(3-4):203–226, 2003.

P.C. Lichtner. Continuum formulation of multicomponent-multiphase reactive transport, in reactive transport in porous media. *Reviews in Mineralogy*, 34:1 81, 1996a.

P.C. Lichtner. Modeling of reactive flow and transport in natural systems. *Paper presented at the Rome Seminar on Environmental Geochemistry, Castelnuovo di Porto, Rome*, 1996b.

G.D. Lima and B.E. Sleep. The spatial distribution of eubacteria and archaea in sand-clay columns degrading carbon tetrachloride and methanol. *Journal of Contaminant Hydrology*, 94:34–48, 2007.

G. Liu and W.P. Ball. Back diffusion of chlorinated solvent contaminants from a natural aquitard to a remediated aquifer under well-controlled field conditions: predictions and measurements. *Ground Water*, 40(2):175–184, 2002.

R. Lookman, D. Paulus, E. Marnette, C. Pijls, A. Ryngaert, L. Diels, and F. Volkering. Ground water transfer initiates complete reductive dechlorination in a pce-contaminated aquifer. *Groundwater Monitoring & Remediation*, 27(3):65–74, 2007.

D.M. Mackay. *Pump and Treat in Low Permeability Media; Chapter 7 in* In Situ *Remediation of DNAPL Compounds in Low Permeability Media Fate/Transport,* In Situ *Control Technologies, and Risk Reduction.* Prepared by Oak Ridge National Laboratory, Oak Ridge, Tennessee, 1996.

D.M. Mackay and J.A. Cherry. Groundwater contamination: Pump and treat remediation. *Environ. Sci. Technol.*, 23(6):630–636, 1989.

D.M. Mackay, D.L. Freyberg, and P.V. Roberts. A natural gradient experiment on solute transport in a sand aquifer 1. approach and overview of plume movement. *Water Resources Research*, 22(13):2017–2029, 1986.

L.K. MacKinnon and N.R. Thomson. Laboratory-scale in situ chemical oxidation of a perchloroethylene pool using permanganate. *Journal of Contaminant Hydrology*, 56(1-2): 49–74, 2002.

J.K. Magnuson, M.F. Romine, D.R. Burris, and M.T. Kingsley. Trichloroethene reductive dehalogenase from dehalococcoides ethenogenes: sequence of tcea and substrate range characterization. *Appl. Environ. Microbiol.*, 66(12):5141–5147, 2000.

G. Manoli, J.C. Chambon, P.L. Bjerg, C. Scheutz, P.J. Binning, and M.M. Broholm. A remediation performance model for enhanced metabolic reductive dechlorination of chloroethenes in fractured clay till. *Journal of Contaminant Hydrology*, 131(1-4):64–78, 2012.

B.K. Marvin, J. Chambers, A. Leavitt, and C.G. Schreier. *Chemical and Engineering Challenges to In Situ Permanganate Remediation.* Battelle Press, 2002.

K.U. Mayer, S.G. Benner, E.O. Frind, S.F. Thornton, and D.N. Lerner. Reactive transport modeling of processes controlling the distribution and natural attenuation of phenolic compounds in a deep sandstone aquifer. *Journal of Contaminant Hydrology*, 53(3-4):341–368, 2001a.

K.U. Mayer, D.W. Blowes, and E.O. Frind. Reactive transport modelling of an in situ reactive barrier for the treatment of hexavalent chromium and trichloroethylene in groundwater. *Water Resour. Res.*, 37(12):3091–3103, 2001b.

U.K. Mayer, E.O. Frind, and D.W. Blowes. Multicomponent reactive transport modeling in variably saturated porous media using a generalized formulation for kinetically controlled reactions. *Water Resources Research*, 38(9):13.1–13.21, 2002.

X. Maymo-Gatell, T. Anguish, and S.H. Zinder. Reductive dechlorination of chlorinated ethenes and 1,2-dichloroethane by *Dehalococcoides ethenogenes* 195. *Appl. Environ. Microbiol.*, 65(7):3108–3113, 1999.

J.E. McCray, J. Munakata-Marr, J.A. Silva, S. Davenport, and M.M. Smith. Multi-scale experiments to evaluate mobility control methods for enhancing the sweep efficiency of injected subsurface remediation amendments. *SERDP Project ER-148*, 2010.

Merck. *The Merck Index: An Encyclopedia of Chemicals, Drugs, and Biologicals.* Royal Society of Chemistry, 2013.

R. Millington and J. Quirk. Gas diffusion in porous media. *Science*, 130:100–102, 1959.

W.W. Mohn and J.M. Tiedje. Microbial reductive dehalogenation. *Microbiology and Molecular Biology Reviews*, 56(3):482507, 1992.

J.A. Muller, B.M. Rosner, G. Von Abendroth, G. Meshulam-Simon, P.L. McCarty, and A.M. Spormann. Molecular identification of the catabolic vinyl chloride reductase from dehalococcoides sp. strain vs and its environmental distribution. *Appl. Environ. Microbiol.*, 70(8):4880–8, 2004.

J.W. Mullin and A.W. Nienow. Diffusion coefficients of potassium sulfate in water. 9(4): 526–527, 2002.

K.G. Mumford, N.R. Thomson, and R.M. Allen-King. Bench-scale investigation of permanganate natural oxidant demand kinetics. *Enviro.n Sci. Technol.*, 39(8):2835–40, 2005.

NRC. *Alternatives for groundwater cleanup.* The National Academies Press, 1994.

NRC. *Contaminants in the Subsurface.* The National Academies Press, 2005.

NRC. *Alternatives for managing the nation's complex contaminated groundwater sites*. The National Academies Press, 2013.

A. Ogata and R.B. Banks. A solution of the differential equation of longitudinal dispersion in porous media. *Geological Survey Professional Paper 411-A*, 1961.

J.F. Pankow and J.A. Cherry. *Dense Chlorinated Solvents and other DNAPLs in Groundwater*. Waterloo Press, Portland, Oregon, 1996.

B.L. Parker, R.W. Gillham, and J.A. Cherry. Diffusive disappearance of immiscible-phase organic liquids in fractured geologic media. *Ground Water*, 32(5):805–820, 1994.

B.L. Parker, S.W. Chapman, and M.A. Guilbeault. Plume persistence caused by back diffusion from thin clay layers in a sand aquifer following {TCE} source-zone hydraulic isolation. *Journal of Contaminant Hydrology*, 102(12):86 – 104, 2008.

F. Parsons, P.R. Wood, and J. DeMarco. Transformation of tetrachloroethene and trichloroethene in microcosms and groundwater. *Journal (American Water Works Association)*, 76(2):56–59, 1984.

S.V. Patankar. *Numerical Heat Transfer and Fluid Flow*. McGraw-Hill, 1980.

S.G. Pavlostathis and P. Zhuang. Reductive dechlorination of chloroalkenes in microcosms developed with a field contaminated soil. *Chemosphere*, 27:585–595, 1993.

F.C. Payne, J.A. Quinnan, and S.T. Potter. *Remediation Hydraulics*. CRC Press, 2008.

D.W. Peaceman and H.H. Rachford. Numerical calculation of multidimensional miscible displacement. *Society of Petroleum Engineers Journal*, 2:327–339, 1962.

T.K. Perkins and O.C. Johnston. A review of diffusion and dispersion in porous media. *Society of Petroleum Engineers*, 3(1):70–84, 1963.

K.R. Rehfeldt and L.W. Gelhar. Stochastic analysis of dispersion in unsteady flow in heterogeneous aquifers. *Water Resources Research*, 28(8):2085–2099, 1992.

David Rickard. Kinetics of fes precipitation: Part 1. competing reaction mechanisms. *Geochimica et Cosmochimica Acta*, 59(21):4367 – 4379, 1995.

M.N.E. Rifai, W.J. Kaufman, and D.K. Todd. *Dispersion Phenomena in Laminar Flow Through Porous Media*. Univ. of California, 1956.

M.O. Rivett, S. Feenstra, and J.A. Cherry. Transport of a dissolved-phase plume from a residual solvent source in a sand aquifer. *Journal of Hydrology*, 159:27–41, 1994.

M.O. Rivett, S. Feenstra, and J.A. Cherry. A controlled field experiment on groundwater contamination by a multicomponent dnapl: creation of the emplaced-source and overview of dissolved plume development. *Journal of Contaminant Hydrology*, 49(1-2):111–149, 2001.

S. Saenton, T.H. Illangasekare, K. Soga, and T.A. Saba. Effects of source zone heterogeneity on surfactant-enhanced napl dissolution and resulting remediation end-points. *Journal of Contaminant Hydrology*, 59:27–44, 2002.

P.G. Saffman. Dispersion due to molecular diffusion and macroscopic mixing in flow through a network of capillaries. *Journal of Fluid Mechanics*, 2(7):194–208, 1960.

T. Sale. *Chemically Enhanced* In Situ *Recovery; Chapter 11 in* In Situ *Remediation of DNAPL Compounds in Low Permeability Media Fate/Transport,* In Situ *Control Technologies, and Risk Reduction.* Prepared by Oak Ridge National Laboratory, Oak Ridge, Tennessee, 1996.

T. Sale, J. Zimbron, and D. Dandy. Effects of reduced contaminant loading from analog dnapl sources on down-gradient water quality in an idealized two layer system. *Journal of Contaminant Hydrology*, 102, 2008.

T. Sale, B.L. Parker, C.J. Newell, and J.F. Devlin. Management of contaminants stored in low permeability zones. *SERDP Project ER-1740*, 2014.

A.E. Scheidegger. Statistical hydrodynamics in porous media. *Journal of Applied Physics*, (25):994–1001, 1954.

A.E. Scheidegger. On the theory of flow of miscible phases in porous media. *Porc. IUGG General Assembly*, pages 236–242, 1957.

C. Scheutz, N.D. Durant, P. Dennis, M.H. Hansen, T. Jørgensen, R. Jakobsen, E.E. Cox, and P.L. Bjerg. Concurrent ethene generation and growth of dehalococcoides containing vinyl chloride reductive dehalogenase genes during an enhanced reductive dechlorination field demonstration. *Environ. Sci. Technol.*, 42(24):9302–09, 2008.

C. Scheutz, M.M. Broholm, N.D. Durant, E.B. Weeth, T.H. Jorgensen, P. Dennis, C.S. Jacobsen, E.E. Cox, J.C. Chambon, and P.L Bjerg. Field evaluation of biological enhanced reductive dechlorination of chloroethenes in clayey till. *Environ. Sci. Technol.*, 44:5134–5141, 2010.

M. Schnarr, C. Truax, G. Farquhar, E. Hood, T. Gonullu, and B. Stickney. Laboratory and controlled field experiments using potassium permanganate to remediate trichloroethylene and perchloroethylene dnapls in porous media. *Journal of Contaminant Hydrology*, 29(3): 205–224, 1998.

M.H. Schroth, M. Oostrom, T.W. Wietsma, and J.D. Istok. In-situ oxidation of trichloroethene by permanganate: effects on porous medium hydraulic properties. *Journal of Contaminant Hydrology*, 50(1-2):79–98, 2001.

F. Schwille and J.F. Pankow. *Dense Chlorinated Solvents in Porous and Fractured Media - Model Experiments.* Lewis Publishers, Boca Raton, FL, 1988.

C. Shackelford and J. Lee. Analyzing diffusion by analogy with consolidation. *J. Geotech. Geoenviron. Eng.*, 131(11):1345–1359, 2005.

R.L. Siegrist, M. Crimi, and T.J. Simpkin. *In Situ Chemical Oxidation for Groundwater Remediation (SERDP ESTCP Environmental Remediation Technology)*. Springer, 2011.

E.S. Simpson. Transverse dispersion in liquid flow through porous media. *U.S. Geological Survey, Professional Paper 411-C*, 1962.

C.S. Slichter. Field measurement of the rate of movement of underground waters. *U.S. Geological Survey, Water Supply Paper*, (140), 1905.

C.I. Steefel and A.C. Lasaga. A coupled model for transport of multiple chemical species and kinetic precipitation/dissolution reactions with application to reactive flow in single phase hydrothermal systems. *Amer. Journal of Science*, 294:529–592, 1994.

H.F. Stroo, A. Leeson, J.A. Marqusee, P.C. Johnson, C.H. Ward, M.C. Kavanaugh, T.C. Sale, C.J. Newell, K.D. Pennell, C.A. Lebron, and M. Unger. Chlorinated ethene source remediation: lessons learned. *Environ. Sci. Technol.*, 46(12):6438–47, 2012.

E.A. Sudicky, J.A. Cherry, and E.O. Frind. Migration of contaminants in groundwater at a landfill: A case study: 4. a natural-gradient dispersion test. *Journal of Hydrology*, 63 (1-2):81108, 1983.

E.A. Sudicky, R.W. Gillham, and E.O. Frind. Experimental investigation of solute transport in stratified porous media 1. the nonreactive case. *Water Resources Research*, 21(7):1035 – 1041, 1985.

G.I. Taylor. Dispersion of soluble matter in solvent flowing slowly through a tube. *Proceedings of the Royal Society*, (219):186–203, 1953.

N.R. Thomson, E.D. Hood, and G.J. Farquhar. Permanganate treatment of an emplaced dnapl source. *Groundwater Monitoring and Remediation*, 27(4):74–85, 2007.

N.R. Thomson, M.J. Fraser, C. Lamarche, J.F. Barker, and S.P. Forsey. Rebound of a coal tar creosote plume following partial source zone treatment with permanganate. *Journal of Contaminant Hydrology*, 102(1-2):154–171, 2008.

M.A. Urynowicz, B. Balu, and U. Udayasankar. Kinetics of natural oxidant demand by permanganate in aquifer solids. *Journal of Contaminant Hydrology*, 96:187–194, 2008.

G. van der Kamp, L.D. Luba, J.A. Cherry, and H. Maathuis. Field study of a long narrow sewage contaminant plume. *Ground Water*, 32(6):1008–1016, 1994.

S. Vancheeswaran, M.R. Hyman, and L. Semprini. Anaerobic biotransformation of trichlorofluoroethene in groundwater microcosms. *Environ. Sci. Technol.*, 33(12):2040–45, 1999.

J.E. VanderKwaak, P.A. Forsyth, K.T.B. MacQuarrie, and E.A. Sudicky. *WatSolv - Sparse Matrix Iterative Solver, users guide.* Univ. of Waterloo, Waterloo, Ontario, Canada, 1997.

T.M. Vogel and P.L. McCarty. Biotransformation of tetrachloroethylene to trichloroethylene, dichloroethylene, vinyl chloride, and carbon dioxide under methanogenic conditions. *Appl. Environ. Microbiol.*, 49(5):1080–1083, 1985.

M. Wang, G. Wildburg, J. H. van Esch, P. Bennema, R. J. M. Nolte, and H. Rinsdorf. Surface-tension-gradient-induced pattern formation in monolayers. *Phys. Rev. Letters*, 71: 40034006, 1993.

M.P. Whelan, E.A. Voudrias, and A. Pearce. Dnapl pool dissolution in saturated porous media: procedure development and preliminary results. *Journal of Cont. Hydrology*, 15: 223–237, 1994.

M. Wolthers, S.J. Van der Gaast, and D. Rickard. The structure of disordered mackinawite. *Amer. Mineral.*, 88:2007–2015, 2003.

X. Xu and J. Luo. Marangoni flow in an evaporating water droplet. *Applied Phys. Letters*, 91, 2007.

Y.E. Yan and F.W. Schwartz. Oxidative degradation and kinetics of chlorinated ethylenes by potassium permanganate. *Journal of Contaminant Hydrology*, 37(3-4):343–365, 1999.

K. Yuhara. A model experiment of saline diffusion in flow of water through porous media. *Geophysics*, (9):127–134, 1954.

DERIVATION OF CONTAMINANT PLANE-SOURCE MODEL

Beginning with a fundamental PDE for transport in a porous media:

$$(15) \qquad -v_w \cdot \frac{\partial C_{aq}}{\partial x} + D_L \cdot \frac{\partial^2 C_{aq}}{\partial^2 x} + D_t \cdot \frac{\partial^2 C_{aq}}{\partial^2 y} + D_t \cdot \frac{\partial^2 C_{aq}}{\partial^2 z} - \frac{R_M}{\phi} - \frac{G_M}{\phi} = \frac{\partial C_{aq}}{\partial t}$$

The model states the assumptions:

- System is at steady-state:

$$\frac{\partial C_{aq}}{\partial t} = 0$$

- Pool width ('y' into page) is infinite:

$$\frac{\partial^2 C_{aq}}{\partial^2 y} = 0$$

- Transport in x-direction will be primarily by convection:

$$D_L \cdot \frac{\partial^2 C_{aq}}{\partial^2 x} = 0$$

- No reactions:

$$\frac{R_M}{\phi} = 0$$

- No mass gain or loss:

$$\frac{G_M}{\phi} = 0$$

Applying the assumptions to Equation 15:

$$v_w \cdot \frac{\partial C_{aq}}{\partial x} - D_t \cdot \frac{\partial^2 C_{aq}}{\partial^2 z} = 0$$

Defining:

$$\alpha = \frac{D_t}{v_w}$$

(16)
$$\frac{\partial C_{aq}}{\partial x} = \alpha \cdot \frac{\partial^2 C_{aq}}{\partial^2 z}$$

Defining boundary conditions:

1) $C_{aq}(x, z) = 0$ for all $x \leq 0$ and $z = \infty$

2) $C_{aq}(x, z) = C_{sol}$ for all $x > 0$ and $z = 0$

3) $C_{aq}(x, z) = 0$ for all $x = 0$ and $z \geq 0$

Using a Boltzman transform variable:

$$\eta = \frac{z}{\sqrt{4 \cdot \alpha \cdot x}}$$

The LHS of Equation 16 becomes:

$$\frac{d}{dx}C_{aq} = \frac{d}{d\eta}C_{aq} \cdot \frac{d}{dx}\eta = \frac{d}{d\eta}C_{aq} \cdot \frac{d}{dx}\frac{z}{\sqrt{4 \cdot \alpha \cdot x}}$$

$$\frac{d}{dx}\frac{z}{\sqrt{4 \cdot \alpha \cdot x}} = -\frac{z}{2 \cdot x \cdot \sqrt{4 \cdot \alpha \cdot x}}$$

Therefore:

(17)
$$\frac{d}{dx}C_{aq} = \frac{d}{d\eta}C_{aq} \cdot \frac{-\eta}{2 \cdot x}$$

RHS of Equation 16:

$$\alpha \cdot \frac{d^2 C_{aq}}{dz^2} = \alpha \cdot \frac{d}{dz}\left(\frac{d}{d\eta}C_{aq} \cdot \frac{d}{dz}\eta\right) = \alpha \cdot \frac{d}{dz}\left(\frac{d}{d\eta}C_{aq} \cdot \frac{d}{dz}\frac{z}{\sqrt{4 \cdot \alpha \cdot x}}\right)$$

$$= \alpha \cdot \frac{d}{d\eta}\left(\frac{d}{d\eta}C_{aq} \cdot \frac{d}{dz}\frac{z}{\sqrt{4 \cdot \alpha \cdot x}}\right) \cdot \frac{d}{dz}\eta = \alpha \cdot \frac{d}{d\eta}\left(\frac{d}{d\eta}C_{aq} \cdot \frac{d}{dz}\frac{z}{\sqrt{4 \cdot \alpha \cdot x}}\right) \cdot \frac{d}{dz}\frac{z}{\sqrt{4 \cdot \alpha \cdot x}}$$

$$\frac{d}{dz}\frac{z}{\sqrt{4 \cdot \alpha \cdot x}} = \frac{1}{\sqrt{4 \cdot \alpha \cdot x}}$$

Therefore:

(18)
$$\alpha \cdot \frac{d^2 C_{aq}}{dz^2} = \frac{1}{4 \cdot x} \cdot \frac{d^2 C_{aq}}{d\eta^2}$$

Putting Equations 17 and 18 back into Equation 16:

$$\frac{\eta}{-2 \cdot x} \cdot \frac{d}{d\eta}C_{aq} = \frac{1}{4 \cdot x} \cdot \frac{d^2}{d\eta^2}C_{aq}$$

Simplifying:

(19)
$$\frac{d^2}{d\eta^2}C_{aq} + 2 \cdot \eta \cdot \frac{d}{d\eta}C_{aq} = 0$$

Redefining B.C.'s in terms of η:

    1) $C_{aq}(x, z) = 0$ for all $x \leq 0$ and $z = \infty$: $\eta = \infty$, $C_{aq} = 0$

    2) $C_{aq}(x, z) = C_{sol}$ for all $x > 0$ and $z = 0$: $\eta = 0$, $C_{aq} = C_{sol}$

Now solving the ODE through 2 integration steps. First integration, set:

$$\psi = \frac{d}{d\eta}C_{aq}$$

Rewriting equation 19:

$$\frac{d}{d\eta}\psi = -2 \cdot \eta \cdot \psi$$

$$\int \frac{1}{\psi}d\psi = \int -2 \cdot \eta d\eta$$

$$Ln(\psi) = -\eta^2 + C_1 \qquad or \qquad \psi = C_1 \cdot e^{-\eta^2}$$

Second Integration:

$$\frac{d}{d\eta} C_{aq} = C_1 \cdot e^{-\eta^2}$$

$$C_{aq}(\eta) - C_{aq}(0) = C_1 \cdot \int_0^\eta e^{-\eta^2} d\eta + C_2$$

$$C_{aq}(\eta) = C_1 \cdot \int_0^\eta e^{-\eta^2} d\eta + C_2 + C_{sol}$$

$$C_{aq}(0) = C_{sol} = C_1 \cdot \int_0^0 e^{-\eta^2} d\eta + C_2 + C_{sol}, \qquad C_2 = 0$$

$$C_{aq}(\eta) = C_1 \cdot \int_0^\eta e^{-\eta^2} d\eta + C_{sol}$$

$$C_{aq}(\infty) = 0 = C_1 \cdot \int_0^\infty e^{-\eta^2} d\eta + C_{sol}, \qquad C_1 = \frac{-C_{sol}}{\int_0^\infty e^{-\eta^2} d\eta}$$

$$C_{aq}(\eta) = C_{sol} - C_{sol} \cdot \frac{\int_0^\eta e^{-\eta^2} d\eta}{\int_0^\infty e^{-\eta^2} d\eta}$$

$$\frac{C_{aq}(\eta)}{C_{sol}} = 1 - \frac{\int_0^\eta e^{-\eta^2} d\eta}{\int_0^\infty e^{-\eta^2} d\eta} = 1 - \frac{2}{\sqrt{\pi}} \cdot \int_0^\eta e^{-\eta^2} d\eta = erfc(\eta)$$

Substitute definition of η:

$$C_{aq}(x, z) = C_{sol} \cdot erfc\left(\frac{z}{\sqrt{4 \cdot \alpha \cdot x}}\right)$$

Substitute definition of α:

$$C_{aq}(x, z) = C_{sol} \cdot erfc\left(\frac{z}{\sqrt{4 \cdot \frac{D_t}{v_w} \cdot x}}\right)$$

Simplify:

$$C_{aq}(x, z) = C_{sol} \cdot erfc\left(\frac{z}{2} \cdot \sqrt{\frac{v_w}{D_t \cdot x}}\right)$$

Change to definition of the erf:

$$C_{aq}(x, z) = C_{sol} \left(1 - erf \left(\frac{z}{2} \sqrt{\frac{v_w}{D_t \cdot x}} \right) \right) \tag{20}$$